Final Technical Report

Project Title: Light Metals Permanent Mold Casting

Award Number: DE-FC36-04GO14230

Project Period: January 2004 – March 31, 2014

Principal Investigator(s):
Yemi Fasoyinu, 905-645-0779, Yemi.Fasoyinu@NRCan.gc.ca

Recipient Organization:

CanmetMATERIALS, Natural Resources Canada
183 Longwood Road South, Hamilton, ON, L8P 0A5, Canada

Laboratory Former Address:

CANMET MTL (Materials Technology Laboratory), Natural Resources Canada
568 Booth Street, Ottawa, ON, KIA 0G1, Canada

Participants (cost sharing): January 2004 – June 30, 2009

Eck Industries, Inc.
Grenville Castings Limited
Magma Foundry Technologies, Inc.
Alcan International Ltd.

Participants (cost sharing): June 2012 – March 31, 2014

Eck Industries, Inc.
B.S Metallurgy, Inc.
Product Development &Analysis (PDA) LLC

March 2014

Acknowledgment, Disclaimer and Proprietary Data Notice

Acknowledgment: This report is based upon work supported by the U. S. Department of Energy under Award No.DE-FC36-04GO14230

Disclaimer: Any findings, opinions, and conclusions or recommendations expressed in this report are those of the author(s) and do not necessarily reflect the views of the Department of Energy.

Proprietary Data Notice: None in report

Table of Contents

List of Figures iv

List of Tables vi

1 Executive Summary 1

2 Introduction 2

3. Background 3

3.1 Specific Goals and Objectives 4
TASK 1 - Selection of Prototype Component 4
TASK 2 - Hot Tearing Studies 4
TASK 3 – Prototype Casting Trials (at CANMET) 4
TASK 4 – Mechanical Properties and Metallographic Evaluation 4
TASK 5 - Technology Transfer 4

3.2 Team Members 5

4 Results and Discussion 6

4.1 TASK 1: Selection of Prototype Components 6
4.1.1 Regular Restrained Mold 6
4.1.2 Instrumented Restrained Mold 6
4.1.3 Engine Mount Casting 8
4.1.4 Rocker Arm Casting 8

4.2 TASK 2 - Hot Tearing and Computer Simulation Studies 9
4.2.1 Phase I: Experimental Details 9
4.2.2 Hot Tearing Results from Constrained Rod Molds 11
4.2.3 Computer Simulation 14
4.2.4 Instrumented Constrained Rod Mold 18
4.2.5 Phase II: Experimental Details 24
4.2.6 Results and Discussion 24
4.2.7 Summary and Conclusions 30

4.3 TASK 3 Prototype Casting Trials 31
4.3.1 Melting and Casting 31
4.3.2 Results and Discussion 32

4.4 TASK 4 Mechanical Properties and Microstructures 36
4.4.1 Experimental Procedure 36
4.4.2 Results and Discussion 36
4.4.3 Metallography and Microstructure 41
4.4.4 Summary and Conclusions 49

4.5 TASK 5 - Technology Transfer (Casting Trials at Partner Foundry) 50

4.5.1 Phase I: Prototype Castings 50
4.5.2 Melting and Casting 51
3.5.3 Characterization 56
4.5.4 Control of Hot Tearing 59
4.5.5 Summary and Conclusions 59
4.5.2 Phase II: 4.5.2 Mounting Bracket Casting 61
4.5.2.1 Computer Simulation 61
4.5.2.2 Simulation Results 67
4.5.2.3 Summary and Conclusions 74
4.5.2.4 Casting Trials 75
4.5.2.5 Casting Trial Highlights 77
4.5.2.6 Microstructures from Selected Bracket Components 85
4.5.2.7 Summary and Conclusions 91
4.5.3 Characterization (Mechanical Properties) 92
4.5.3.1Test bars 92
4.5.3.2 Results and Discussion 92
4.5.3.3 Summary and Conclusions 100

5 Benefits Assessment 101

6 Commercialization 101

7 Accomplishments 101
7.1 Control of Hot Tearing 101
7.2 Publications 102

8 Conclusions 102

9 Recommendations 104

10 References 104

11 Appendices 106

List of Figures

Figure 4.1.1 Restrained rod hot-tearing molds. 6
Figure 4.1.2 Instrumented restrained mold showing the location of thermocouples. 7
Figure 4.1.3 Engine mount mold halves. 8
Figure 4.1.4 Rocker arm mold halves and metal core. 9
Figure 4.2.1 Typical sectioned RPT samples (a) before, and (b) after degassing. 9
Figure 4.2.2 Macrostructures of disc castings (a) before, and (b) after adding grain refiners. 10
Figure 4.2.3 Photographs of 3-rod constrained casting showing location of hot tearsing. 12
Figure 4.2.4 Simulation results for alloy 206.0 at 290°C and 450°C. 16
Figure 4.2.5 Comparative hot tearing potential at 290 and 450°C for alloy 206.0. 17
Figure 4.2.6 Simulation results for alloy 535.0 at 290 and 450°C. 18
Figure 4.2.7 Alloy 206.0 showing the effects mold temperatures on hot tearing. 20
Figure 4.2.8 Anodized microstructures of 206.0 (a) before and (b) after grain refinement. 21
Figure 4.2.9 Restrained casting from alloy 535.0 without hot tearing 21
Figure 4.2.10 Cooling curves and its first derivative near the ingate and the rounded end of the 26 cm rod poured from unrefined melts of alloy 206. 22
Figure 4.2.11 Cooling curves and its first derivatives from the top, middle, and the bottom of the sprue poured from unrefined melts of alloy 206. 22
Figures 4.2.12 Refined metal poured into molds preheated to (a) 300°C and (b) 400°C. 25
Figure 4.2.13 Examples of cooling curves at the rod/sprue and rod/ball junctions 27
for a 10 inch rod at solidus temperature. 27
Figure 4.2.14 Examples of cooling curves at the rod/sprue and rod/ball junctions for a 10 inch rod at solidus temperature from which the cooling rate was estimated. 28
Figure 4.3.1 Photographs of engine mount castings without and with hot tear. 33
Figure 4.3.2 Radiographs from A206.0 and A535 33
Figure 4.3.3 Photographs of a mounted rocker arm mold and rocker arm casting. 34
Figure 4.3.4 Examples of hot tear and surface shrinkage in rocker arm castings. 35
Figure 4.4.1 Effect of Cu content on the tensile properties of alloy 206. 39
Figure 4.4.2 Effect of test temperature on the tensile properties of alloy 206 with 5.1%Cu. 39
Figure 4.4.3 Effect of Mg content on the tensile properties of alloy 535 40
Figure 4.4.4 Hot-tear region of constrained rod castings from alloys 206 and 535. 41
Figure 4.4.5 Microstructures from alloy 206 poured in mold preheated to 200°C. 42
Figure 4.4.6 Microstructures from alloy 206 poured in mold preheated to 350°C. 43
Figure 4.4.7 Microstructures from alloy 206 poured in mold preheated to 400°C. 44
Figure 4.4.8 Anodized and etched microstructures showing the progression of hot tear. 44
Figure 4.4.9 Unetched microstructures of test bars of alloy 206 before and after heat treatment. 45
Figure 4.4.10 Microstructures of test bars of alloy 206 before and after heat treatment. Keller's etch. 45
Figure 4.4.11 Microstructures from test bars of alloy 206. 46
before and after heat treatment. Keller's etch. 46
Figure 4.4.12 Alloy 206, SEM of the fracture surface of test bar showing dendritic structure. The EDS of the general area and eutectic area are shown in (e) and (f). 47
Figure 4.4.13 Unetched and etched microstructures of test bars of alloy 535 before 48
in addition, after heat treatment, 500x. 48
Figure 4.4.14 Alloy 535, SEM of (a) fracture surface, (b) dendritic structure of (a), and (c) EDS. 48
Figure 4.5.1 Mounted 4-cavity swivel mold on tilt-pour machine. 50
Figure 4.5.2 Schematic of sand core and swing arm casting with gating system and feed tube. 51
Figure 4.5.3 Mounted swing arm mold on LP machine with T/C and cooling channel probes. 51
Figure 4.5.4 Photographs of swivel castings with and without the gating system. 54
Figure 4.5.5 Radiographs of swivel casting from A206 and A535. No hot tear or shrinkage cavity. 54
Figure 4.5.6 Photographs of elbow casting with and without the gating system 55

Figure 4.5.7 Radiographs of elbow casting from A206 and A535. 55
Figure 4.5.8 Swing arm casting with gating system, sand core, and finished casting. 56
Figure 4.5.9 Predicted and observed hot tear location on casting on casting. 56
Figure 4.5.10 Sectioned and macroetched swivel head castings from alloys 206 and 535. 57
Figure 4.5.11 Anodized microstructures from grain refined swivel-head casting from alloys 206 and 535. Etched with 1.8% fluoboric acid (HBF4) in water (Barkers's anodizing method). 57
Figure 4.5.12 Microstructures from swing arm castings. 58
Figure 4.5.13 SEM of fracture surface from swing arm casting. 58
Figure 4.5.14 Bracket component poured from A356 61
Figure 4.5.15 Bracket casting with gating system. 62
Figure 4.5.16 Thermocouple locations for the casting trials and simulation. 62
T1 and T2 are locations of thermocouples in the mold. 62
Figure 4.5.17 Hot tearing predicted in the cross bracket. 67
Figure 4.5.18 Casting #12 showing hot tearing location in the upper cross member junctions. 68
Figure 4.5.19 Casting #10 showing hot tearing in the transition from the post to the journal area. 68
Figure 4.5.20 Minor hot tearing tendencies at the top cross bar. 69
Figure 4.5.21 Minor secondary shrinkage predicted underneath top risers 69
Figure 4.5.22 Example of mold filling results. 70
Figure 4.5.23 Potential areas where contraction stresses can develop and 71
promote mechanical hot tearing are shown by the arrows. 71
Figure 4.5.24 Areas where minor shrinkage is predicted when die opens 71
Figure 4.5.25 Predicted maximum principal stress and maximum principal strain when die was opened after 120 seconds. 72
Figure 4.5.26 Predicted areas where hot tearing will develop towards the end of solidification 72
Figure 4.5.27 Minor hot tearing tendencies at the bottom cross bar. 73
Figure 4.5.28 Minor secondary shrinkage predicted underneath un-insulated top riser. 73
Figure 4.5.29 Closed mold showing location of the two thermocouples. 75
Figure 4.5.30 Spot where mold surface temperature (IR #3) was measured, near the pouring cup 75
Figure 4.5.31 Spot where mold surface temperature (IR #4) was measured, ...76
flange under the hoop section. 76
Figure 4.5.32 Photograph of casting with gating system. 78
Figure 4.5.33 Photograph of finished component. 78
Figure 4.5.34 Examples of X-ray radiographs showing area where surface shrinkage was observed. 79
Figure 4.5.35 Mold and pouring temperatures from melt A206-1. 83
Figure 4.5.36 Mold and pouring temperatures from melt A206-2. 83
Figure 4.5.37 Mold and pouring temperatures from melt B206. 84
Figure 4.5.38 Mold and pouring temperatures from melt 535. 84
Figure 4.5.39 A sectioned casting showing locations A and B. 85
where samples for microstructure evaluation were removed. 85
Figure 4.5.40 Unetched as-cast microstructures from component #35 alloy A206. 85
Figure 4.5.41 Unetched as-cast microstructures from component #64 alloy 535. 86
Figure 4.5.42 As-cast microstructures from component #35 alloy A206. 87
Figure 4.5.43 As-cast microstructures from component #44 alloy B206. 87
Figure 4.5.44 Heat treated microstructures from component #51 alloy B206 88
Figure 4.5.45 As-cast microstructures from component #64 alloy 535. 88
Figure 4.5.46 Photograph of fracture surface from casting #10 alloy A206, 1.2x. 89
Figure 4.5.47 SEM photographs of fracture surface from casting #10 of A206. 89
Figure 4.5.48 Unetched microstructures from casting #10 perpendicular to the fracture surface. 90
Figure 4.5.49 Etched microstructures from broken casting #10. 90
Figure 4.5.50 Bracket casting showing areas where test bars were removed. 93
Figure 4.5.51 Photographs of machined and separately cast test bars. 93
Figure 4.5.52 (a) Tensile properties and (b) elongation from as-cast and after heat treatment. 94
Figure 4.5.53 Microstructures from test bars poured from B206 in as-cast and 95
after heat treatment. Keller's etch, 500x. 95
Figure 4.5.54 Mechanical properties of test bars machined from bracket casting of A206-1. 97
Figure 4.5.55 Mechanical properties of test bars machined from bracket casting of A206-2 97

Figure 4.5.56 Mechanical properties of test bars machined from bracket casting of B206. 98
Figure 4.5.57 Mechanical properties of separately cast test bars of A206....98
Figure 4.5.58 Microstructures from test bars machined from the bracket component in vertical (17-1) and horizontal (17-2) orientation. Etchant is Keller's reagent....99
Figure 4.5.59 SEM of fracture surface of tensile bars in vertical (17-1) and horizontal (17-2) orientation. Dendritic structure and shrinkage voids are shown. 100

List of Tables

Table 4.2.1 Processing parameters for computer simulation 11
Table 4.2.2 Chemical analysis of alloy 206 for hot tearing studies 11
Table 4.2.3 Chemical analysis of alloy 535 for hot tearing studies 11
Table 4.2.4 Processing parameters of alloy 206 melt # N6080....13
Table 4.2.5 Processing parameters of alloy 206 melt # N6081....13
Table 4.2.6 Processing parameters of alloy 206.0 melt # N6090....14
Table 4.2.7 Processing parameters of alloy 535.0 melt # N6082....14
Table 4.2.8 Summary of the simulation results of the restrained rod castings....15
Table 4.2.9 Processing parameters of alloy 206 melt # N7057....19
Table 4.2.10 Processing parameters of alloy 206 melt # N7072....19
Table 4.2.11 Processing parameters of alloy 206 melt # N7073....19
Table 4.2.12 Processing parameters of alloy 535 melt # N7074....20
Table 4.2.13 Chemical analysis of alloy 206 24
Table 4.2.14 Effects of mold temperature and grain refiner addition on hot tearing 26
Table 4.2.15 Estimated cooling rate from melt N2051A-4 mold preheated to 200°C....29
Table 4.2.16 Estimated cooling rates from melt N2052A-4 mold preheated to 350°C 29
Table 4.2.17 Estimated cooling rates from melt N2054A-4 mold preheated to 400°C 29
Table 4.3.1 Chemical analysis of A535 31
Table 4.3.2 Chemical analysis of A/B206 32
Table 4.3.3 Processing parameters for engine bracket castings 33
Table 4.3.4 Processing parameters of the rocker arm castings 34
Table 4.4.1 Chemical analysis of alloy 206 37
Table 4.4.2 Chemical analysis of alloy 535 37
Table 4.4.3 Mechanical properties of alloy 206 in the F, T4 and T7 tempers 38
Table 4.4.4 Effect of test temperature on properties of alloy 206.0, melt N6090 39
Table 4.4.5 Mechanical Properties of alloy 535 in the F and T5 tempers....40
Table 4.5.1 Chemical analysis of A535 53
Table 4.5.2 Chemical analysis of A/B206 53
Table 4.5.3 Processing temperatures for swivel castings....53
Table 4.5.4 Processing parameters for A356 63
Table 4.5.5 Processing parameters for A206 64
Table 4.5.6 Summary of iterations and die cycle for A206 65
Table 4.5.7 Processing parameters for 535 66
Table 4.5.8 Summary of iterations and die cycle for 535 66
Table 4.5.9 Chemical analysis of alloy A206 77
Table 4.5.10 Chemical analysis of alloy B206 77
Table 4.5.11 Chemical analysis of alloy 535 77
Table 4.5.12 Processing temperatures from thermocouples 81
and infrared pyrometer for A206-1 81
Table 4.5.13 Processing temperatures from thermocouples 81
and infrared pyrometer for A206-2 81
Table 4.5.14 Processing temperatures from thermocouples 82
and infrared pyrometer for alloy B206 82

Table 4.5.15 Processing temperatures from thermocouples 82
and infrared pyrometer for alloy 535.....82
Table 4.5.16 Chemical analysis of alloy 206.....94
Table 4.5.17 Average Properties and standard deviation from ASTM B108 test bar of alloy 206.....94
Table 4.5.18 Chemical analysis of alloy A/B206 96
Table 4.5.19 Chemical analysis of alloy 535.....96
Table 4.5.20 Average properties from bars machined from component.....97

1 Executive Summary

The current federal regulations on the fuel economy and emissions make it imperative that the current vehicles need to be more fuel efficient. The fuel efficiency can be improved in many ways, including power train modifications, electrification, and light weighting of the vehicle. Usually automotive manufacturers incorporate a combination of these technologies. Every 10% reduction in weight can improve the fuel efficiency by 6% and reduce GHG emissions by 3%.

Current vehicles use mostly ferrous components for structural applications. It is possible to reduce the weight of the vehicle by substituting these parts with those made from light metals such as aluminum and magnesium. Many alloys and manufacturing processes can be used to produce these light metal components and casting is known to be most economical. One of the high integrity casting processes is permanent mold casting which is the focus of this research report.

Many aluminum alloy castings are used in automotive applications and the majority of them are produced by the sand casting process. Also, aluminum-silicon (Al-Si) alloys are the most widely used alloy systems for automotive applications. It is possible that by using high strength aluminum alloys based on an aluminum-copper (Al-Cu) system and permanent mold casting, the performance of these components can be enhanced significantly. This will also help to further reduce the weight. However, many technological obstacles need to be overcome before using these alloys in automotive applications in an economical way. There is very limited information in the open literature on gravity and low-pressure permanent mold casting of high strength aluminium alloys.

This report summarizes the results and issues encountered during the casting trials of high strength aluminum alloy 206.0 (Al-Cu alloy) and moderate strength alloy 535.0 (Al-Mg alloy). Five engineering components were cast by gravity tilt-pour or low pressure permanent mold casting processes at CanmetMATERIALS (CMAT) and two production foundries. The results of the casting trials show that high integrity engineering components can be produced successfully from both alloys if specific processing parameters are used. It was shown that a combination of melt processing and mold temperature is necessary for the elimination of hot tears in both alloys.

A focused study, using constrained rod castings in metal molds on the effects of grain refinement and mold temperature on the hot tearing resistance of both alloys, exhibited that the combination of grain refinement and mold temperatures had resulted in lower strain rates which was proven to be necessary to prevent the formation of hot tearing during the solidification. The associated simulation efforts indicated that the constrained rod castings poured in metal molds at lower temperatures (around 290˚C) develop higher maximum principal strain rates during the last stages of solidification as compared to those cast in molds held at more than 400°C. This trend was similar to both alloys and simulation results closely match the hot cracking trends observed experimentally. The reduced hot cracking in the hotter mold is attributed to the reduced principal strain during the last stages of solidification.

The report also presents the results from the evaluation of mechanical properties, in both as-cast and heat-treated conditions using separately cast ASTM B108 tensile bars. It was also shown that the mechanical properties of the castings produced met or exceeded the required aerospace standards. The results from this work should make it easier for automotive designers to confidently use the high strength aluminum alloys in vehicles.

2 Introduction

Weight reduction of vehicles is one of the major efforts being undertaken by automakers worldwide in their increased emphasis to improve fuel economy. The use of aluminum and magnesium alloys as replacements for the existing ferrous components is one strategy to reduce the weight of vehicles. These light metal components can be produced through many high integrity manufacturing processes such as gravity and low pressure permanent mold casting. Some of the advantages of permanent mold casting process compared to sand casting processes are better surface finish, precise and consistent dimensional control and improved mechanical properties.

A number of foundries currently produce aluminium components for the automotive, electrical, marine and agricultural sectors by gravity tilt-pour and low pressure permanent mold casting processes. A majority of these castings are produced from aluminium-silicon family alloys, namely 356.0 (Al-Si) and 319.0 (Al-Si-Cu). These alloys, despite being easy to cast, do not possess very high strengths and have only moderate toughness. Other high strength aluminum alloys based on the Al-Cu system can reduce the weight further as compared to Al-Si alloys.

The high strength Al-Cu alloy 206 is usually produced by sand casting for aerospace applications. Similarly Al-Mg alloy 535 has a good combination of strength and ductility, shock resistance, and dimensional stability in the as-cast condition and is used in automotive, marine and military applications. Both of these alloys are prone to hot tearing (hot shortness) when poured in permanent molds due to their long freezing ranges. There is limited information in the literature on the gravity and low-pressure permanent mold casting of high strength aluminium alloys 206 and 535.

The use of magnesium for automotive applications is gaining momentum as increased weight savings is being targeted. There are several ongoing research efforts on the development of new creep resistance magnesium alloys that have improved high temperature properties for automotive applications. It is anticipated that some automakers may increase their use of magnesium from the 4 kg per vehicle in 2005 to about 100 kg by 2020. Currently, the major production route of magnesium alloy components used in automotive applications is by high-pressure die-casting. However, due to porosity, most of the high pressure die cast components cannot be heat-treated. Gravity tilt-pour, and low-pressure permanent mold casting of powertrain components from magnesium alloys can lead to reduced porosity defects, and thus allow for the heat treatment of the prototype components for improved performance. The use of magnesium in other applications is also expected to increase due to its high-strength-to-weight-ratio.

Therefore the selection of alloys 206 and 535 and some magnesium alloys for more rigorous engineering applications is currently hampered by lack of adequate data on the foundry characteristics and the mechanical properties in metal permanent molds. This research was initiated to address some of the issues identified above.

3 Background

Aluminum alloy A535.0 is well suited for automotive, marine and military applications because of its good corrosion resistance in mild alkaline and salt spray exposure, and a good combination of strength and ductility, shock resistance, and dimensional stability in the as-cast condition [1, 2]. The alloy has poor hot tearing resistance when poured in metal molds due partly to its long solidification range of 80˚C (144˚F), with liquidus and solidus temperatures of 630°C (1166°F) and 550°C (1022°F) respectively. This alloy exhibits good mechanical properties in the as-cast condition, and when heat-treated, a more cost effective heat treatment (T5) followed by air cooling can be used. Hence, it does not require the more expensive solution heat treatment followed by water quenching and aging (T6) commonly used for alloys 356.0 and 319.0.

Similarly to alloy A535.0, alloy A206.0 is also subjected to hot cracking when poured in metal molds due partly to its long solidification range of 80°C (144°F), with liquidus and solidus temperatures of 650°C (1202°F) and 570°C (1058°F) respectively. Additions of Ti-B based commercial grain refiners can improve the hot tear resistance of both alloys when poured in metal molds [3-5]. The alloy is used in automotive, aerospace and other applications where high mechanical performance is needed [1, 2]. Alloy A206.0 is a higher purity version of the regular 206.0 that is used in aerospace and other high integrity applications. Alloy B206.0 has similar purity as A206.0 but its titanium level is limited to 0.10max, whereas the titanium level in A206.0 ranges from 0.15 to 0.25 %. Alloy B206.0 was registered based on the work of Sigworth[5] who made the discovery that the alloy responds better to particulate grain refinement when the overall level of dissolved Ti was lower than the 0.15% Ti in the current specification.

According to Kearney and Raffin [6], hot tearing can be defined as a strain-induced fracture that occurs during the solidification or subsequent cooling of a metal casting as a result of hindered contraction. The hot tears can be large and visible to the naked eye and sometimes very small and only visible after die penetrant inspection of the component. Some of the variables that have been shown to influence hot tearing include alloy composition, solidification conditions, and mold and casting design. Some useful casting design guidelines and principles to prevent the formation of hot tearing have been presented in previous publications [6, 7]. There is limited information published on the gravity and low-pressure permanent mold casting of engineering components in alloys A535.0 and 206.0 for the automotive industry. Hence, the selection of both alloys for rigorous engineering applications is hampered by this lack of adequate foundry processing data. With the increased interest in vehicle weight reduction and cost savings, development of viable permanent mold casting of A535.0 and 206.0 should be of interest to the automotive industry.

As part of the project plan, casting of prototypes took place at experimental casting laboratory (ECL) of CanmetMATERIALS (CMAT), ECK Industries Inc., and Grenville Castings Ltd. Both foundries are part of our industrial partners in the project. This report present the results and issues encountered during the casting of the five components from alloys 206.0 and 535.0 by gravity tilt-pour and low-pressure permanent mold casting processes.

3.1 Specific Goals and Objectives

The main objectives of this project are to:

- Establish the processing parameters for selected prototype automotive, marine and other components during gravity and low pressure permanent mold casting of selected aluminum and magnesium alloys;
- Determine the microstructure and mechanical properties in the as-cast as well as heat-treated conditions of the alloys mentioned above.

These objectives are met by conducting experiments as explained below:

TASK 1 - Selection of Prototype Component

- Select prototype castings for the casting trials at CanmetMATERIALS (CMAT) in consultation with AFS, ECK Industries Inc., and other partners.

TASK 2 - Hot Tearing Studies

- Pour test castings in an instrumented constrained metal mold from non-grain refined and grain refined melts of alloy 206.
- Carry out computer simulation of the constrained rod castings to identify potential hot spots.
- Study the effects of mold and pouring temperatures on the stresses developed during solidification with a view to aid the prediction of hot tearing.
- Study the effects of mold temperature on hot tearing.

TASK 3 – Prototype Casting Trials CMAT

- Carry out computer simulation of prototype component to identify potential hot spots, local cooling rates, and thermal gradients. Pour prototype component and provide detail information on molten metal processing (e.g. grain refinement), mold preparation, mold temperature, pouring temperature, etc.).
- Study the effects of mold and pouring temperatures on casting quality. Based on the simulation and experimental work, establish the casting design rules which will help avoid hot tearing conditions, e.g. thick to thin section transitions.

TASK 4 – Mechanical Properties and Metallographic Evaluation

- Pour ASTM B108 test bars and determine the mechanical properties in the as-cast condition and after heat treatment.
- Evaluate the cast component for hot tearing, porosity, and other casting defects.
- Evaluate the microstructures of test samples sectioned from the cast components.

TASK 5 - Technology Transfer

- Demonstrate developed technology at partners' foundry by pouring selected components under industrial casting conditions.
- Present results at AFS technical committee meetings and incorporate results into CMI courses, including design guidelines.

3.2 Team Members

Dr. Yemi Fasoyinu is the principal investigator and project leader from January 2004 to March 31, 2014. He created the project proposal in 2004 with contributions from industry partners. He completed the permanent mold casting of selected prototype components at CMAT Experimental Casting Laboratory and casting trials at industry partner foundries. In addition, he carried out laboratory base hot tearing studies and computer simulation of the component used for the casting trials to gain a better understanding on the effect of processing parameters on hot tearing formation in the selected alloys. He completed the mechanical properties and microstructure evaluation of alloys 206 and 535. The second stage of the project is focused on the effect of mold temperatures and addition of grain refiner on hot tearing, establishing of processing parameters during the casting of a production component in a metal mold and computer simulation of a production component. During his work he was supported by Dr. Mahi Sahoo (retired) and Dr. Kumar Sadayappan. He was also supported by the CanmetMATERIALS technical team from experimental casting laboratory, mechanical testing and metallography evaluation.

ECK Industries, Inc. team: Mr. David Weiss provided technical guidance and Dan Hoefert provided technical support for the casting trials during January 2004 to March 31, 2014.

Mr. Paul Burke, Grenville Castings Ltd., Perth, Ontario, Canada, assisted with casting and mold design, and casting of a prototype component during 2004 to 2008.

Mr. Steve Sikorski, Magma Foundry Technologies, Inc. carried out computer hot tear modeling of the constrained test casting during 2004 to 2008.

Mr. Rob Baily, B.S Metallurgy, Inc., provided overall project management during the casting trials at ECK Industries, Inc. during June 2012 to March 31, 2014.

Mr. Jiten Shah, Product Development & Analysis (PDA) LLC, carried out casting process modeling (filling, solidification, residual stress and hot tear modeling) of a bracket production component selected for the casting trials at ECK Industries, Inc. during June 2012 to March 31, 2014.

4 Results and Discussion

4.1 TASK 1: Selection of Prototype Components

Four castings, two for hot tearing testing and two components, were selected for evaluation at CMAT Experimental Casting Laboratory. While the constrained rods mold, engine mount and rocker arm castings were tested in Phase I the instrumented hot tear mold was also used in Phase II.

4.1.1 Regular Restrained Mold

The hot tearing resistance of both alloys was evaluated by using restrained rod permanent molds, one with 4-arm and the other with 3-arm designs. The molds were designed by ALCAN and have been shown to be sensitive in the evaluation of hot tearing tendency in selected aluminum alloys [11]. The molds were machined from H13 tool steel and coated with insulating coating, and sometimes followed by graphite wash to improve surface finish and facilitate easier casting ejection. The mold and metal temperatures were measured during the casting trial. The sprue also serves as the riser and the rods are restrained during solidification. The lengths of the rods in the 4-arm mold are 5, 9, 13 and 16 cm (2, 3.5, 5 and 6.5 in.), and in the 3-arm mold 16, 21 and 26 cm (6.5, 8 and 10 in.) respectively. It is noted that majority of the test castings poured in the 4-arm mold during our casting trials were usually free of hot tears, except for the longest rod. The 3-arm mold gives better sensitivity for both alloys; hence it was used for subsequent experiments. The diameter of the rods in both mold designs is 9.5 mm (0.38 in.) and the rounded end diameter is 19 mm (0.75 in.). These molds are shown in Figures 4.1.1(a) and (b).

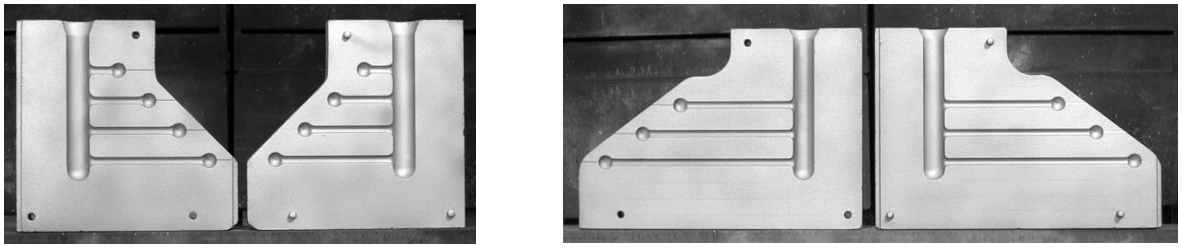

(a) Four-arm molds halves. (b) Three-arm molds halves.

Figure 4.1.1 *Restrained rod hot-tearing molds.*

4.1.2 Instrumented Restrained Mold

The three constrained rods in the metal mold are fed by a common vertical sprue. Figures 4.1.2 (a) and (b) illustrates the front and back of the molds. The lengths of each rod from the sprue junction to the rounded end are 16, 21 and 26 cm (6.5, 8 and 10 in.) respectively. The diameter of each rod is 9.5 mm (0.38 in.) and the rounded end diameter is 19 mm (0.75 in.). The sprue also serves as a riser and the rods are restrained during solidification.

The 3-arm mold was instrumented with nine thermocouples (T/C's) at selected locations to determine the temperature-time data during solidification. Three of the T/C's were located in the sprue (T/C's 1, 2, and 3), close to the rod ingates (T/C's 4, 5, and 6) and near the rounded ends (T/C's 7, 8, and 9). The tip of the T/C's extended about 2 mm through the mold wall into the mold cavity at the nine locations. The 2 mm length was chosen so that the T/C's can be removed from the casting after each pour and the mold made ready for the next casting. The length and diameter of the sprue are 19 cm (7.5 in) and 1.9 cm (0.75 in.) respectively. The rods are about 3.8 cm (1.5 in.) from one another center to center. The dimension of the

Type-K, Chromel-Alumel, T/C's is: 1.5 mm in diameter and 30 cm in length. The total casting cycle time was about 150 seconds. The temperature-time data from the T/C's were recorded using a computer data acquisition system, Sciemetric Series 7000. This is a 16 channel data logger, up to 800 samples per second, with 16-bit digital-to-analogue (D/A) conversion, and hardware data filtering (averaging) capability. The sampling rate was 20 per second. The mold temperatures were kept in the range 300°C to 450°C.

Comparative temperature-time data were recorded by the thermocouples located at the rod/sprue and rod/rounded end junctions on each of the rods during solidification. The temperature-time data were recorded during solidification using a computer data acquisition system, Sciemetric Series 7000, a 16 channel data logger, processing up to 800 samples per second, with 16-bit digital-to-analogue (D/A) conversion, and hardware data filtering (averaging) capability. The sampling rate was 20/s.

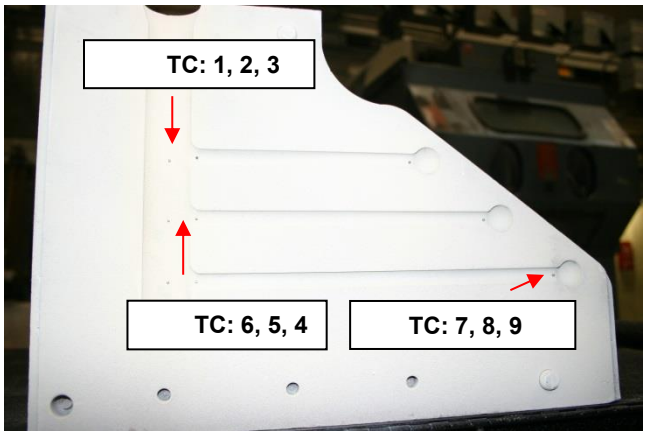

(a) Front of mold, showing the tip of the 9 T/C's.

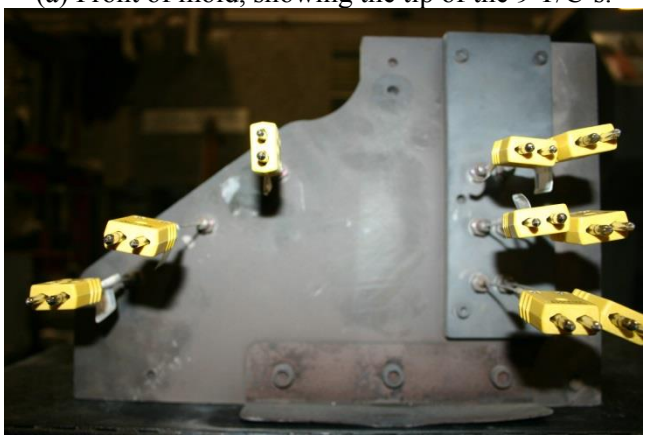

(b) Back of mold showing T/C locations.

Figure 4.1.2 *Instrumented restrained mold showing the location of thermocouples.*

4.1.3 Engine Mount Casting

An engine mount casting was produced by low pressure casting process during the casting trials at CANMET-MTL. The engine mount mold was designed by Grenville Castings Ltd. and fabricated at CANMET-MTL from H13 tool steel. Ejector pins were incorporated into the mold design to facilitate casting ejection. Photographs of the engine mount mold halves are shown in Figures 4.1.3.

The molds were preheated in a furnace to about 250˚C before coating and were coated with an insulating coating (Dycote 14ESS), followed by graphite base coating on top to improve surface finish and aid casting ejection.

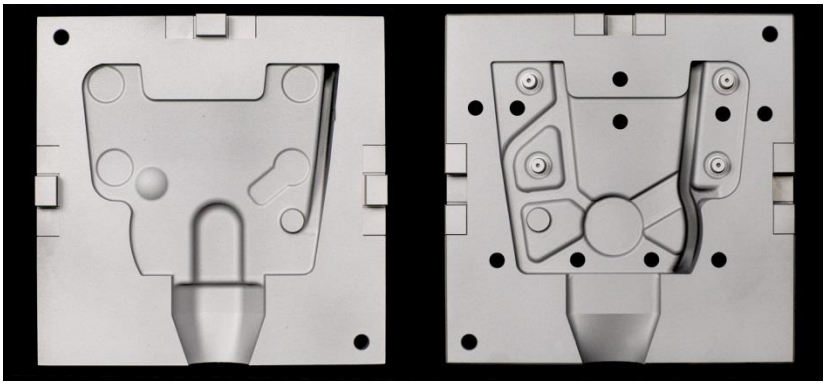

Figure 4.1.3 *Engine mount mold halves.*

4.1.4 Rocker Arm Casting

The rocker arm mold design was reproduced from a mold designed by ECK Industries Inc. for use on a commercial tilt-pour casting machine (Figure 4.1.4). The rocker arm mold is relatively complex, with deep recesses and it was machined from gray cast iron plate castings. A hollow tapered metal core, 102 x 114 x 70 mm (4 x 4.49 x 2.76 in.) was used for the rocker arm mold (to reduce the heat sink) during pouring.

The rocker arm mold was not optimized for either alloy A535.0 or A206.0, there were no ejector pins, and castings were extracted manually. One of the important considerations in the design and fabrication of the gravity tilt-pour mold was that it could be mounted on our IMR casting machine, Model C40. The maximum height of the mold is limited to 254 mm (10 in.) to allow for clearance. The mold and core temperatures were measured using a digital contact pyrometer.

Similar to the engine mount molds, rocker arm molds and cores were preheated in a furnace to about 250˚C before coating. They were coated with an insulating coating (Dycote 14ESS), followed by graphite base coating on top to improve surface finish and aid casting ejection.

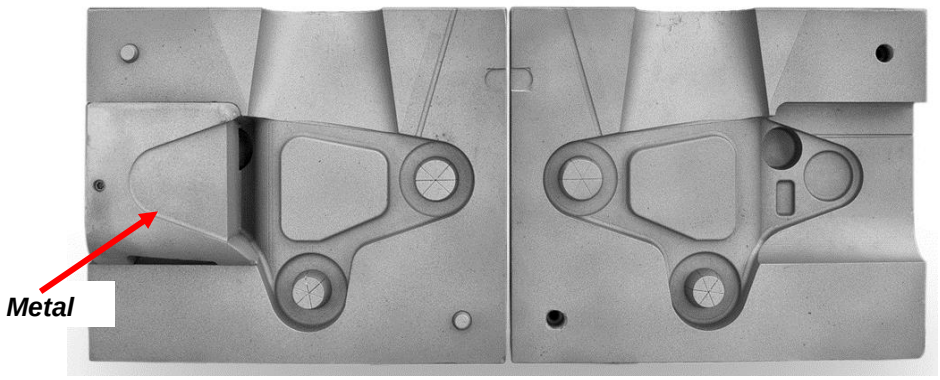

Figure 4.1.4 *Rocker arm mold halves and metal core.*

4.2 TASK 2 - Hot Tearing and Computer Simulation Studies

Alloys 206 and 535 are subjected to hot tearing (cracking) when poured in metal molds due partly to their long solidification range. The main focus of this section of the report is to present the results on the effects of grain refinement and mold temperatures on the hot tearing resistance of both alloys during solidification in metal molds. The experiments were conducted in two distinct phases and the results are presented separately.

In addition, results of computer simulation of the effect of mold temperature on hot tearing was compared with the hot tearing trends observed experimentally when both alloys were poured in metal molds.

4.2.1 Phase I: Experimental Details

Melting and Casting

20 to 40 kg charge material of alloys 206.0 and 535.0 were melted in a clay-graphite crucible in a resistance or a push-up induction furnace. The charge materials were prepared from ingots of aluminum alloy B206.0, master alloys of Al-Cu and Al-Mn, and pure ingots of aluminum and magnesium alloys. The castings were poured at 50° - 100C superheat. The chemical composition was determined using Baird Optical Emission Spectrometer (OES) and dissolved hydrogen in the melt was evaluated by the reduced pressure test (RPT) technique. RPT samples were sectioned to observe the level of gas in the metal by comparing it to published standards [9]. Figures 4.2.1 shows typical sectioned RPT samples before and after degassing. Melts were generally degassed to #1 standard of quality (Figure 4.2.1 b) that is an acceptable quality for high-quality casting.

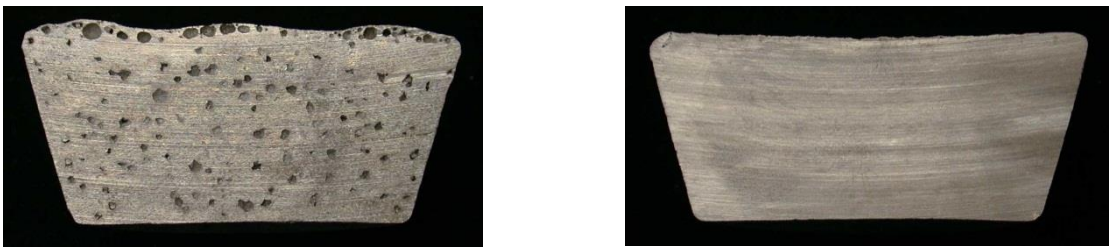

(a) Before degassing. (b) After degassing.

Figure 4.2.1 *Typical sectioned RPT samples (a) before, and (b) after degassing.*

Addition of 10-15 g/kg of the Al-5Ti-1B master alloy provided fully grain refined metal. The effectiveness of the grain refiner was verified by casting 76 mm (3 in.) diameter by 25 mm (1 in.) thick disc "hockey puck" samples before and after grain refiner addition as reported in a previous study 10. These pucks are shown in Figure 4.2.2. Majority of the test castings poured during the casting trials were from the nominal composition of unrefined and refined alloy 206.

(a) Before refinement (b) After grain refinement with Ti/B

Figure 4.2.2 *Macrostructures of disc castings (a) before, and (b) after adding grain refiners.*

The restrained rod castings were poured from degassed metal from both unrefined and refined metal (using Al-5%Ti-1%B master alloy). The rod castings were poured at about 100°C superheat for both alloys. The pouring time was about 10 seconds and the casting was allowed to cool in the mold for 60 seconds before it was ejected. The casting cycle time was about 150 s. The castings were examined visually for hot tearing.

Computer Simulation

The use of computer simulation to optimize casting and mold designs has made significant inroad into the metal casting industry and has given metal casters the opportunity to reduce product development time and scrap rate. The results of previous casting trials at CANMET-MTL show that hot tearing in alloys 206.0 and 535.0 of the restrained rod castings was reduced at higher mold temperatures 11. It was decided to run a computer simulation of the restrained rod castings using the experimental processing data to get a better understanding of this phenomenon. For this study, MAGMASOFT® software package was used for the computer simulation. Some of the processing parameters used for the simulation are shown in Table 4.2.1. Other processing input data not listed in the table but part of the software database includes the fraction solid as a function of temperature during solidification. It is important to note that the software did not consider the effects of grain refinement on the simulation because the current software package does not have that capability. This capability will be incorporated into future software package. The maximum principal strain rate developed during solidification was calculated during simulation and correlated with the fraction solid as a function of temperature and the potential for hot tearing (hot tearing index) was determined. The results from the computer simulation were compared with the experimental observation from previous casting trials.

Table 4.2.1 *Processing parameters for computer simulation*

Parameters	Restrained Rod Casting
Alloys Poured	206 and 535
Mold Material	H13
Mold Temperatures	290°C (554°F) and 450°C (842°F)
Pouring Temperatures	733°C (1351°F)
Pouring Time (s)	10
Casting Ejection Time (s)	60

Chemical Composition

The chemical analyses for alloys 206 and 535 are shown in Tables 4.2.2 and 4.2.3. Also shown in these tables are the ASTM composition limits for both alloys. The chemical compositions are close to the range recommended for both alloys. The Cu level in one melt (melt N6081) of alloy 206 was lower than the lower limit of the ASTM specification to study the effect of lower Cu on hot tearing.

Table 4.2.2 *Chemical analysis of alloy 206 for hot tearing studies*

Melt No.	Cu	Si	Fe	Mn	Mg	Ti
ASTM	4.2 – 5.0	0.10 max	0.15 max	0.20 - 0.50	0.15 - 0.35	0.15 - 0.30
N6080	5.1	0.044	0.069	0.37	0.280	0.170
N6081	3.96	0.039	0.068	0.31	0.199	0.072
N6090	5.1	0.038	0.050	0.38	0.280	0.066
N7057	5.0	0.047	0.065	0.37	0.280	0.055
N7072	4.65	0.044	0.050	0.30	0.290	0.043
N7073	4.70	0.049	0.080	0.23	0.280	0.051

Table 4.2.3 *Chemical analysis of alloy 535 for hot tearing studies*

Melt No.	Mg	Mn	Si	Fe	Cu	Ti
ASTM	6.2 - 7.5	0.10 - 0.25	0.15 max	0.15 max	0.05 max	0.10 - 0.25
N6082	6.2	0.45	0.064	0.067	0.016	0.072
N7074	7.1	0.24	0.067	0.070	0.010	0.055

4.2.2 Hot Tearing Results from Constrained Rod Molds

Hot tearing occurs in the hot spots of castings where the strain resulting from the solidification contraction is concentrated when the contraction of a solidifying casting is excessively restrained by the mold or cores. The restraint of the rods was facilitated by the ball at the end of each rod, and the longer the rod the higher would be the stress / strain that is built-up during solidification. Therefore an alloy that is susceptible to hot tearing will usually yield more broken rods during solidification. Figures 4.2.3(a) to (d) show examples of sections where hot tears are observed in the restrained rod castings. It is observed that hot tearing is usually formed closer to the in-gates [Figure 4.2.3(b)], midsection of the rod [Figure 4.2.3(c)] and near the rounded end of the rod [Figure 4.2.3(d)]. Tables 4.2.4 to 4.2.7 show the processing temperatures from the un-instrumented 3-arm mold for both alloys. The “HT” and “NHT” in the tables indicate for “hot tear” and “no hot tear”.

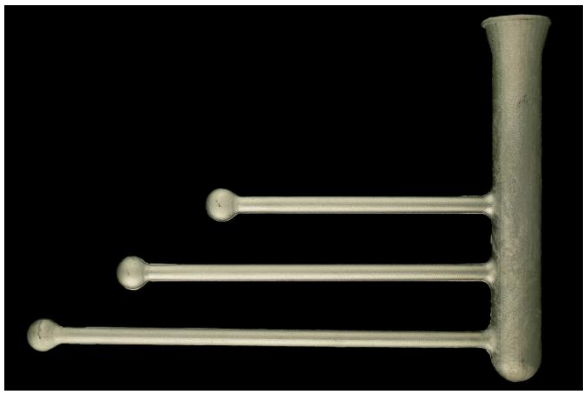

(a) 3-rod restrained casting.

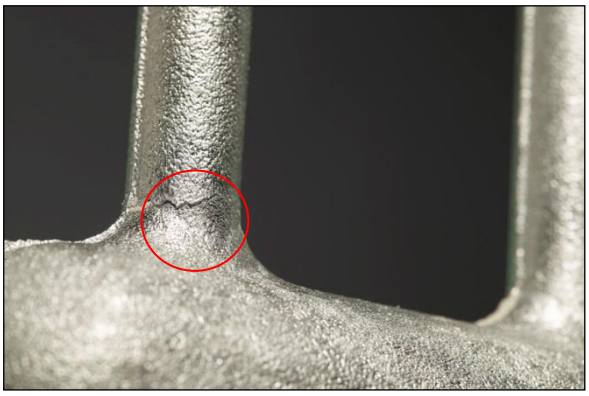

(b) Close to the ingate.

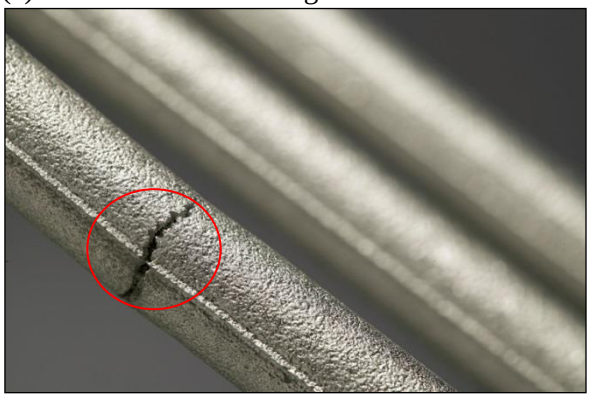

(c) Towards midsection of rod.

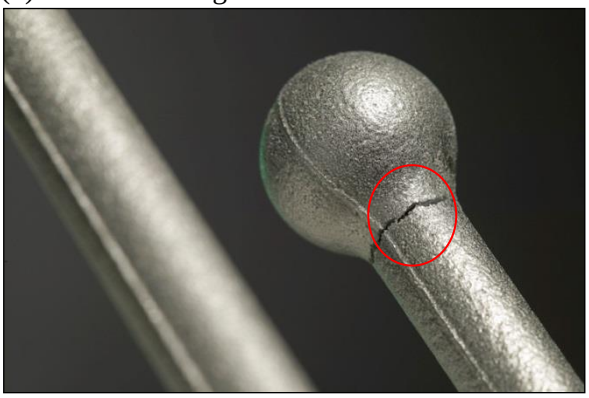

(d) Towards base of round section.

Figure 4.2.3 *Photographs of 3-rod constrained casting showing location of hot tearing.*

Alloy 206

The mold and pouring temperatures in Tables 4.2.4 to 4.2.6 ranged from 330°C to 425°C and 734°C to 754°C (a superheat of 84°C to 104°C) respectively. Hot tearing is usually observed in rod castings poured from melts that has not been grain refined. For example, in Table 4.2.4 , nine of the eleven castings poured from unrefined (castings #1 and 2) and refined (castings #3 to 11) melts show hot tearing. It is noted that the mold temperature in those castings were ≤ 350°C and the two castings (castings #8 and 9) that show limited hot tearing were poured into molds at 350°C and 370°C. It is also noted that none of the three rods in castings #3 and 9 (Table 4.2.5) show signs of hot tearing. Some improvement in the hot tearing was observed when the mold temperature was ≥400°C (Tables 4.2.5 and 4.2.6). The improvement in the hot tearing may also be associated with the lower copper (~4%Cu) in the data shown in Table 4.2.5. It is observed that as the mold temperature falls below 400°C, hot tearing tendency is marginally increased.

Table 4.2.4 *Processing parameters of alloy 206 melt # N6080*

Casting No.	Temperature (°C)		3-Arm Mold Rod Length (cm)			Comments
	Mold	Melt	26	21	16	
1	330	753	HT	HT	HT	0.004% Ti
2	350	753	HT	HT	HT	
3	340	734	HT	HT	HT	0.067% Ti
4	340	743	HT	HT	HT	
5	330	745	HT	HT	HT	0.17 %Ti
6	330	752	HT	HT	HT	
7	330	751	HT	HT	HT	
8	350	750	NHT	HT	NHT	
9	370	749	NHT	HT	NHT	
10	330	750	HT	HT	HT	0.26% Ti
11	330	749	HT	HT	HT	

Table 4.2.5 *Processing parameters of alloy 206 melt # N6081*

Casting No.	Temperature (°C)		3-Arm Mold Rod Length (cm)			Comments
	Mold	Melt	26	21	16	
1	409	749	HT	HT	NHT	0.005% Ti
2	420	751	HT	HT	NHT	
3	410	750	NHT	NHT	NHT	0.059% Ti
4	410	752	NHT	HT	NHT	
5	350	754	HT	HT	HT	
6	341	751	HT	HT	HT	
7	407	750	HT	NHT	NHT	
8	400	750	HT	HT	HT	
9	421	751	NHT	NHT	NHT	
10	410	750	HT	HT	NHT	

Table 4.2.6 *Processing parameters of alloy 206.0 melt # N6090*

Casting No.	Temperature (°C)		3-Arm Mold Rod Length (cm)			Comments
	Mold	Melt	26	21	16	
1	412	749	HT	NHT	NHT	0.004% Ti
2	424	749	HT	HT	HT	
3	420	754	NHT	NHT	NHT	0.066% Ti
4	425	752	NHT	NHT	HT	
5	410	751	HT	HT	HT	
6	380	750	HT	HT	HT	
7	370	749	HT	HT	HT	
8	390	751	HT	HT	NHT	

Alloy 535

The mold and pouring temperatures from the 3-arm mold is summarized in Table 4.2.7. The mold and pouring temperatures ranged from 170°C to 450°C and 730°C to 733°C (a superheat of 100°C to 103°C) respectively. Alloy 535 is less prone to hot tearing than alloy 206. For example, it is observed that casting #'s 1 and 2 poured in molds preheated to 450°C and 422°C respectively, without grain refinement (0.006%Ti) were free of hot tear. Whereas, casting #'s 3 to 6 poured in molds at lower than 400°C from the unrefined metal show various degree of hot tear. It is also observed that casting # 7 poured from refined metal (0.064% Ti) into a mold at 170C also show hot tears in the longer rods. These results seem to show that hot tearing can still be an issue from grain refined metal if the mold temperature is not optimized.

Table 4.2.7 *Processing parameters of alloy 535.0 melt # N6082*

Casting No.	Temperature (C)		3-Arm Mold Rod Length (cm)			Comments
	Mold	Melt	26	21	16	
1	450	733	NHT	NHT	NHT	0.006% Ti
2	422	733	NHT	NHT	NHT	
3	347	733	HT	HT	NHT	
4	345	731	HT	HT	NHT	
5	300	730	HT	HT	HT	
6	290	730	HT	HT	HT	
7	170	731	HT	HT	NHT	0.064% Ti

4.2.3 Computer Simulation

Based on the initial casting trials it was decided to run a computer simulation of the restrained casting using the processing data used for casting trials at CANMET-MTL. A summary of the computer simulation results showing the relationship between mold temperature, solid fraction, and the principal strain developed during solidification are shown in Table 4.2.8. Comparative computer simulation results from the ALCAN hot tear mold preheated to 290C and 450C for alloy 206.0 are shown in Figures 4.2.4 and 4.2.9. Similar results are shown in Figure 4.2.6 for alloy 535.0. It is noted that, although the experimental results were from refined and unrefined metal, the computer simulation did not incorporate the effect of grain refinement because of current technology gap in both software and database development.

Table 4.2.8 *Summary of the simulation results of the restrained rod castings*

Alloy	Mold Temp. (°C)	Principal Strain Rate	Solid Fraction (%)	Comments
206	450	7	90-100	Low hot tear potential
	290	500	90-100	Severe hot tear potential
535	450	50	70-85	Low hot tear potential
	290	250	90-100	Severe hot tear potential

The computer simulation results shown in Figures 4.2.4 and 4.2.5 for alloy 206 from molds preheated to 290°C and 450°C show that the maximum principal strain developed during the last stages of solidification is lower at the higher mold temperature. Grain refinement was not taken into account during simulation. The ranges of fraction solid and maximum principal strain are shown on the side scale. The white areas are 100 % solid. The reduced tendency to hot tearing in the hotter mold is associated with this reduced principal strain during the last stages of solidification. Due to the lower mold temperature (Figure 4.2.5a) the casting solidified faster, in 52 s, the rod to gate interface was approximately 90-100 % solid and contains a much higher strain peak (side scales in the figures) compared to the higher mold temperature (Figure 4.2.4b). It is noted that the white areas on the side scale are 100% solid. This is associated with the fact that when the material reaches 90-100% fraction solid, and close to the time of casting ejection the material is put under some strain. The simulation matches the hot tearing trend seen in alloy 206 (Table 4.2.5) and alloy 535 (Table 4.2.7) by varying the mold temperature. Figures 4.2.5(a) and (b) show pictorial view of hot tear progression in alloy 206 at 290 and 450°C respectively.

For alloy 535 at lower mold temperature the casting solidified faster, and at 36 s the rod to ingate interface is approximately 90-100% solid and contains much higher strain peak (Figure 4.2.6a) compared to the higher mold temperature (Figure 4.2.6b). It was found that at the time of casting ejection, the area contains a high strain rate but the amount of fraction solid ranges from 50 to 85% solid. The potential for hot tearing was low because there are no high strain peaks occurring in the 90-100 % solid region.

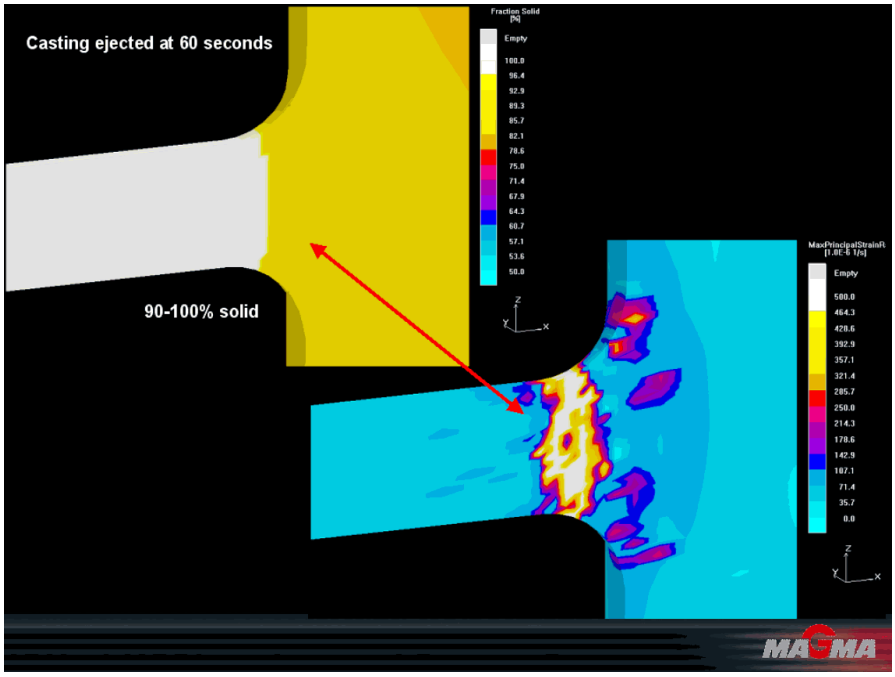

(a) Mold at 290°C.

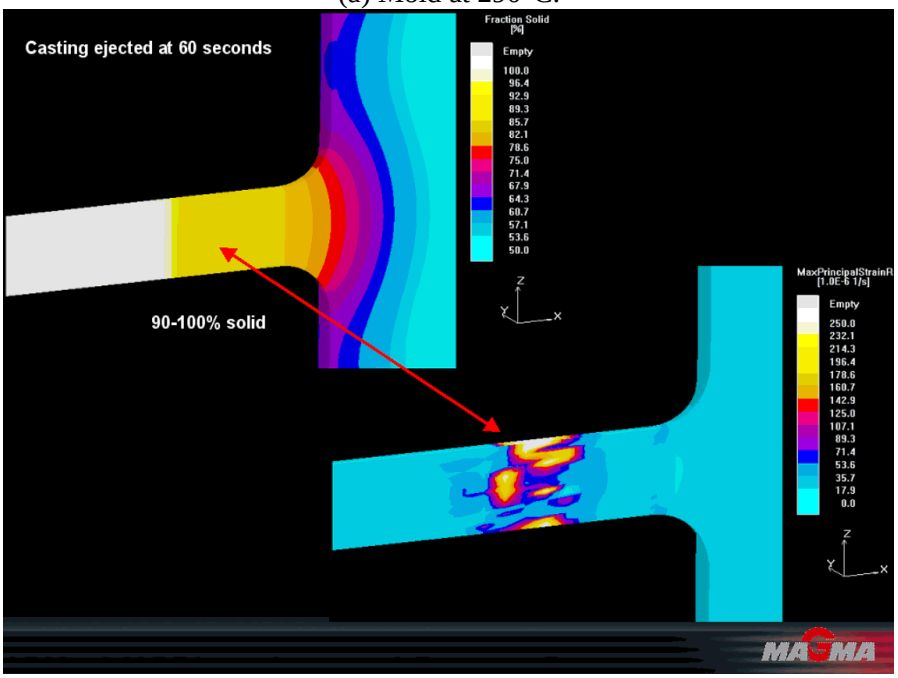

(b) Mold at 450°C.

Figure 4.2.4 *Simulation results for alloy 206.0 at 290°C and 450°C.*

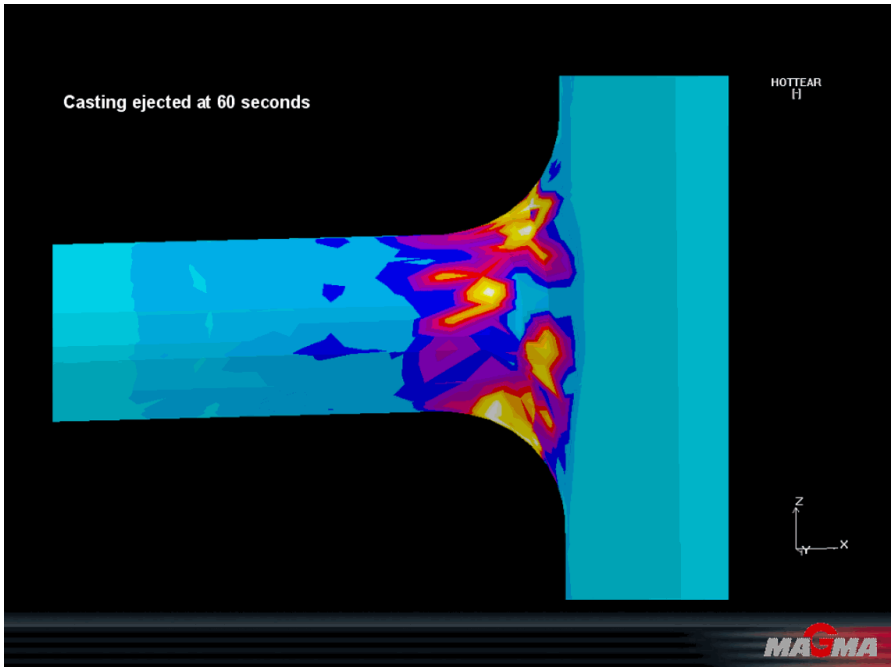

(a) Mold at 290°C.

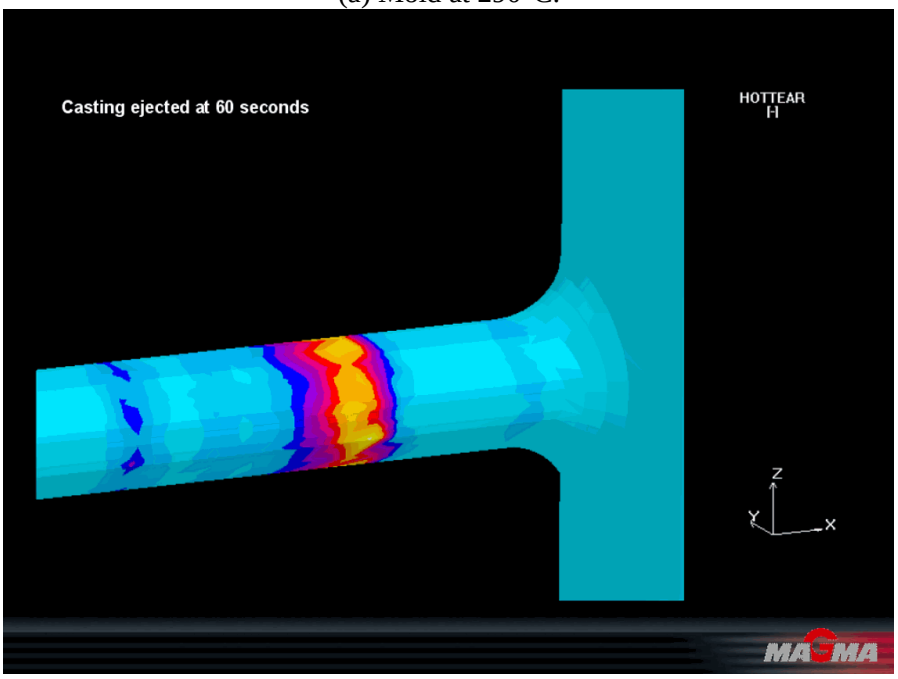

(b) Mold at 450°C.

Figure 4.2.5 *Comparative hot tearing potential at 290 and 450°C for alloy 206.0.*

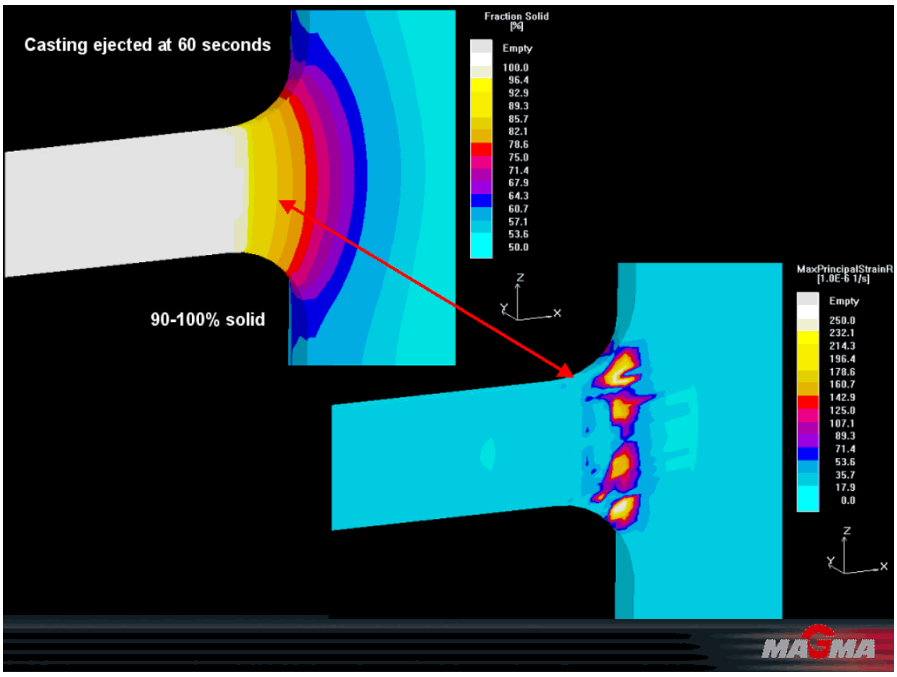

(a) Mold at 290°C.

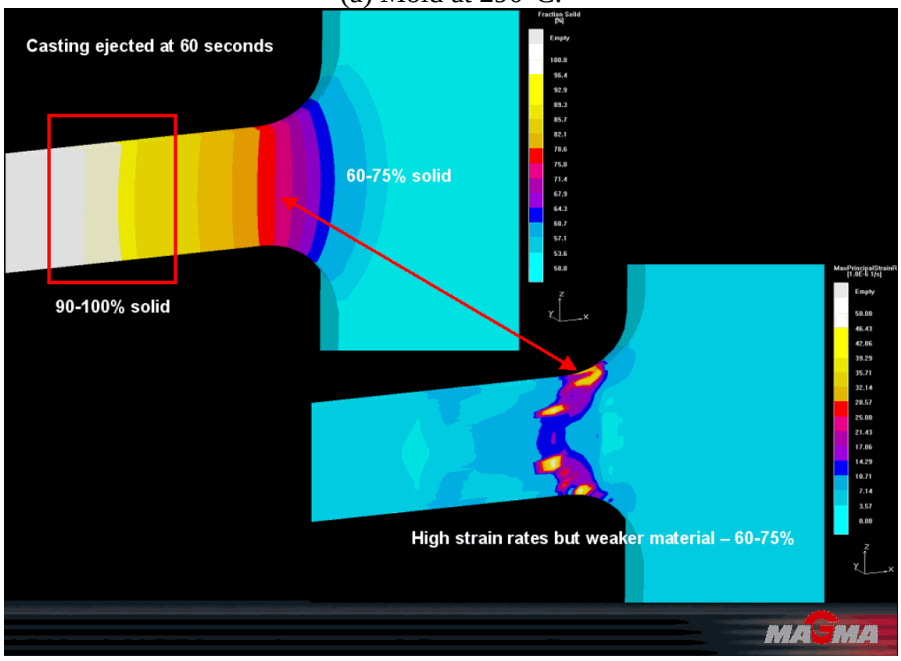

(b) Mold at 450°C.

Figure 4.2.6 *Simulation results for alloy 535.0 at 290 and 450°C.*

4.2.4 Instrumented Constrained Rod Mold

Tables 4.2.9 to 4.2.11 gives a summary of the processing temperatures from three melts of alloy 206. The mold and pouring temperatures ranged from 267-445°C and 749-755°C (a superheat of 99-105°C) respectively. It is observed that the shortest rod (16 cm) exhibited the least hot tearing for both unrefined and refined metal. As previously observed in the mold that was not instrumented, addition of grain refiner

and preheating of the mold to ≥400°C are necessary to preclude the formation of hot tearing in this alloy. This previous observation is confirmed in the instrumented mold as shown Tables 4.2.9 to 4.2.11, that a combination of grain refinement and mold temperature ≥400°C is required to prevent hot tearing in alloy 206.0. For example, castings #1 and #2 poured before grain refinement in molds preheated to 420°C and 423°C (Table 4.2.10) show hot tearing in the 21 cm and 26 cm rod castings. Whereas, none of the rods in castings #5 and #6 poured from grain refined metal in molds at 423°C and 445°C show hot tearing. Similarly, casting #8 (Table 4.2.10) and #4 and 5 (Table 4.2.11) show hot tearing, despite grain refinement because of low mold temperature.

Table 4.2.9 *Processing parameters of alloy 206 melt # N7057*

Casting No.	Temperature (°C)		3-Arm Mold Rod Length (cm)			Comments
	Mold	Melt	26	21	16	
1	305	750	HT	HT	HT	0.006% Ti
2	267	751	HT	HT	HT	
3	345	749	NHT	HT	NHT	0.055% Ti
4	345	749	HT	HT	NHT	

Table 4.2.10 *Processing parameters of alloy 206 melt # N7072*

Casting No.	Temperature (°C)		3-Arm Mold Rod Length (cm)			Comments
	Mold	Melt	26	21	16	
1	420	752	HT	HT	NHT	0.005%Ti
2	423	752	HT	HT	NHT	
3	370	752	HT	HT	HT	
4	387	750	HT	HT	HT	
5	423	750	NHT	NHT	NHT	0.043% Ti
6	445	749	NHT	NHT	NHT	
7	366	749	NHT	NHT	NHT	
8	315	752	HT	HT	NHT	

The processing temperatures from one melt of alloy 535.0 are summarized in Table 4.2.12. The mold and pouring temperatures in these tables ranged from 280-439°C and 729-739°C (a superheat of 99-109°C) respectively. As noted previously, alloy 535.0 is less susceptible to hot tearing than alloy 206.0. None of the nine constrained castings show hot tearing even when the mold temperature was less than 400°C for both unrefined and grain refined metal.

Table 4.2.11 *Processing parameters of alloy 206 melt # N7073*

Casting No.	Temperature (°C)		3-Arm Mold Rod Length (cm)			Comments
	Mold	Melt	26	21	16	
1	435	750	HT	HT	NHT	0.006 %Ti
2	432	749	HT	HT	NHT	
3	412	755	HT	HT	HT	
4	358	750	HT	HT	NHT	0.051 %Ti
5	381	751	HT	HT	NHT	

Table 4.2.12 *Processing parameters of alloy 535 melt # N7074*

Casting No.	Temperature (°C)		3-Arm Mold Rod Length (cm)			Comments
	Mold	Melt	26	21	16	
1	439	729	NHT	NHT	NHT	
2	352	731	NHT	NHT	NHT	
3	374	733	NHT	NHT	NHT	0.005 %Ti
4	307	734	NHT	NHT	NHT	
5	295	732	NHT	NHT	NHT	
6	433	731	NHT	NHT	NHT	
7	438	731	NHT	NHT	NHT	0.055%Ti
8	307	739	NHT	NHT	NHT	
9	280	729	NHT	NHT	NHT	

Examination of several instrumented rod castings with and without hot tearing show that the hot tears were not created by the location of the thermocouples but rather by the processing conditions (e.g., mold temperature and grain refiner). Examples of photographs of selected castings from alloy 206.0 showing T/C and hot tearing locations are shown in Figures 4.2.7(a) and (b). Examples of anodized microstructure showing the effects of grain refinement are shown in Figures 4.2.8(a) and (b). The dendrite nature of the solidification structure is readily apparent in Figure 4.2.8(a). Photographs of casting #2 from Table 4.2.12 from alloy 535.0 showing T/C locations and without hot tearing are shown in Figures 4.2.9 (a) and (b). It is noted that the mold temperature was 352°C.

(a) N7072-8, 315°C, 0.043%Ti, hot tear. (b) N7072-6, 445°C, 0.043%Ti, no hot tear.

Figure 4.2.7 *Alloy 206.0 showing the effects mold temperatures on hot tearing.*

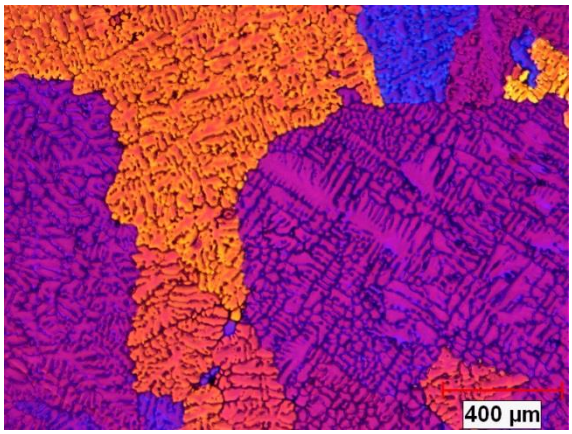

(a) N6080-1, 330C, not refined, 37.5x.

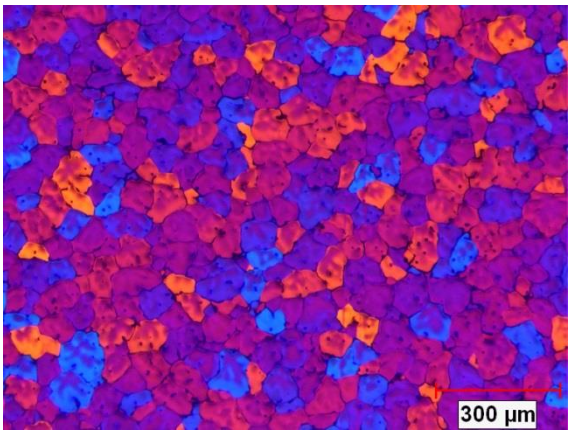

(b) N6080-10, 330C, refined, 50x.

Figure 4.2.8 *Anodized microstructures of 206.0 (a) before and (b) after grain refinement.*

(a) N7074-2, 352C, 0.005%Ti, ingate.

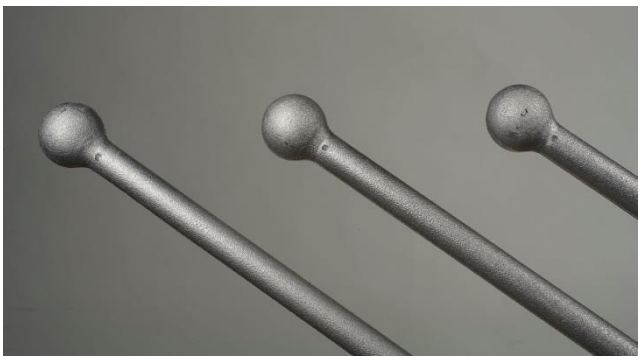

(b) Same as (a) close to the rounded end.

Figure 4.2.9 *Restrained casting from alloy 535.0 without hot tearing*.

Examples of the cooling curves and its first derivative from one of the restrained rod castings in alloy 206 are shown in Figure 4.2.10. It is recalled that the liquidus and solidus temperatures of the alloy are 650 and 570°C respectively. It is shown that there are significant differences in the temperature at the ingate and close to the rounded end of the rod castings. After about 30 s, Figure 4.2.10, the difference between the two temperatures is about 130°C. The solidification of the rod at the ingate started at around 647°C. There is a small plateau region in the cooling curve around 645°C for about 10 s suggesting the formation of dendrites as solidification progresses. It is remarkable that the temperature of the rod at the ingate had dropped to 550°C, 20°C below the solidus temperature of the alloy within the first 15 s of solidification. The T/C located close to the rounded end indicated 450°C, a 120°C below the solidus.

These results show that significant temperature drop can be expected during the solidification of the hot tear test castings. Backerud et al. 12, 13 have determined the dendrite coherency point (a point at which dendrites developed during solidification starts to impinge on each other to form a solid phase network throughout the entire casting) for a number of aluminum casting alloys in their two-thermocouple thermal analysis method. For alloy A206.0, they reported that dendrite coherency point occurred at 641C at 30 % fraction solid. The occurrence of dendrite coherency at such relatively low fraction solid explains why the feeding of solidification shrinkage in this alloy is difficult. As previously mentioned, grain refinement reduces the size of the dendrites and facilitates the intergranular flow of liquid metal during solidification. The second derivative of the cooling curves gave some indication of the rate of cooling of metal in the solidifying sample. Similarly, examples of the cooling curves and its first derivative from the top, middle, and bottom of the sprue of the restrained casting are shown in Figure 4.2.11. The temperature from the

T/C located at the top are higher than the middle and bottom throughout the solidification process. There is a small plateau region in the three cooling curves lasting about 10 s that may be associated with the eutectic reaction as solidification progresses.

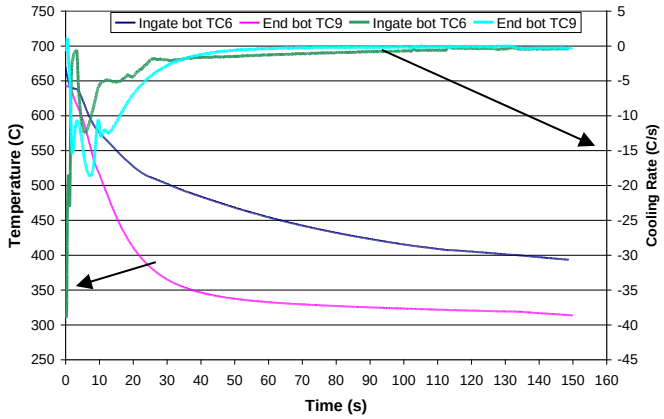

Figure 4.2.10 *Cooling curves and its first derivative near the ingate and the rounded end of the 26 cm rod poured from unrefined melts of alloy 206.*

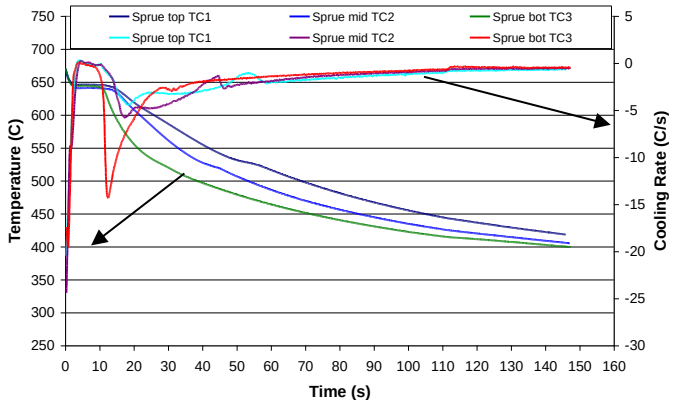

Figure 4.2.11 *Cooling curves and its first derivatives from the top, middle, and the bottom of the sprue poured from unrefined melts of alloy 206.*

During early stages of solidification, mass feeding of solidification shrinkage can occur relatively easily to feed developed shrinkage cavity to relief contraction stresses without hot tearing. Towards the final stages of solidification, the casting structure becomes a coherent mass due to the formation of a dendrite network, and liquid metal cannot flow easily to fill the voids caused by solidification and contractual shrinkage. Therefore, hot tear defects can be mitigated by implementing good casting design principles and solidification conditions to compensate for strains in the casting caused by both types of shrinkage. The need to fill the void space can produce significant stresses in parts of the casting, and if these stresses are greater than the ultimate strength of the metal at any time during solidification, hot tearing can occur. Therefore, the use of steep thermal gradients to control solidification so that molten metal is readily available to feed shrinkage, and elastic or self-relief systems in casting and mold design to prevent excessive stresses from developing during casting solidification is often recommended [6].

Many studies have shown that the extent of the liquidus-solidus temperature range is one of the major contributors to hot tearing during solidification. For example, Lees [14] observed that hot tearing was not observed during the solidification of high purity aluminum and the eutectic alloys even when cast under severe restraint; and that the addition of alloying elements such as silicon or copper promoted hot tearing.

When there is a large solidification range, the last region to solidify is subjected to contraction stresses over a greater temperature interval. It is believed that during the mushy stage, the temperature is well above the solidus temperature, hence the extension of the hot zone is distributed and interdentritic liquid areas are relatively wide and mass flow of the pasty mass occurs. The interdendritic fracture appearance of hot tears and their origin at near-solidus temperatures indicate that the basic mechanism of hot tear is related to the separation at the film stage of solidification which exists when the solidus temperature is approached and only a minute amount of liquid remains. According to Pellini [15], in passing through the solidus temperature range, during heating or cooling, the metal develops a condition of continuous liquid films at the grain boundaries. He noted that this behavior is fundamental to alloy systems and is accordingly not subject to control. Because of the fundamental nature of this behavior, it is used to determine the position of solidus lines in phase diagrams (by heating a number of specimens to various temperatures, followed by quenching, and metallographic examination for signs of liquid films at grain boundaries). The lowest temperature at which liquid films is observed is taken as the solidus temperature. At the liquid films stage, there is no appreciable strength and the unit strain developed can be very high and lead to hot tearing. When the mold temperature was increased from 290 to 450°C, the cooling rate during solidification is decreased and tension in the rod casting is reduced. This is evident from the simulation results when the principal strain rate calculated was lower.

For alloys that solidify dendritically over a long freezing range, hot tearing is more prevalent close to 100% solid fraction because of lack of liquid metal to feed the voids created by contraction and shrinkage during solidification. It is believed that hot tearing occurs close to the solidus temperature of the alloy where the growth of the primary interlocking dendrites commonly associated with long freezing range alloys is present with some residual liquid film. The trapped residual liquid freezes progressively until the process is complete at the solidus temperature. Therefore, for alloys such as 206 and 535 that exhibit long freezing ranges, the growth of the primary interlocking dendrites can occur very early in the solidification process and residual liquid that is trapped within the dendrite network will not be able to feed the solidification shrinkage. The reduction in hot tearing after grain refinement of alloys 206 and 535 could be associated with the break down and refinement of the interdendritic structure leading to improved feeding and a decrease in the amount of residual liquid during the last stages of solidification. With the hotter mold, the casting has a longer time for feeding during solidification to eliminate hot tearing. These results seem to show that hot tearing in alloys 206 and 535 improved when the mold temperature was ≥400°C. As the mold temperature falls below 400°C, the castings begin to show signs of hot tearing. It is believed that the hot mold provided effective thermal gradient that improved feeding and reduced hot tearing during solidification.

The computer simulation results shown in Figures 4.2.4 to 4.2.6, seem to be consistent with the strain theory of hot tearing proposed by Pellini [15] to explain the mechanism of hot tearing during the later stages of solidification. He noted that strain accumulation occurs within the liquid films surrounding the solid grains within a small temperature range which varies with alloy composition during the later stages of solidification. The presence of the liquid films provide the metal condition which permits hot tearing and that the actual occurrence of hot tearing is determined by mechanical factors in the region where liquid films is present. The significance of this theory is that hot tearing is strain controlled phenomenon and when the strain accumulated within the hot spots reaches a critical value, hot tearing will occur. Bishop et al. [16] have shown that for sound Al-4%Cu alloy castings, hot tears were observed at temperatures between 538 and 557°C, and the solidus of the alloy was determined to be between 538 and 543°C. This result was based on using a series of radiographs of a casting during solidification in a mold. On the basis of these results, they concluded that hot tearing for this alloy begins at or slightly above the solidus temperature where solidification is almost complete and the remaining liquid is present as interdendritic films. The two alloys under discussion, exhibits long freezing range, solidify dendritically, and the potential for the formation of liquid films during the last stages of solidification is relatively high. However, when the mold temperature was increased from 290 to 450°C, the cooling rate is decreased and tension (strain) in

the hot spot region of the rod casting is reduced, and the principal strain rate developed is lowered as was shown by the computer simulation results.

4.2.5 Phase II: Experimental Details

Molds

In Phase II, only the instrumented constrained bar mold (Figure 4.1.2) was used for evaluating the Al-Cu alloy, B206, as this alloy suffers from severe hot tearing compared to alloy 535. This way the effect of various process parameters such as grain refinement and mold temperature can be illustrated more clearly.

Only six thermocouples were used in this study. Thermocouples 1, 3, and 5 are located at the rod ingates, and 2, 4, and 6 are located near the rounded ends. The tip of each thermocouple extended about 2 mm into the mold cavity at the six locations. This arrangement will provide information on the behavior of liquid metal at the wall section.

Casting

The hot tearing was evaluated at three mold temperatures: 200ºC, 350ºC, and 400ºC. Two castings were poured at each of the three mold temperatures evaluated and examined visually for hot tearing. Samples for microstructure evaluation were sectioned from unrefined and refined rod castings.

Chemical Composition

The summary of chemical composition prepared for the melts are shown in Table 4.2.13. Also shown are the Aluminum Association (AA) composition specification for alloy 206 and the composition of B206.2 ingot from which the melts were prepared. The compositions used in this investigation generally fall within the AA composition specification.

Table 4.2.13 *Chemical analysis of alloy 206*

Alloy	Composition, Wt. %							
	Si	Fe	Cu	Mn	Mg	Ni	Zn	Ti
AA Spec 206	0.05 max	0.10 max	4.2 - 5.0	0.20 - 0.50	0.15 - 0.35	0.05 max	0.10 max	0.15 - 0.30
B206.2	0.048	0.06	4.74	0.21	0.25	0.01 max	0.01 max	0.01 max
B206 -1	0.048	0.076	4.6	0.393	0.33	-	-	0.06
B206-2	0.044	0.058	4.2	0.385	0.28	-	-	0.06

4.2.6 Results and Discussion

Grain Refinement and Mold Temperature

The key findings on the effects of mold temperatures and addition of grain refiner to the melts are summarized in Table 4.2.14. The castings poured from the unrefined metal at the three mold temperatures evaluated show significant hot tearing. The three rods generally breaks off completely near at the sprue/rod junction and sometimes close to the rod/rounded end. The castings poured from the refined

metal also exhibit hot tearing when molds are preheated to 200°C. The severity of cracking gradually reduces as the castings are poured in molds preheated to 350°C and 400°C. Many of the rods did not break off completely at sprue/rod junction as observed at 200°C for unrefined and refined metals. Figures 4.2.12(a) and (b) show examples of castings with and without hot tearing. The breaking off of the constrained rods at the rod/sprue junctions during solidification may be associated with higher strain rate at the lower mold temperature. The reduced hot tearing at higher mold temperatures (350°C and 400°C) may be associated with reduced strain rate as previously shown by computer simulation for this constrained casting. A complete summary of processing temperatures and observations made on the castings poured during the casting trials are summarized in Tables 1 to 6 in Appendix 1.

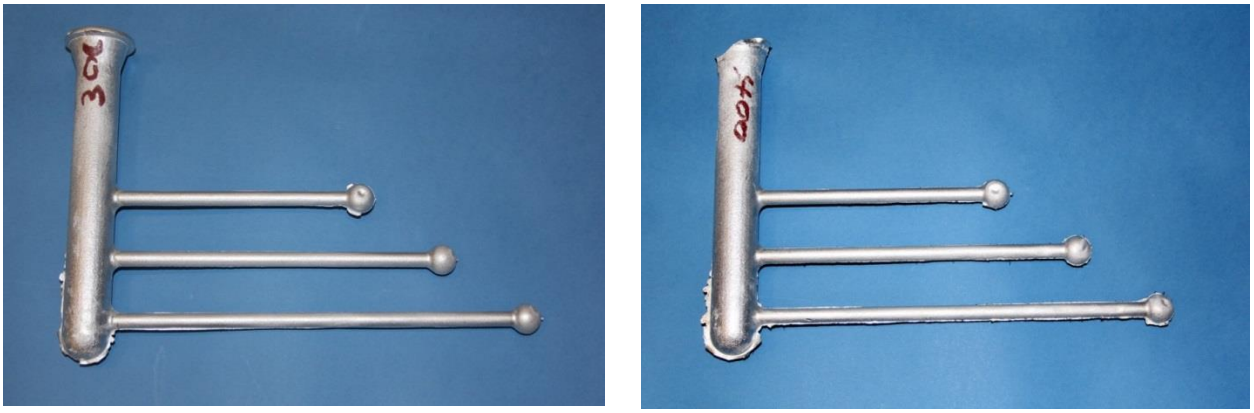

(a) Hot tear at rod/sprue junction. (b) No hot tear.

Figures 4.2.12 *Refined metal poured into molds preheated to (a) 300°C and (b) 400°C.*

Table 4.2.14 *Effects of mold temperature and grain refiner addition on hot tearing*

MoldTemp. (°C)	Metal Treatment	
	Unrefined	Refined
200	All rod casting show severe hot tearing and broke off at rod/sprue junction and sometimes at rod/rounded end.	All rod casting show severe hot tearing and broke off at rod/sprue junction and sometimes at rod/rounded end.
350	All rod casting show hot tearing and broke off at rod/sprue junction and sometimes at rod/rounded end.	All rod casting show hot tearing and broke off at rod/sprue junction and sometimes at rod/rounded end.
400	The rod castings show hot tearing. Some rods especially the longer rods broke off at the rod/sprue junction and sometimes close to the rod/rounded end. In some cases, no hot tears on the shorter rods.	Hot tearing significantly reduced after grain refinement. None of the rods broke off completely at the rod/sprue junction. In a few cases, there was no hot tearing on all the rod castings.

Cooling Curves

The temperature-time data from thermocouples located at the rod/sprue and rod/rounded end junctions on selected constrained rods during the solidification of in molds preheated to 200ºC, 350ºC, and 400ºC are shown in Figures 4.2.13(a) to (c). The detailed cooling curves for the three rod lengths and mold temperatures and are given in Appendix 2.

As it can be seen from the curves the highest temperatures recorded by the thermocouples are lower than the original liquidus temperature of the alloy, 650°C. This is due to reason that the thermocouples were not located at the center of the rods but very close to the wall section of the casting. The data indicates that due to the high cooling rates obtained in the metal molds the wall section of the casting solidifies rapidly.

The cooling rates based on highest liquidus temperatures attained during solidification were estimated by using the time it took for the metal to reach the solidus temperature of 570°C from the highest temperature. These are calculated from the sections of cooling curves as shown in Figures 4.2.14(a) to (c) and summarized in Tables 4.2.15 to 4.2.17. The following observations can be made from the data and temperature curves:

.

- The cooling rates attained at the rod/sprue and rod/rounded end junctions are different for each of the rod lengths. As expected, the cooling rates are higher for the castings poured in the mold preheated to 200°C as compared to those poured in hotter mold.
- In addition, the length of the bars has an influence on the cooling rates. The longest bar has the highest cooling rates in all the mold temperatures.
- At low mold temperatures, the cooling rates in the riser end are higher than that recorded in the end of the bars. This is reverse of the trend observed in other castings.

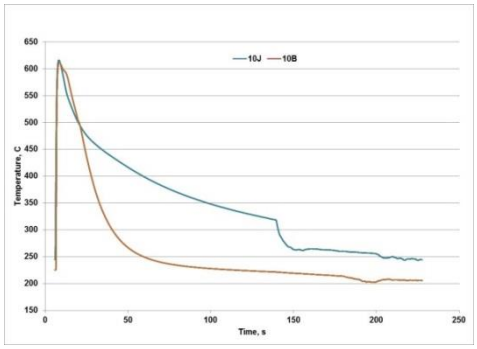

(a) Cooling curves for mold at 200°C.

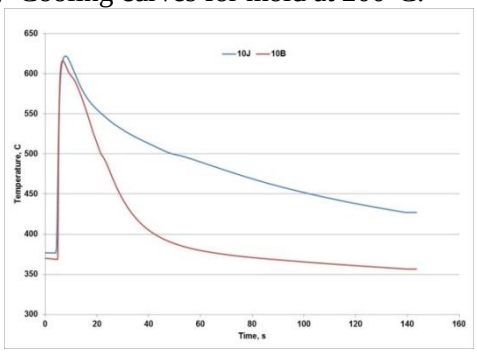

(b) Cooling curves for mold at 350°C.

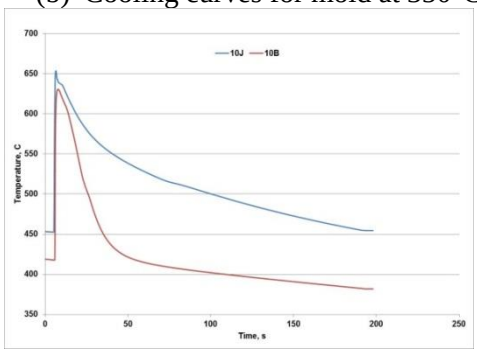

(c) Cooling curves for mold at 400°C.

Figure 4.2.13 *Cooling curves at the rod/sprue and rod/ball junctions for a 10 inch rod at solidus temperature.*

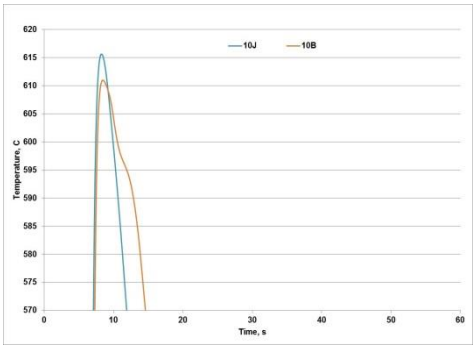

(a) Cooling curves for mold at 200°C.

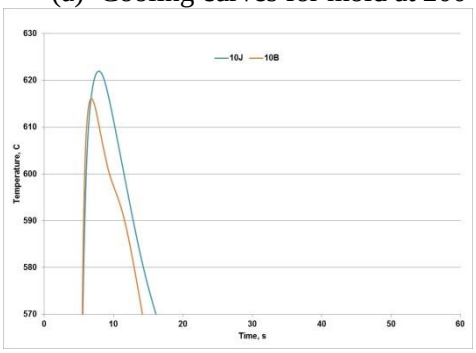

(b) Cooling curves for mold at 350°C.

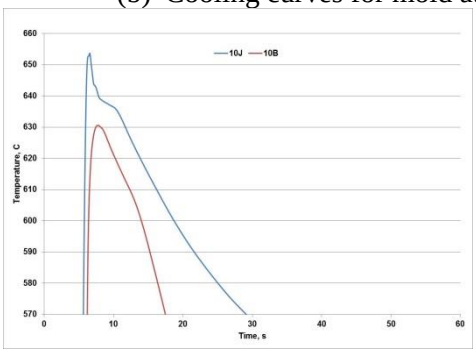

(c) Cooling curves for mold at 400°C.

Figure 4.2.14 *Cooling curves at the rod/sprue and rod/ball junctions for a 10 inch rod at solidus temperature from which the cooling rate was estimated.*

Table 4.2.15 *Estimated cooling rate from melt N2051A-4 mold preheated to 200°C*

Rod Length / TC Location	Liquidus Temp, °C	Time, s	Solidus Temp, °C	Time, s	Cooling Rate °C/s
6.5 inch					
Rod/sprue	618	9	570	13	12
Rod/ball	603	9	570	13	8.3
8 inch					
Rod/Sprue	608	9	570	12	12.7
Rod/ball	610	9	570	14	8
10 inch					
Rod/Sprue	616	8	570	12	11.5
Rod/ball	611	8	570	15	5.9

Table 4.2.16 *Estimated cooling rates from melt N2052A-4 mold preheated to 350°C*

Rod Length / TC Location	Liquidus Temp, °C	Time, s	Solidus Temp, °C	Time, s	Cooling Rate, °C/s
6.5 inch					
Rod/Sprue	600	9.5	570	19	3.2
Rod/ball	604	8	570	14	5.7
8 inch					
Rod/Sprue	598	9	570	19	2.8
Rod/ball	615	7	570	14	6.9
10 inch					
Rod/Sprue	622	8	570	16	6.3
Rod/ball	616	7	570	14	6.2

Table 4.2.17 *Estimated cooling rates from melt N2054A-4 mold preheated to 400°C*

Rod Length / TC Location	Liquidus Temp, °C	Time, s	Solidus Temp, °C	Time, s	Cooling Rate, °C/s
6.5 inch					
Rod/Sprue	640	7	570	51	1.6
Rod/ball	631	9	570	19.6	5.7
8 inch					
Rod/Sprue	641	7	570	46	1.8
Rod/ball	616	8	570	16	5.8
10 inch					
Rod/Sprue	653	7	570	30	3.6
Rod/ball	630	8	570	17	6.1

4.2.7 Summary and Conclusions

1. Based on the experimental and computer simulation results, hot tearing in alloys 206 and 535 depend strongly on the mold temperature.

2. It was demonstrated that a combination of grain refinement and preheating of metal mold to ≥400°C is necessary to prevent the formation of hot tearing during the solidification of alloy 206 in the restrained metal mold. The computer simulation results closely match the hot cracking trends observed experimentally during the casting trials.

3. For grain refined alloy 535, it is recommended that the mold temperature should exceed 300°C to avoid hot tearing.

4. The comparative computer simulation results of the restrained rod castings poured in metal molds at 290°C and 450°C, from alloys 206 and 535 show that hot tearing is reduced at the higher mold temperature. The improvement in hot tearing resistance is associated with the reduced principal strain developed at the higher mold temperature during the last stages of solidification (90-100% fraction solid). Therefore, casting conditions that would create a combination of a high strain rate and high solid fraction during the later stages of solidification should be avoided.

5. The cooling curves from the thermocouples attached to the restrained rod castings show that significant differences in temperatures close to the ingate and rounded end of the rod castings can be expected. This can also contribute to the strain developed in the casting during solidification.

6. Hot tearing can be eliminated or significantly reduced from both alloys by effective thermal management of the mold temperature and optimization of the grain structure of both alloys during solidification.

4.3 TASK 3 Prototype Casting Trials

4.3.1 Melting and Casting

Ingots of aluminum alloys 535.0 and 206.0 were melted in a clay-graphite crucible in either a resistance or a push-out induction furnace at CANMET-MTL. The charge size ranged from 35 to 120 kg. Alloy 535.0 was melted under an argon gas cover to reduce oxidation loss and 206.0 were melted in air. The chemical composition was determined using Baird Optical Emission Spectrometer (OES) to ensure compliance with specification. The metal was degassed with dry argon gas or a proprietary degassing tablet. The measurement of gas and grain refinement was carried out as explained in previous sections.

The engine mount and rocker arm castings were poured from melts fully grain refined with TiBor, an Al-5%Ti-1%B master alloy. The pouring ladle for the rocker arm castings was preheated to reduce temperature drop during pouring. The pouring basin attached to the mold was filled in the tilt-pour starting position, such that the mold cavity filled as the casting machine rotated to the horizontal position. The pouring cycle time (mold filling, solidification, and die opening) was about 90 seconds. The castings were poured at 100˚C superheat or less.

The low pressure casting trial was performed on an IMR casting machine Model BP155S equipped with a single-head manipulator, control panel for the manipulator, and a PLC for the casting operation. The applied pressure ranged from 350 to 400 mbar for both alloys. The engine mount and rocker arm castings were visually inspected for hot tear and other surface defects. Some of the engine mount castings were X-rayed following the ASTM E-155 (series 11) procedure to evaluate the casting soundness.

Chemical Composition

The chemical analyses from A535 and A/B206 during the casting trials are given in Tables 4.3.1 and 4.3.2 respectively. It is noted that the boron content was not determined but estimated to be in the range 5 to 20 ppm. The specified composition limits for both alloys are also shown in these tables. The chemical compositions are close to the range recommended for both alloys, except for the silicon levels that are higher in the B206.0 melt for the swing arm casting. The silicon pick-up was from the ceramic feed tube that was used to limit overheating of the block. Using silicon free material should solve this problem. It is noted that for A535 (melt N5235) and A206 (melt N5201), the magnesium and copper level were deliberately lowered to study the effects of lower magnesium and copper level on hot tearing.

Table 4.3.1 *Chemical analysis of A535*

Melt No.	Mg	Mn	Si	Fe	Cu	Ti
AA spec	6.2-7.5	0.1-0.25	0.15 max	0.15 max	0.05 max	0.1-0.25
Engine Mount and Rocker Arm Castings						
N5115	6.9	0.18	0.040	0.060	0.010	0.130
N5193	7.2	0.19	0.050	0.070	0.010	0.120
N5136	7.0	0.18	0.070	0.059	0.004	0.150
N5171	7.0	0.18	0.047	0.060	0.010	0.035
N5188	7.1	0.29	0.035	0.050	0.010	0.035
N5235	5.0	0.20	0.066	0.068	0.005	0.033
N6125	7.6	0.20	0.051	0.08	0.012	0.150

Table 4.3.2 *Chemical analysis of A/B206*

Melt No.	Cu	Si	Fe	Mn	Mg	Ti
AA spec	4.2 – 5.0	0.1	0.15	0.2 - 0.5	0.15 - 0.35	0.15 - 0.30
Engine Mount and Rocker Arm Castings						
N5111	4.5	0.022	0.090	0.28	0.320	0.224
N5192	4.8	0.040	0.070	0.34	0.214	0.065
N5137	5.0	0.040	0.086	0.37	0.230	0.053
N5201	3.8	0.040	0.070	0.25	0.200	0.080
N6124	5.0	0.041	0.059	0.38	0.29	0.075

4.3.2 Results and Discussion

Engine Mount Casting

The processing temperatures and the number of castings poured during the low pressure casting trials are given Table 4.3.3. The mold temperature ranges from 290 to 425ºC for the low pressure casting trials. Alloys A535 and A206 castings were poured at 672-730˚C (42-100˚C superheat), and 696-754˚C (46-104˚C superheat) respectively. An applied pressure of 350 to 400 mbar (5.1 to 5.8 psi) gave full castings for both alloys. In order to get a sound casting throughout, a holding time of 30 seconds was used with a maximum pressure of 400 mbar. The major issue during preliminary casting trials was cracking during ejection as the part tended to drag during ejection due to an insufficient ejector system. The number of ejector pins was increased to prevent the twisting of the casting during ejection. After this modification, castings were ejected without twisting and the severity of hot tear was reduced and sometimes eliminated in both alloys. Photographs of the engine mount castings from A535 and 206 without and with hot tear are shown in Figures 4.3.1(a) and (b) respectively. It is noted that majority of the hot tear occurred at sharp corners. To correct this problem, introduction of a generous radius at the corners should eliminate the hot tear [6, 7]. X-ray radiographic inspection revealed hot tear and sponge shrinkage that range from category 1 to 8 based on ASTM E155 (series 11) standards. Sponge shrinkage categories greater than 3 may not be acceptable for engineered components. Figures 4.3.2(a) and (b) show examples of X-ray radiographs defects in selected castings. The sponge shrinkage was usually on the vertical ribs of the casting furthest from the ingate and at places where there is change in cross section. It is believed that the long freezing range in both alloys contributed to the poor feeding and formation of shrinkage porosity defects. The introduction of cooling channels in the mold would help to encourage directional solidification to improve soundness.

Rocker Arm Casting

The processing temperatures of the rocker arm castings are given in Table 4.3.4. The rocker arm mold and core temperatures ranged from 165 to 265˚C and 120 to 260˚C. Alloys 535 and 206 were poured at 680-705˚C (50-75˚C superheat), and 695-705˚C (45-55˚C superheat) respectively. The rocker arm molds were generally filled at 50˚C superheat or lower.

Table 4.3.3 *Processing parameters for engine bracket castings*

Melt No.	No. of castings poured	Processing temperature range (˚C)	
		Mold	Pouring
A206			
N5111	23	300-390	700-714
N5192	8	320-375	696-705
N6124	10	290-425	742-754
A535			
N5115	18	350-360	672-692
N5193	14	330-400	683-705
N6125	12	355-405	709-730

(a) N5115-2, A535, no hot tear. (b) N5111-18, A206, hot tear.

Figure 4.3.1 *Photographs of engine mount castings without and with hot tear.*

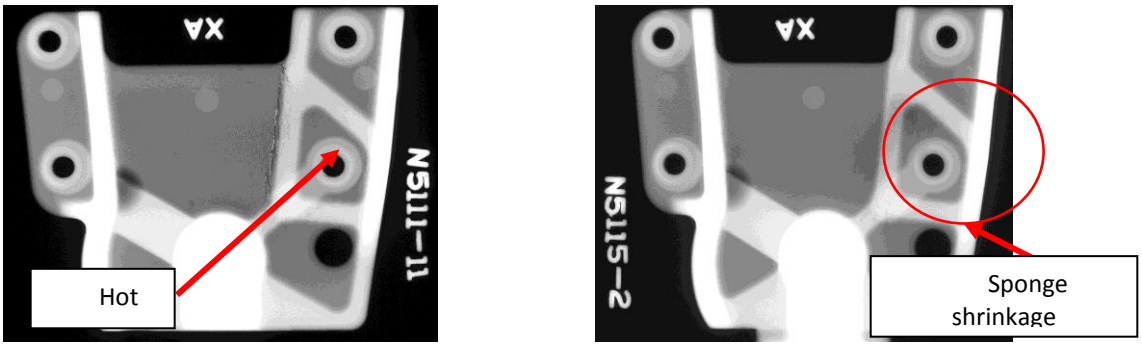

(a) N5111-11 XA, A206. (b) N5115-2 –XA, A535.

Figure 4.3.2 *Radiographs from A206.0 and A535.*

Table 4.3.4 *Processing parameters of the rocker arm castings*

Melt No.	No. of castings poured	Processing temperature range (°C)		
		Mold	Core	Pouring
A535				
N5136	11	218-265	150-230	680-684
N5171	13	195-240	140-230	680-705
N5188	5	165-205	120-225	678-704
N5235	10	190-248	145-230	677-682
N5147	10	195-270	145-220	683-700
A206				
N5137	11	180-233	160-230	695-705
N5201	7	192-260	145-260	695-705

Photographs of a mounted rocker arm mold with its metal core, and a rocker arm casting with its gating system are shown in Figures 4.3.3(a) and (b) respectively. The use of a hollow metal core was beneficial as it reduced rapid heat loss to the core by the molten metal. Five of the ten castings poured from alloy A535 with reduced magnesium level (melt #N5235) were free of hot tear cracks. Lowering of the copper level (melt #N5201) to 3.8% in A206.0 produced marginal improvement in hot tear resistance. Hot tear and surface shrinkage similar to that shown in Figures 4.3.4 (a) and (b) were present on some of the castings.

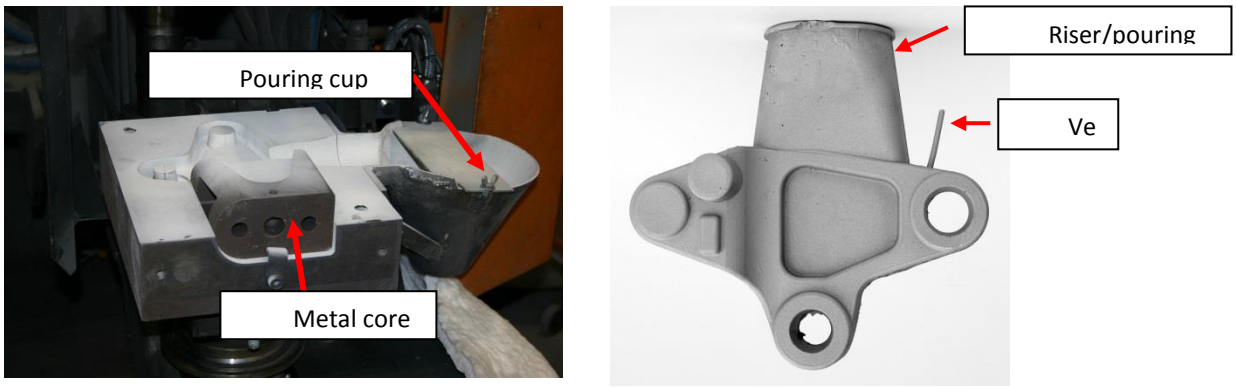

(a) Mounted rocker arm mold. (b) Rocker arm casting with gating system.

Figure 4.3.3 *Photographs of a mounted rocker arm mold and rocker arm casting.*

Apart from the hot tear problem, extraction of the castings from the mold cavity was difficult due to the deep recesses, and the casting tended to stick to one side of the die. Having a top coat of graphite wash on the insulating coating was not always effective as a mold release. It is noted that ejector pins were not used in this mold because of the limited capacity of the machine. The thermal expansion of the core can possibly force the casting towards the mold wall and increase the difficulty of ejection. The use of a composite mold (mold and core of different thermal expansion properties), and core with lower thermal expansion than the mold material could alleviate this problem.

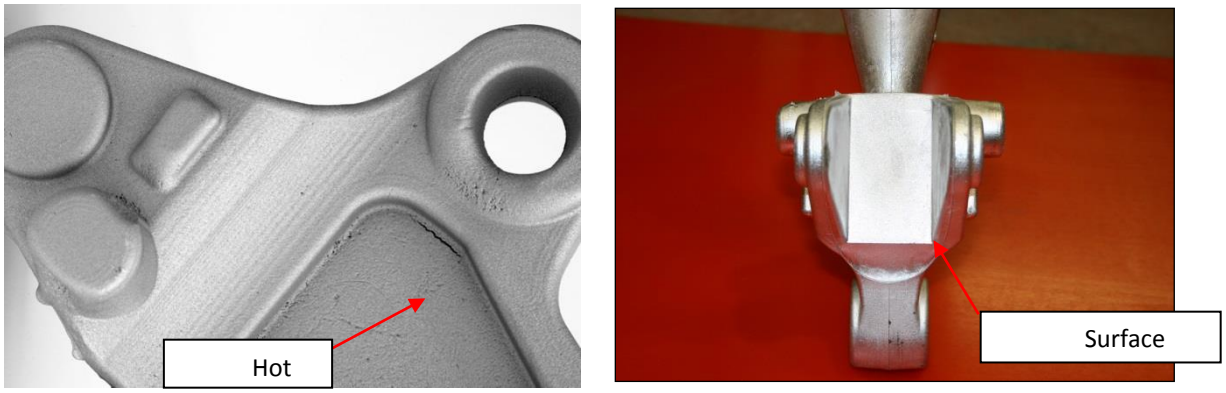

(a) Alloy 535 showing hot tear. (b) Surface shrinkage.

Figure 4.3.4 *Examples of hot tear and surface shrinkage in rocker arm castings.*

4.4 TASK 4 Mechanical Properties and Microstructures

4.4.1 Experimental Procedure

Mechanical Properties and Heat Treatment

The mechanical properties (UTS, YS, and % elongation) from the ASTM B108 tensile bars were determined following standard ASTM procedures. The test bars from both alloys were X-rayed, following the ASTM E-155 procedure to evaluate casting soundness. Alloy 206.0 test bars were subjected to both T4 and T7 temper heat treatments. The T4 temper solutionizing heat treatment consists of heating samples from room temperature to 495ºC in 2 h, holding at 495ºC for 2 h, then increasing the temperature to 525ºC and holding there for 8 h. When the solutionizing heat treatment cycle was completed, the samples were immediately quenched in water at 80ºC. Some test bars were further subjected to an immediate artificial aging treatment done at 200ºC for 4 h (T7 temper). In addition, a few test bars from alloy 206.0 were held at 200ºC for 20 min before determination of the tensile properties. For alloy 535.0, test bars were subjected to a T5 temper heat treatment (held for 5 h at 400ºC, followed by air cooling).

Metallography and Microstructure

Samples for metallographic and microstructural evaluation were sectioned from the prototype castings and the gauge section of the fractured ASTM test bars. The samples were polished and etched using Keller's reagent (2.5 mL HNO3, 1.5 mL HCl, 1 mL HF, and 95 mL H2O), and some samples were anodized using a solution of 1.8% fluoboric acid in water following the Barkers's anodizing method to reveal the grain structure before and after grain refiner addition. Limited grain structure and size comparison were made from anodized samples for both alloys. Some of the swivel-head castings were sectioned transverse to the parting line through the thickest section (45 mm) of the casting and macroetched using Poulton's reagent (60 mL HCL, 30 mL HNO3, 5 mL HF and 5 mL H2O) to reveal their internal quality. The fracture surfaces of selected samples were studied by SEM. The SEM image contrast from topographic and compositional differences were obtained using the low-energy secondary electrons (SE), the higher-energy backscattered electrons (BSE), and the energy dispersive X-ray spectroscopy (EDS) to evaluate the solidification structure and the presence of oxides and other non-metallic inclusions. Specimens were sectioned from selected constrained rod castings along the parting line through the hot-tear region. Several pictures of the hot-tear cross section were taken in the as-polished condition. The Clemex Vision Lite software with specific mosaic capabilities was used to capture the images and combine them into single composite photographs.

4.4.2 Results and Discussion

Chemical Composition

The chemical analyses from alloys 206 and 535 are shown respectively in Tables 4.4.1 and 4.4.2. The Aluminum Association (AA) composition specifications for both alloys are shown in these tables. The chemical compositions are close to the range recommended for both alloys, except for the silicon levels that are higher in the 206 melt for the swing-arm casting. The silicon pick-up was probably from the ceramic feed tube that was used to limit overheating of the block. The copper levels in alloy 206 (melts N5201, N6081, and N7026) and magnesium levels in alloy 535 (melt N5235) were reduced to study the effects of lower copper and magnesium contents on the mechanical properties of both alloys.

Table 4.4.1 *Chemical analysis of alloy 206*

Melt No.	Cu	Si	Fe	Mn	Mg	Ti
AA spec	4.2 – 5.0	0.10 max	0.15 max	0.20 - 0.50	0.15 - 0.35	0.15 - 0.30
Engine Mount and ASTM Test Bar Castings						
N5111	4.5	0.022	0.090	0.28	0.320	0.224
N5192	4.8	0.040	0.070	0.34	0.214	0.065
N5137	5.0	0.040	0.086	0.37	0.230	0.053
N5201	3.8	0.040	0.070	0.25	0.200	0.080
N6080	5.1	0.044	0.069	0.37	0.280	0.170
N6081	3.8	0.039	0.051	0.31	0.199	0.072
N6090	5.1	0.038	0.050	0.38	0.280	0.066
N6124	5.0	0.041	0.059	0.38	0.290	0.075
N7026	3.8	0.046	0.070	0.40	0.450	0.065
N7038	4.8	0.044	0.060	0.38	0.200	0.058

Table 4.4.2 *Chemical analysis of alloy 535*

Melt No.	Mg	Mn	Si	Fe	Cu	Ti
AA spec	6.2 - 7.5	0.10 - 0.25	0.15 max	0.15 max	0.05 max	0.10 - 0.25
Engine Mount and ASTM Test Bar Castings						
N5115	6.9	0.18	0.040	0.060	0.010	0.130
N5193	7.2	0.19	0.050	0.070	0.010	0.120
N5136	7.0	0.18	0.070	0.059	0.004	0.150
N5171	7.0	0.18	0.047	0.060	0.010	0.035
N5188	7.1	0.29	0.035	0.050	0.010	0.035
N5235	5.0	0.20	0.066	0.068	0.005	0.033
N6082	6.2	0.45	0.064	0.067	0.016	0.072
N6125	7.6	0.20	0.051	0.08	0.012	0.150

Mechanical Properties

Alloy 206 (F, T4 and T7 Tempers)

The average mechanical properties and standard deviation from ASTM B108 test bars of alloy 206 are summarized in Tables 4.4.3. These data were generated from a minimum of three and a maximum of twelve test bars per melt. The ASTM B108 test bar mold was preheated to about 400˚C before pouring the test bars for consistent mold filling. X-ray radiography results of the test bars show that the bars were relatively free from centerline shrinkage defects, but some inclusions were observed on the fracture surfaces of some of the test bars. The Aerospace Material Specifications (AMS) for the yield strength (YS), ultimate tensile strength (UTS), and % elongation for the T4 temper are 205 MPa, 345 MPa, and 10%, respectively for alloy 206. The corresponding AMS for T7 temper are 275 MPa, 345 MPa, and 3% elongation.

Table 4.4.3 *Mechanical properties of alloy 206 in the F, T4 and T7 tempers*

Sample	Temper	Cu (%)	0.2 %YS (MPa)	UTS (MPa)	Elong (%)
AMS 4236	T4	-	205	345	10
AMS 4235	T7	-	275	345	3
N6090	F	5.1	158 [3]	209 [4]	4.2 [3.4]
N7038		4.8	176 [3]	252 [7]	3.6 [0.7]
N7026		3.8	158 [1]	251 [12]	6.1 [2.0]
N6090	T4	5.1	269 [1]	402 [11]	10.3 [1.9]
N7038		4.8	270 [3]	415 [8]	13.4 [2.7]
N7026		3.8	231 [6]	371 [10]	15.4 [3.2]
N7038	T6	4.8	292 [2]	429 [15]	9.1 [2.7]
N7026		3.8	192 [7]	333 [13]	15.8 [2.4]
N6090	T7	5.1	366 [2]	410 [8]	2.4 [0.4]
N7038		4.8	360 [4]	422 [8]	3.5 [0.6]
N7026		3.8	279 [3]	348 [6]	6.9 [1.1]

The average YS in the as-cast condition ranged from 158 to 176 MPa. There was significant improvement in the YS and UTS after the T4 and T7 heat treatments. These results meet or exceed the AMS shown in Table 4.4.3. Figure 3.4.1 shows that both YS and UTS increase as the Cu content was increased from 3.8 to 5.1%, but the ductility was lower at the higher Cu content. This observation is consistent with previous reports for this alloy 17. The elongation ranged from 3.6 to 6%; the higher elongation is associated with lower Cu content. The average YS after T4 ranged from 231 to 270 MPa, and the corresponding elongation ranged from 15 to 10%. There is no significant difference between the properties at 4.8 and those at 5.1% Cu. The YS was however about 17% lower (from 270 to 231 MPa) when the Cu content was reduced to 3.8%. Considering the T7 data, the YS ranged from 279 to 366 MPa, and the elongation ranged from 7 to 2.4%. Within the T7 temper, about a 31% reduction in YS was observed when the Cu content was reduced to 3.8% from 5.1%.

The effect of test temperature on the mechanical properties from one composition from alloy 206 is shown in Table 4.4.4. This data is plotted in Figure 4.4.2. The tensile properties were reduced at the higher test temperature with corresponding improvement in ductility. For the T7 temper, with 5.1% Cu, the YS at 23˚C was 366 MPa; this was reduced to 307 MPa at 200˚C.

It is noted that some changes in the alloy composition limits could be beneficial in order to improve the hot-tear resistance of this alloy. The Cu limits in the current AA composition specification are 4.2-5.0%, while ingots of this alloy are usually supplied with nominal Cu in the range 4.7-4.9%. It is noted that the AMS at the T4 temper for YS, UTS, and % elongation are 205 MPa, 345 MPa, and 10%, respectively. The corresponding AMS for T7 temper are 275 MPa, 345 MPa, and 3% elongation. The current results show that relatively high tensile properties can be obtained from a 3.8% Cu melt (melt N7026). For example, the average YS, UTS and % elongation at the T7 temper are 279 MPa, 348 MPa, and 7%. These property levels may be adequate for automotive or other component applications, and they are better than specified for alloy 356.0-T6 at 186 MPa, 262 MPa and 5 %.

Table 4.4.4 *Effect of test temperature on properties of alloy 206.0, melt N6090*

Test Temp. (ºC)	Condition	0.2 %YS (MPa)	UTS (MPa)	Elong. (%)
23	T4	269 [1]	402 [11]	10.3 [1.9]
200		214 [5]	306 [4]	13.6 [2.1]
23	T7	366 [2]	410 [8]	2.4 [0.4]
200		307 [3]	323 [3]	6.7 [1.9]

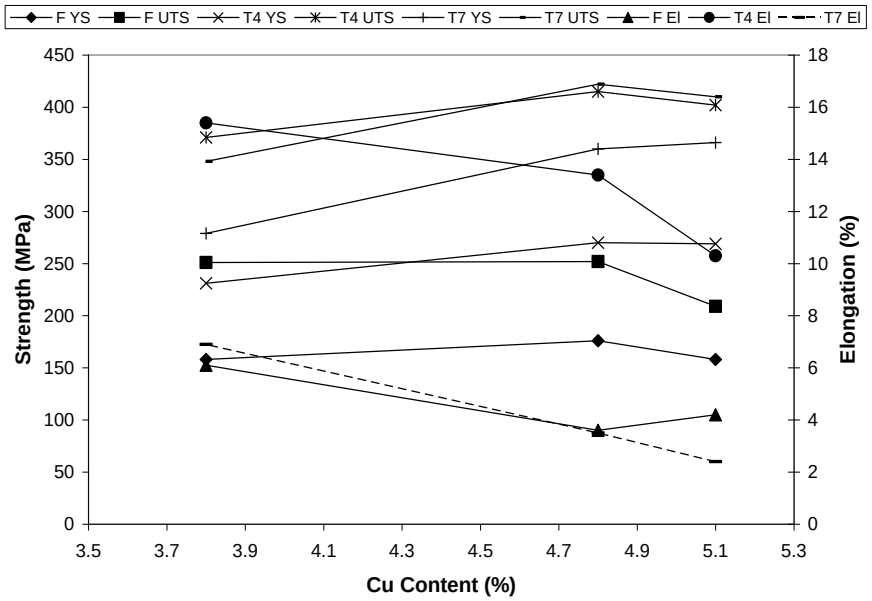

Figure 4.4.1 *Effect of Cu content on the tensile properties of alloy 206.*

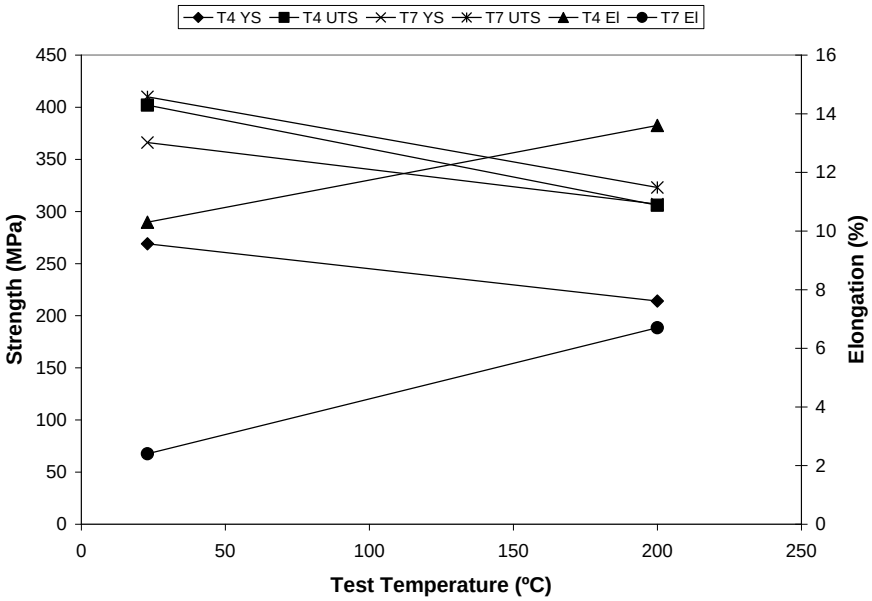

Figure 4.4.2 *Effect of test temperature on the tensile properties of alloy 206 with 5.1%Cu.*

Alloys 535: F and T5 Tempers

The average mechanical properties and standard deviation from ASTM B108 test bars of alloy 535, is summarized in Table 4.4.5. The minimum ASTM specifications for YS, UTS, and % elongation in the as-cast and after T5 heat treatment are 124 MPa, 241 MPa and 8%, respectively.

Table 4.4.5 *Mechanical Properties of alloy 535 in the F and T5 tempers*

Sample	Condition	Mg (%)	0.2 %YS (MPa)	UTS (MPa)	Elong. (%)
ASTM			124	241	8.0
N5193	F	7.2	142 [2]	240 [8]	7.0 [1.4]
N5188		7.1	137 [2]	261 [10]	10.0 [1.9]
N6082		6.2	131 [1]	263 [5]	10.5 [1.1]
N5235		5.0	104 [1]	236 [4]	14.2 [1.3]
N5193	T5	7.2	144 [2]	228 [7]	6.5 [0.7]
N5188		7.1	143 [2]	254 [7]	8.7 [0.6]
N6082		6.2	136 [2]	260 [5]	10.1 [0.8]
N5235		5.0	109 [2]	232 [5]	12.5 [1.0]

The data in Table 4.4.5 is plotted in Figure 4.4.3. The YS increased as the Mg content was increased from 5.0 to 7.2%, but the ductility was lower at higher Mg content. There was no significant improvement in the YS and UTS after the T5 heat treatment. It is not clear why the UTS at T5 for the 7.2% Mg level were lower than that either in the F condition data or at the lower magnesium levels. There was a drop in YS of about 35 MPa when the nominal magnesium level was reduced to 5% from 7% and an improvement in ductility. There was no significant loss in ductility after heat treatment. The elongation ranged from 7 to 14% in the as-cast condition compared with 6.5 to 12.5% after heat treatment.

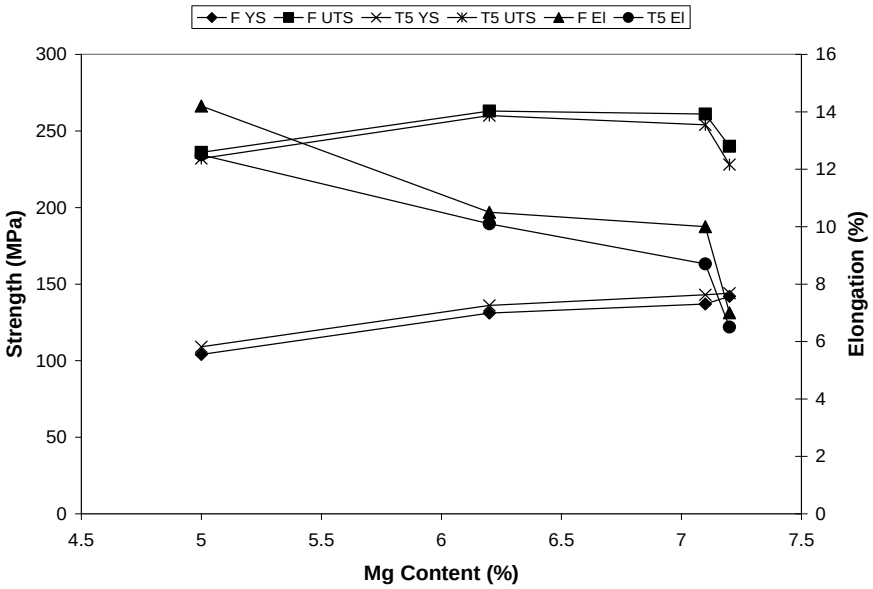

Figure 4.4.3 *Effect of Mg content on the tensile properties of alloy 535.*

4.4.3 Metallography and Microstructure

Constrained Rod Component

Photographs of the constrained rod casting and sections where hot tears were observed are shown in Figure 4.2.3 of this report. The hot-tear regions in the constrained rods were examined. Examples of mosaic images of alloys 206 and 535 combined into single photographs using Clemex Vision Lite software are shown in Figures 4.4.4(a) and (b). The specific advantage of this technique is that a rather large area (~15 mm in this study) was observed, and the morphology of the hot-tearing region is fully captured with superior microscopic details. The dendritic solidification structure is readily apparent in these photographs.

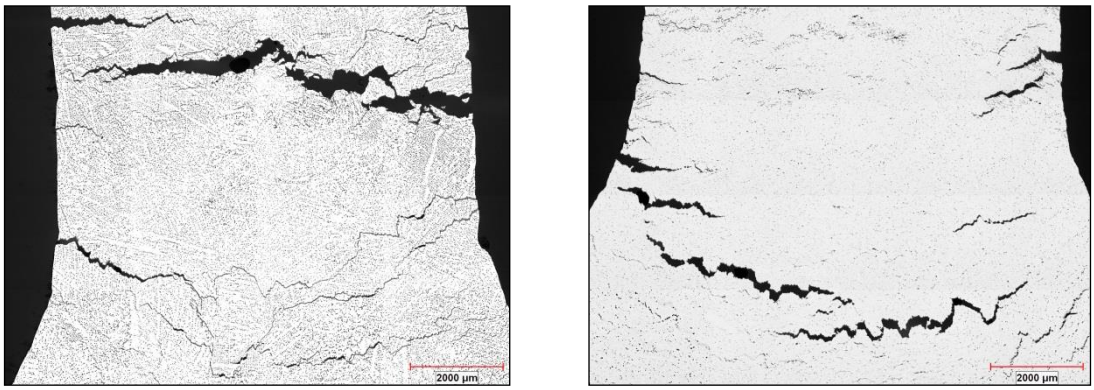

(a) N6080-2, Alloy 206.0, 5.1%Cu, 25x. (b) N6082-6, Alloy 535.0, 6.2%Mg, 25x.

Figure 4.4.4 *Hot-tear region of constrained rod castings from alloys 206 and 535.*

Evaluation of Microstructure

Hot tearing occurs in susceptible alloys when the contraction of solidifying castings is excessively restrained by the mold or cores, especially in hot spots of the casting where the strain resulting from solidification contraction is concentrated. Examples of microstructures from unrefined and refined constrained rod castings at the mold temperatures evaluated are shown in Figures 4.4.5 to 4.4.7. The highly dendritic microstructure from the unrefined metal at the different mold temperatures is readily apparent from these images. After grain refinement, the dendritic structure is broken down and the grain structure significantly reduced. The reduction in hot tearing after grain refinement could be associated with the break down and refinement of the dendritic structure leading to improved feeding of solidification shrinkage. The finer grain structure also contributed to reduce hot tearing because the strain/stress resulting from the solidification contraction can be shared over lager surface area resulting from the finer grain structure. As the mold temperature falls below 400ºC, the castings begin to show signs of hot tearing. The hot mold provided the required thermal gradient during solidification leading to improved feeding.

(a) Sample 1A, Unrefined, 50x.

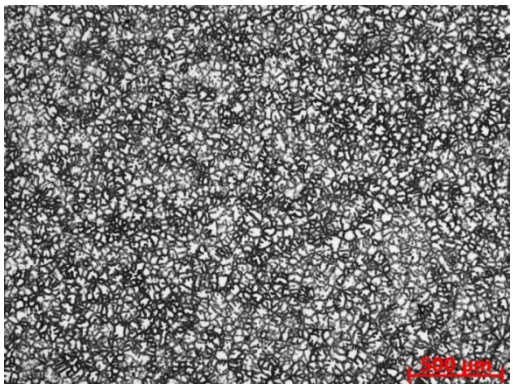

(b) Sample 1B, Refined, 50x.

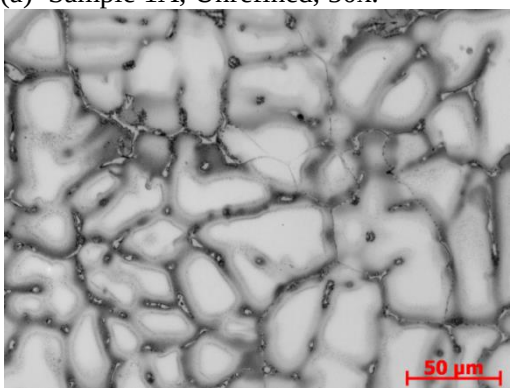

(c) Sample 1A, Unrefined, 500x.

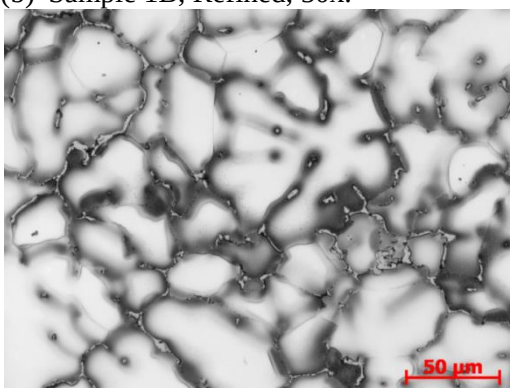

(d) Sample 1B, Refined, 500x.

Figure 4.4.5 *Microstructures from alloy 206 poured in mold preheated to 200°C.*

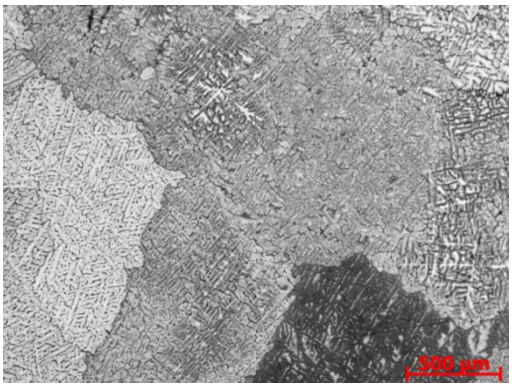

(a) Sample 2A, Unrefined, 50x

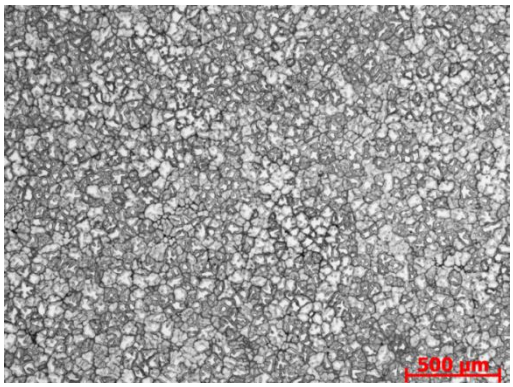

(b) Sample 2B, Refined 50x.

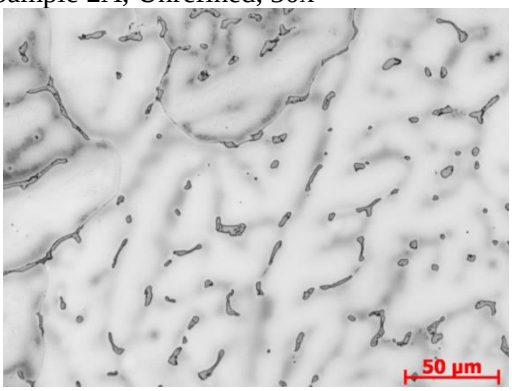

(c) Sample 2A, Unrefined, 500x.

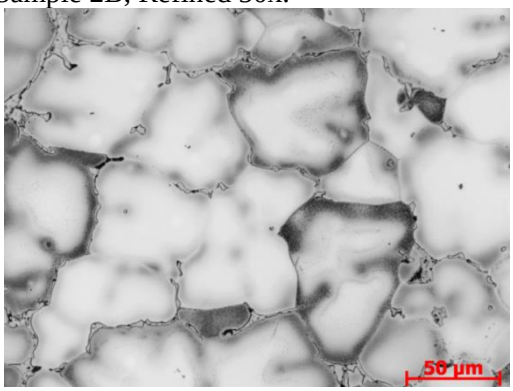

(d) Sample 2B, Refined, 500x.

Figure 4.4.6 *Microstructures from alloy 206 poured in mold preheated to 350°C.*

(a) Sample N2054-A, Unrefined, 50x.

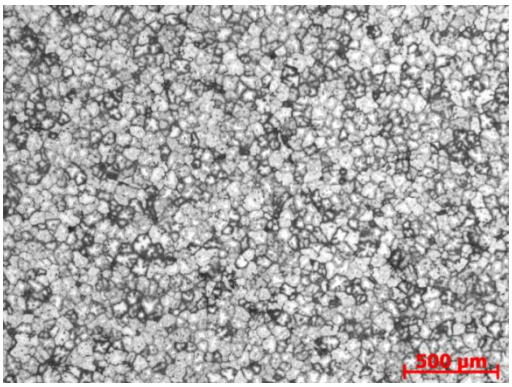

(b) Sample N2054-B, Refined 50x.

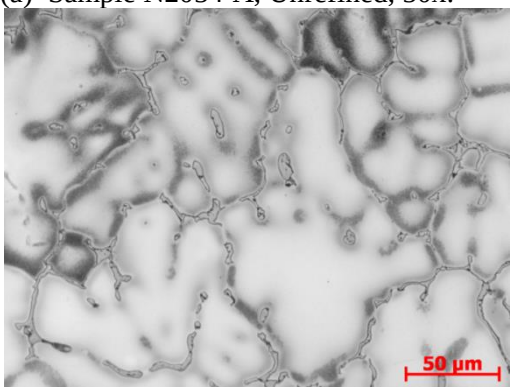

(c) Sample N2054-A, Unrefined, 500x.

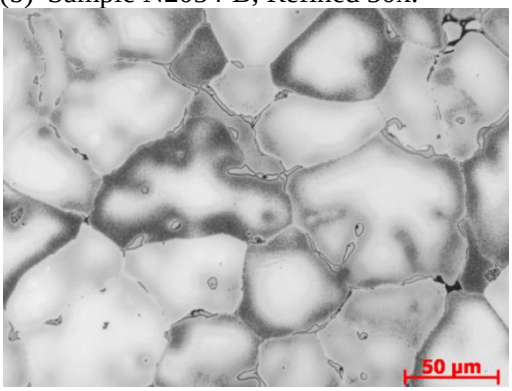

(d) Sample N2054-B, Refined, 500x.

Figure 4.4.7 *Microstructures from alloy 206 poured in mold preheated to 400°C.*

Engine Mount Component

The photographs of the engine mount casting without and with hot tears are shown in Figure 4.3.1 of this report. Examples of anodized and etched microstructures from the engine mount cast from alloy 206 are shown in Figures 4.4.8 (a) and (b). The progression of the hot tear is both along and across the grain boundaries. The dendritic nature of the solidification structure is readily apparent in Figures 4.4.8 (a) and (b). It is noted that a similar dendritic solidification structure was also observed in alloy 535.

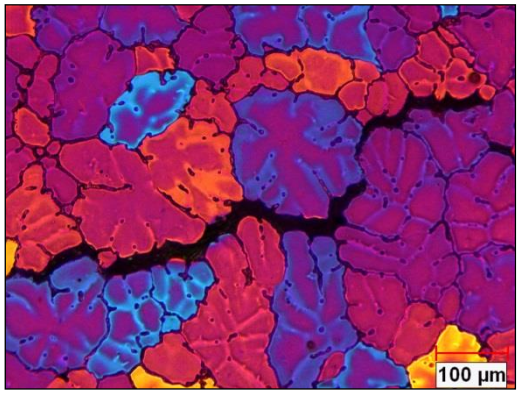

(a) N6124-5-2, 206, anodized, 100x.

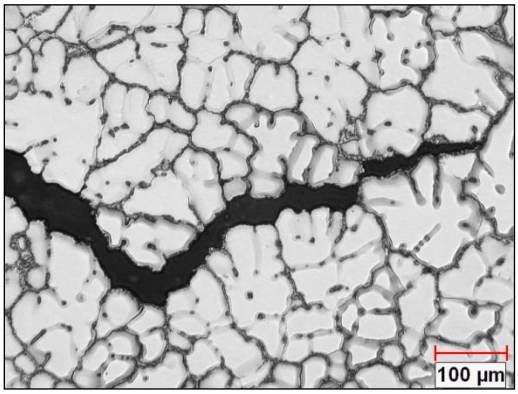

(b) N6124-5-2, 206, Keller's etch, 100x.

Figure 4.4.8 *Anodized and etched microstructures showing the progression of hot tear.*

Microstructures from Test Bars of Alloy 206

Examples of unetched microstructures in the as-cast condition and after heat treatment (T7) from the test bars poured from a 4.8% Cu melt are shown in Figures 4.4.9(a) and (b). The dendritic network of the undissolved eutectic ($CuAl_2$) along the grain boundary in the as-cast condition is shown in Figure 4.4.9(a); it was dissolved after heat treatment as shown in Figure 4.4.9(b).

The microstructures after etching in Keller's reagent are shown in Figures 4.4.10(a) and (b). The relatively fine grain structure of the test bars is revealed after etching. After solution heat treatment, the interdendritic network of the eutectic CuAl2 along the grain boundary (Figure 4.4.11a) was broken down, and fine precipitates of the CuAl2 phase were deposited within the grains and at grain boundaries (Figure 4.4.11b). Similar microstructures were observed for the T4 temper.

The SEM of the fracture surface of a broken test bar at low and high magnifications are shown in Figures 4.4.12(a)-(f). It is noted that this is from the as-cast test bar before heat treatment. The dendritic structure characteristic of long freezing range alloys with some patches of eutectic phase (white) is readily apparent in Figures 4.4.12(c) and (d). The EDS spectra of the general area and eutectic area are shown in Figures 4.4.12(e) and (f). Strong peaks of copper are readily apparent in the eutectic region, Figure 4.4.12(f).

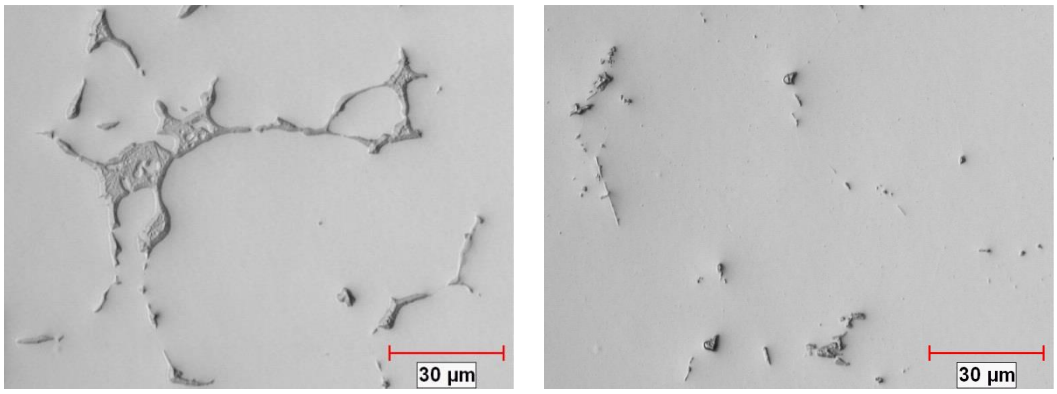

(a) N7038-3B-F, 500x. (b) N7038-7A-T7, 500x.

Figure 4.4.9 *Unetched microstructures of test bars of alloy 206 before and after heat treatment.*

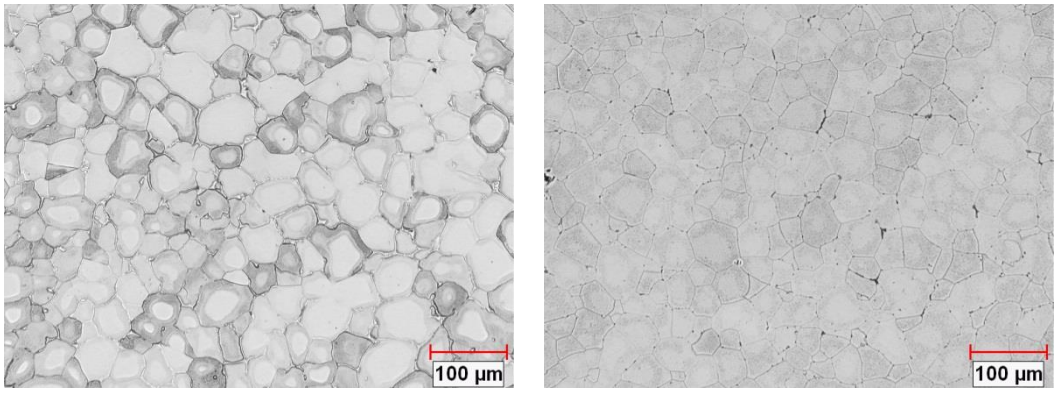

(a) N7038-3B-F, 100x. (b) N7038-7A-T7, 100x.

Figure 4.4.10 *Microstructures of test bars of alloy 206 before and after heat treatment. Keller's etch.*

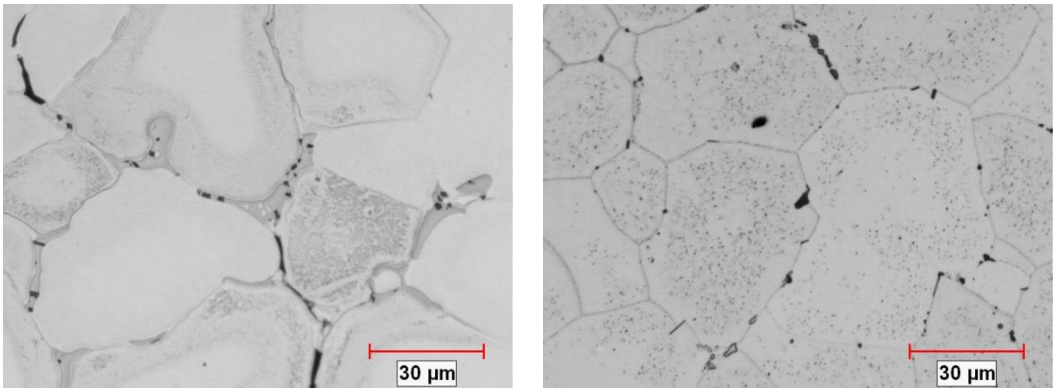

(a) N7038-3B-F, 500x. (b) N7038-7A-T7, 500x.

Figure 4.4.11 *Microstructures from test bars of alloy 206 before and after heat treatment. Keller's etch.*

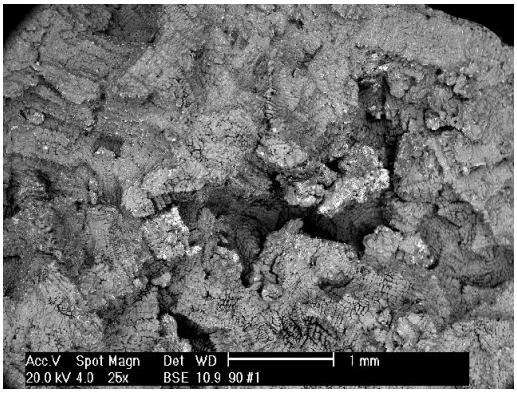

(a) N6090-1, 25x.

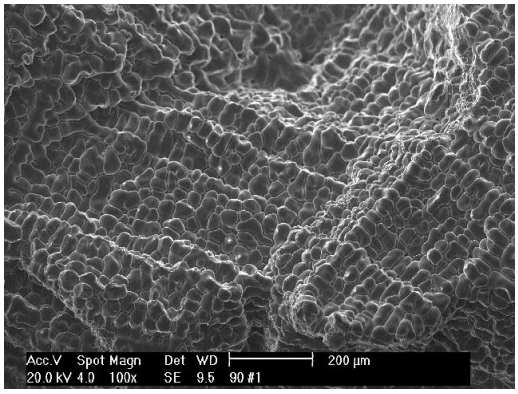

(b) N6090-1, 50x.

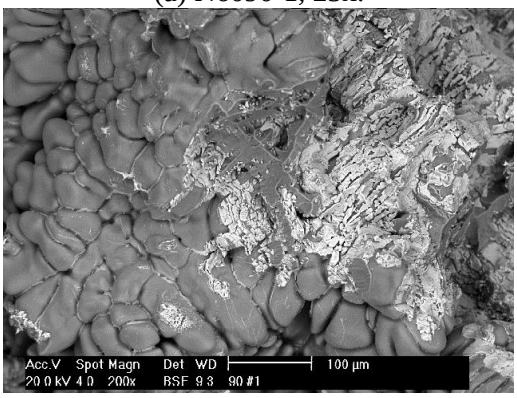

(c) N6090-1, 200x.

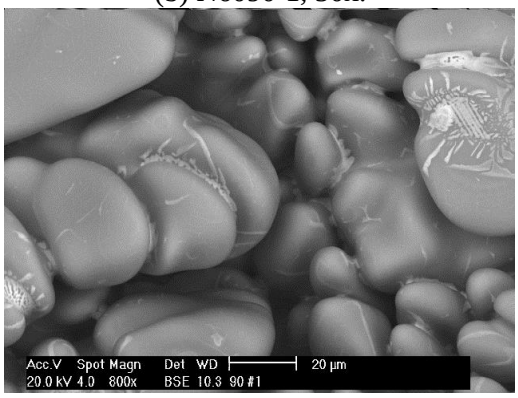

(d) N6090-1, 800x.

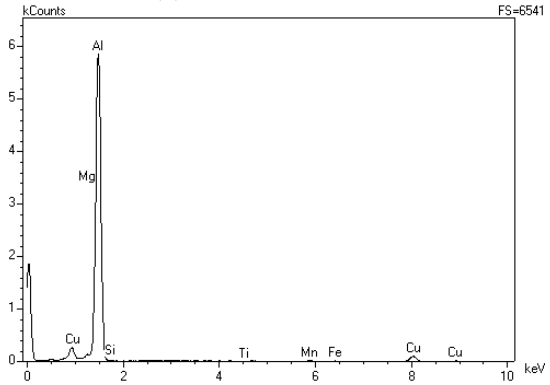

(e) N6090-1, EDS,general area.

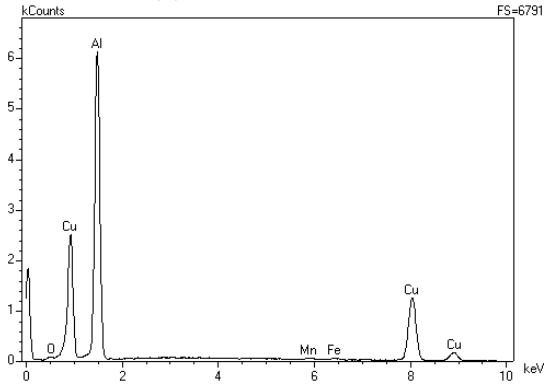

(f) N6090-1, EDS,eutectic,edge.

Figure 4.4.12 *Alloy 206, SEM of the fracture surface of test bar showing dendritic structure. The EDS of the general area and eutectic area are shown in (e) and (f).*

Microstructures from Test Bars of Alloy 535

The microstructures in the as-cast condition and after heat treatment are shown in Figures 4.4.13(a) and (b). Some microporosity (dark area) is associated with the other constituents in the microstructure. The continuous interdendritic network along the grain boundary is readily apparent in Figure 4.4.13(a). These microstructures can be compared to that of Al-Mg alloy 520 in the ASM Handbook, showing insoluble dark particles of possibly $FeAl_3$ and an interdendritic network of possibly Mg_2Al_3 phase along the grain boundary [18]. After T5 heat treatment, most of this phase is dissolved, as shown in Figure 4.4.13(b).

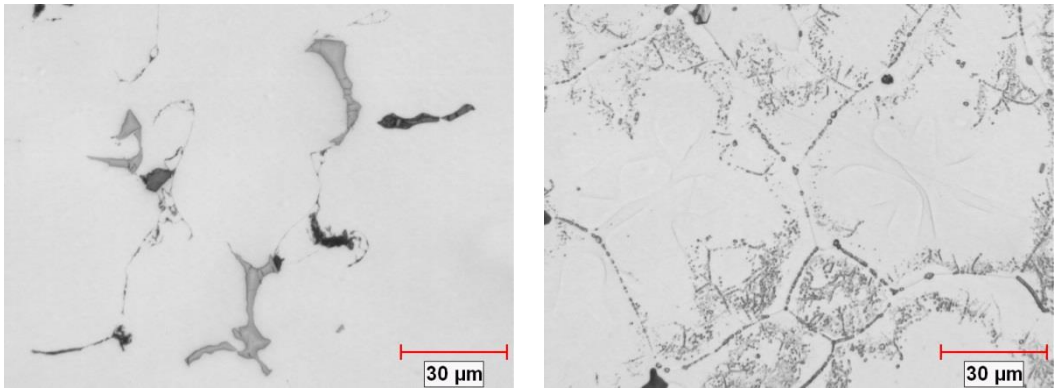

(a) N6082-535-F, 500x, unetched. (b) N6082-535-T5, 500x, etched.

Figure 4.4.13 *Unetched and etched microstructures of test bars of alloy 535 before in addition, after heat treatment, 500x.*

The SEM of the fracture surface of a broken test bar is shown in Figures 4.4.14(a) to (c). The dendritic structure characteristic of long freezing range alloys similar to the observation made for alloy 206 is readily apparent in Figure 4.4.14(b). The EDS of an area with inclusion show strong peaks of aluminum, magnesium and oxygen suggesting an oxide inclusion on the fracture surface.

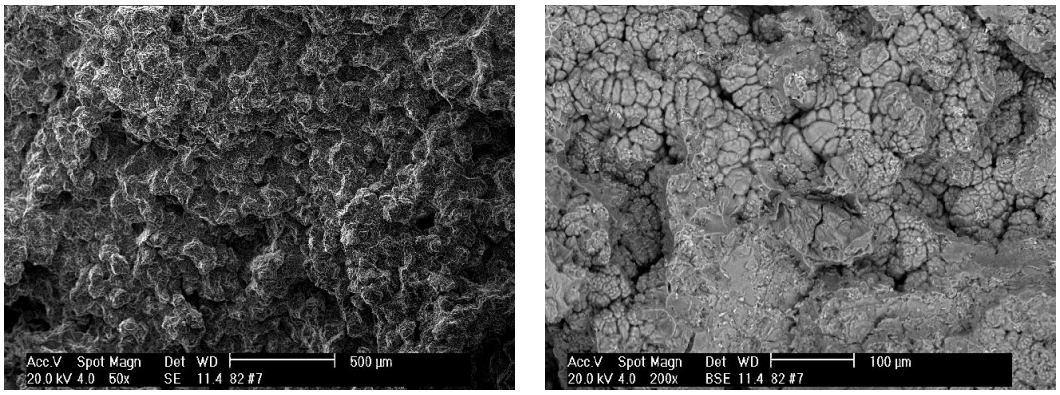

(a) N6082-#7, 50x. (b) N6082-#7, 200x.

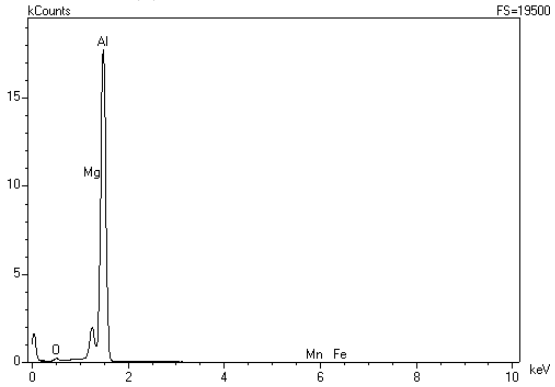

(c) N6082-#7, EDS

Figure 4.4.14 *Alloy 535, SEM of (a) fracture surface, (b) dendritic structure of (a), and (c) EDS.*

4.4.4 Summary and Conclusions

1. The mechanical properties of the separately cast ASTM B108 tensile bars provide good representation of permanent-mold properties for both alloys. As expected, the mechanical properties of alloys 206 and 535 are strong functions of the chemical composition and heat treatment, especially for alloy 206.

2. For alloy 206, some changes in the alloy composition limits could help to improve hot-tear resistance. The Cu limits in the current AA composition specification are 4.2-5.0%. Ingots of this alloy are usually supplied with nominal Cu in the range 4.7-4.9%. The current results show that relatively high tensile properties can be obtained from 3.8 % Cu melt (melt N7026). For example, the average YS, UTS and % elongation at the T7 temper are 279 MPa, 348 MPa, and 7%, respectively. These property levels may be adequate in some automotive and/or other component applications.

3. For alloy 535, the YS and UTS increased as the Mg content was increased from 5.0 to 7.2 % with a corresponding reduction in ductility. There was no significant improvement in the YS and UTS or loss in ductility after the T5 heat treatment. The elongation ranged from 7 to 14% in the as-cast condition compared with 6.5 to 12.5% after heat treatment.

4. The microstructures of the constrained rod castings, the prototype components, and the separately cast ASTM B108 tensile bars show the characteristic dendritic solidification structure from both alloys. The addition of TiBor as grain refiner was effective in reducing the grain size, and the estimated average grain sizes for alloys 206 and 535 are 75 µm and 125 µm, respectively.

5. The anodized and etched microstructures show the progression of the hot tear through the dendritic network and along the grain boundaries. Etching with Keller's reagent was effective in revealing the grain boundaries and the extent of coring in the microstructures in the as-cast condition.

6. The SEM analysis of the hot-tear sections of the prototype castings and the fracture surfaces of the tensile bars show the types of inclusions that can be expected in both alloys as well as the highly dendritic solidification structure. The progression of hot tear along the grain boundaries and within the grains are readily apparent in some of the SEM photographs. The SEM EDS spectrum obtained from the eutectic areas of alloy 206 indicates strong peaks of copper, magnesium, and manganese.

7. Examination of the hot-tear zone in the constrained rod castings by the Clemex Vision Lite software to combine mosaic images into single photographs from both alloys is an effective way to study the detailed morphology of the hot-tearing region.

4.5 TASK 5 - Technology Transfer (Casting Trials at Partner Foundry)

4.5.1 Phase I: Prototype Castings

Swivel and Elbow Castings

The swivel and elbow castings are production parts normally poured from A356.0 by ECK Industries, Inc. using gravity tilt-pour casting machines equipped with effective casting ejector mechanisms. The permanent mold dies were heated by gas. The swivel and elbow molds are four-cavity and one-cavity respectively. A sand shell core was used with the elbow mold and the swivel mold has built in metal cores. The molds were coated with Dycote 8 that has insulating and refractory properties. A top coat of graphite wash was applied as needed to improve surface finish. The mold and metal temperatures were measured during the casting trial. A photograph of a multi-cavity swivel mold is shown in Figure 4.5.1.

Figure 4.5.1 *Mounted 4-cavity swivel mold on tilt-pour machine.*

Swing Arm Casting

The swing arm casting was a new component developed by Grenville Castings Ltd. to be produced from alloy B206.0. Extensive solidification modeling was used to aid the design of the swing arm mold. In addition, information on casting design guidelines from the Hot Tear Control Handbook [6] and an earlier study by Sigworth [7] were used to optimize mold and casting design. The component was developed with the following in mind: (a) the part would have a minimum thickness for rapid freezing and low heat input into the mold block, (b) the part would have high draft and a sand core for mold/part elasticity, and (c) part was to be tilted for low pressure (LP) in the cavity to have an even fill from bottom to top to minimize any oxide folds which could generate tears. Finally, strict thermal management of mold temperatures (incorporation of cooling channels) was maintained during the casting trial to ensure the production of hot tear free castings. Figures 4.5.2 (a) and (b) show schematic of the sand core and component with gating system and feed tube. The mold was machined from H13 tool steel, preheated by gas, and coated with Dycote 14 ESS that has good insulating and refractory properties. Boron nitride was applied as top coat on the bottom die as a release agent. In addition, sometimes graphite was sprayed in some areas to improve surface finish and casting ejection. Cooling channels for water or air were incorporated in the mold design to facilitate the control of mold cooling during the casting trial. Figures 4.5.3 (a) and (b) show mounted mold on the low pressure casting machine.

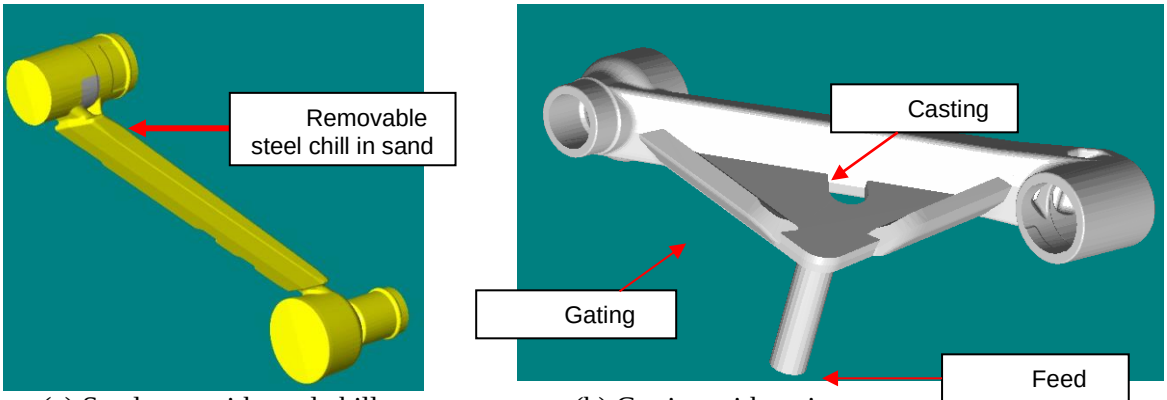

(a) Sand core with steel chill. (b) Casting with gating system and feed tube.

Figure 4.5.2 *Schematic of sand core and swing arm casting with gating system and feed tube.*

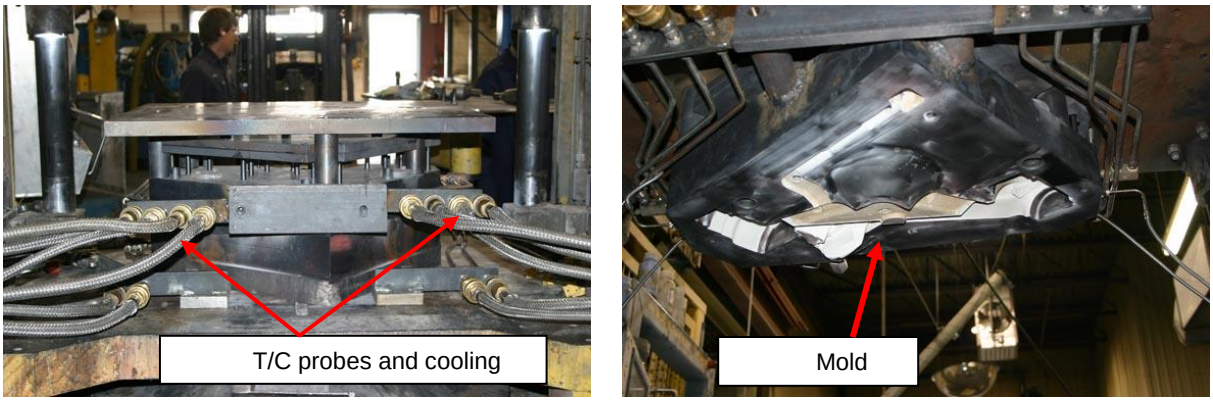

(a)Top and bottom mold halves. (b) Lower mold cavity.

Figure 4.5.3 *Mounted swing arm mold on LP machine with T/C and cooling channel probes.*

The outer perimeter of the mold was controlled to 232˚C (450˚F) (1 in. off cavity) and the inner mold was allowed to reach 400˚C (750˚F) (1 in. off sprue runners) at steady state. In addition, the LP casting machine was modified with the addition of speed controlled soft hydraulic forward and return ejection and the catching system was spring cradled to prevent impact on dropping of the component after mold opening.

4.5.2 Melting and Casting

Swivel and Elbow Castings

The swivel and elbow components are production parts normally poured from aluminum alloy A356.0 by ECK Industries, Inc. using gravity tilt-pour casting machines. Commercial purity ingots of aluminum alloys A535.0 and A206.0 were melted using a gas fired furnace. The charge size was 227 kg (500 lb). These charge materials had been pre-refined with titanium. The dissolved hydrogen was evaluated by the RPT technique. RPT samples were sectioned, and compared with the published standards. The metal was degassed for about 15 minutes with 95%N2/5%SF6 gas mixture before the grain refiner addition. Samples for chemical analysis were obtained before and after grain refiner addition. For both alloys, about 2g/kg of the TiBor master alloy (Al-5%Ti- 1%B) was added to increase the dissolved titanium and boron levels. The composition of alloys used are presented in Tables 4.5.1 and 4.5.2

The metal temperature was monitored by thermocouples immersed in the molten metal. The elbow and swivel castings were poured from fully grain refined metal, and the cycle times were 90 and 255 seconds respectively. Five sets of the swivel castings, and seventeen elbow castings were poured from each of the alloys. The processing temperatures of the swivel castings from alloys A535.0 and 206.0 are given Table 4.5.3

The swivel castings from both alloys and selected elbow castings were visually examined and X-rayed following ASTM E155 standards. The X-ray radiography was obtained from a 150 KV machine with 19.9 MA. The exposure times for the swivel castings from A206.0 and A535.0 were 90 s and 36 s respectively. The exposure time for all the elbow castings was 36 s. In addition to the X-ray analysis, some of the castings were examined using die penetrant inspection to check for hot tear. Some samples were sectioned from the swivel casting for grain structure evaluation.

Swing Arm Casting

Commercial purity ingots of alloy B206.0 were melted at Grenville Castings Ltd in a resistance furnace and transferred to the low pressure casting machine. The charge size was 364 kg (800 lbs). An immersed thermocouple was used to monitor the metal temperature. The molten metal was degassed for about 15 minutes with nitrogen before the grain refiner addition. The dissolved hydrogen was evaluated by the RPT technique. RPT samples were sectioned and compared with the published standards to confirm acceptable gas level.

Samples for chemical analysis were obtained before and after grain refiner addition. The standard Grenville grain refiner practice for A356.0 was to add 455 g (1 lb) TiBor (Al-5%Ti-1%B) master alloy per 45.5 kg (100 lb) charge size. This procedure was followed during the melting of B206.0. It is noted that three levels of TiBor were used during the casting trial to progressively increase the dissolved titanium and boron in the melt.

A filter located at the bottom of the feed tube ensured that any suspended inclusion would not enter the feed tube. The applied pressure was a proportional valve computer controlled linear ramp at a maximum velocity of 30.48 cm/sec (12in/sec) at the choke point which was the sprue. The total cycle time was about 175 s (3 min), made up of 15 s fill time, and 80 s each of holding and cooling times. A total of twenty six castings were poured, the first eight before the addition of grain refiner. The twenty six castings poured were visually examined for hot tears. Some of the castings were X-rayed and subjected to dye penetrant inspection to check for cracks, shrinkage cavity, and other inclusion defects.

Table 4.5.1 *Chemical analysis of A535*

Melt No.	Mg	Mn	Si	Fe	Cu	Ti
AA spec	6.2-7.5	0.1-0.25	0.15 max	0.15 max	0.05 max	0.1-0.25
Swivel and Elbow Castings						
535-1	7.1	0.18	0.083	0.10	0.01	0.071
535-2	7.1	0.18	0.076	0.097	0.01	0.120

Table 4.5.2 *Chemical analysis of A/B206*

Melt No.	Cu	Si	Fe	Mn	Mg	Ti
AA spec	4.2 – 5.0	0.1	0.15	0.2 - 0.5	0.15 - 0.35	0.15 - 0.30
Swivel and Elbow Castings						
A206-1	4.90	0.061	0.065	0.26	0.31	0.23
A206-2	4.90	0.061	0.068	0.26	0.30	0.26
Swing Arm Casting						
Gren-1	4.66	0.223	0.048	0.362	0.269	0.0085
Gren-2	4.40	0.228	0.045	0.356	0.257	0.0156
Gren-3	4.48	0.218	0.049	0.355	0.263	0.0289

Table 4.5.3 *Processing temperatures for swivel castings*

A535					A206				
Cast No.	Temperature				Cast No.	Temperature			
	Mold		Pouring			Mold		Pouring	
	˚F	˚C	˚F	˚C		˚F	˚C	˚F	˚C
1	700	371	1339	726	1	710	377	1342	728
2	690	366	1332	722	2	700	371	1334	723
3	680	360	1337	725	3	690	366	1337	725
4	680	360	1332	722	4	690	366	1339	726
5	675	357	1326	719	5	680	360	1346	730
AVG	685	363	1333	723	AVG	694	368	1340	726

The photographs of the swivel castings with and without the gating system are shown in Figures 4.5.4 (a) and (b) respectively. X-ray radiography and dye penetrant inspection show that the castings are free of hot tear. Examples of X-ray radiography from both alloys are shown in Figures 4.5.5 (a) and (b). The swivel castings from both alloys and selected elbow castings were visually examined and X-rayed following the ASTM E155. The swivel castings from A206 and A535 met Grade A for AMS-STD-2175 (which is equivalent to less than a frame 1 on the ASTM E155 standard), and none of the castings showed hot tears, inclusions or shrinkage porosity. For the elbow castings, where a sand core was used, A206 an A535 were of Grades B and C qualities respectively. A close look at the swivel casting showed that there were no sharp corners, there was generous taper, and the casting design incorporated a generous gating system that provided molten metal to feed solidification shrinkage. In addition, the ejector mechanism worked very well. As shown in Table 4.5.3, the average mold temperatures during the pouring of the swivel casting were 363˚C (685˚F) and 368˚C (694˚F) respectively for A535 and A206, which is hotter than normally used for A356. The pouring temperatures ranged from 719-726˚C for A535 and 723-730˚C for A206. It is believed that a combination of good casting design, fully grain refined metal and good thermal management of the mold (hot mold temperature) accounted for the successful pouring of this component without hot tear. The mold temperature for the elbow component was kept at 357±3˚C (675±5˚F) for A535, and 343 ± 3˚C (650±5˚F) for A206.0, and the pouring temperatures ranged from 771-786˚C (141-156˚C, superheat) and 771-781 (121-131˚C, superheat) respectively.

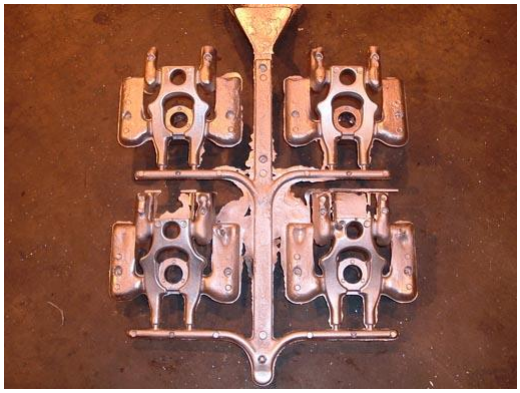

(a) Swivel castings with gating system.

(b) Swivel casting.

Figure 4.5.4 *Photographs of swivel castings with and without the gating system.*

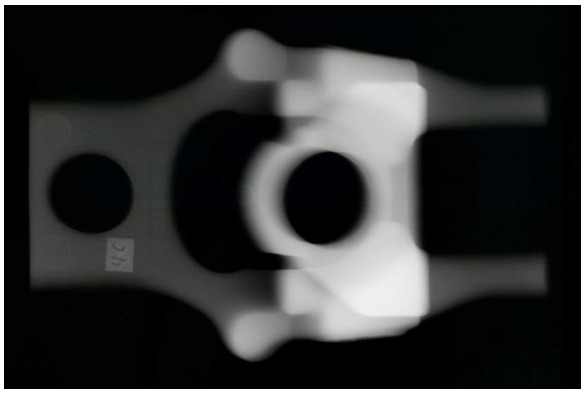

(a) A206.

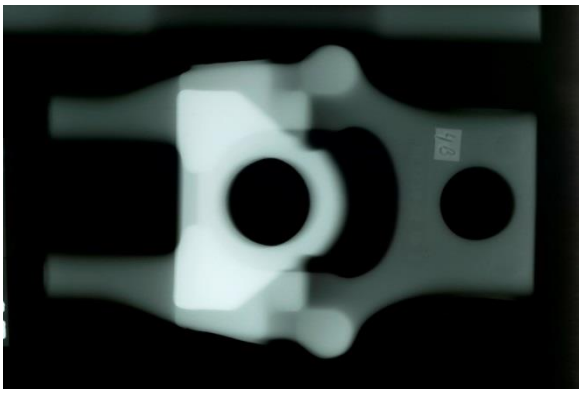

(b) A535.

Figure 4.5.5 *Radiographs of swivel casting from A206 and A535. No hot tear or shrinkage cavity.*

As noted previously, all the castings were poured from fully grain refined metal to improve hot tearing resistance during casting solidification. Examples of anodized grain structure from 19 mm (0.75 in.) thick section of the swivel casting from A206 and A535 are shown in Figures 4.5.11 (a) and (b) respectively. The average grain size for A206 and A535 are 75 μm and 125 μm respectively. The grain size was similar in the 44.5 mm and thin 19 mm thick sections for both alloys. The photographs of the elbow castings with and without the gating system are shown in Figures 4.5.6 (a) and (b) respectively. X-ray radiography and dye penetrant inspection showed that the castings were free of hot tearing. Examples of X-ray radiography from both alloys are shown in Figures 4.5.7 (a) and (b). Similar to the swivel casting, there are no sharp corners, there was generous taper, and the casting design incorporated generous gating system for adequate feeding during solidification.

(a) Casting with gating system and core.

(b) Elbow casting.

Figure 4.5.6 *Photographs of elbow casting with and without the gating system*.

(a) A206.

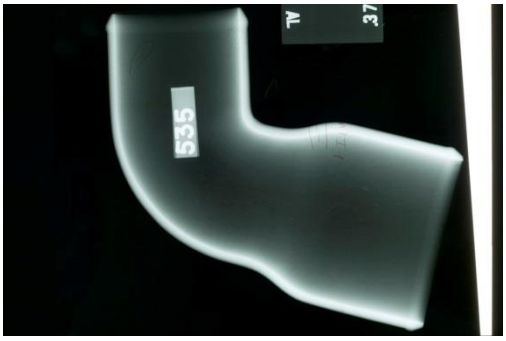

(b) A535.

Figure 4.5.7 *Radiographs of elbow casting from A206 and A535.*

Swing Arm Casting

The part was designed with an open elastic concept from inside out with a collapsible sand core and a goal of 5 to 6 mm walls throughout the casting. In areas where it was not possible to adhere to these criteria, recoverable steel chills was inserted in the sand core and aggressive water cooling provided the needed cooling rate to preclude the formation of hot tears. In addition, cross hatching was added to all stress concentration locations and the parts were ejected as early as possible to limit stress on the parts. The LP casting machine is equipped with PLC based water cooling control by temperature zones. In order to have the best chance of making hot tear free casting, the LP machine was rebuilt with rack and pinion hydraulic ejection system so we could eject as square and soft as possible. Every effort was made to ensure the lowest oxide content with use of multiple filters in the feed tube and casting ingate.

The utilization of intensive solidification modeling to aid mold design was effective in predicting the areas on the part that could produce cracks where the die hit certain maximum temperatures based on the wall thickness and casting geometry. The feeding distance of the alloy and gating were limited and the model suggested that it be distributed across much of the part for feeding. This also helped to limit the hot spots that could contribute to tearing. The utilization of sand shell core with a hollow center provided the required core collapsibility after solidification. The incorporation of the reusable steel chills within the core provided aggressive chilling in the inside radii that would have had a propensity to tear. Water-cooling of the perimeter of the part opposite of the gates was used to create a strong gradient and reduce solidification time. Photographs of the swing arm casting with the gating system and the sand core and finished casting are shown in Figures 4.5.8 (a) and (b) respectively. Figures 4.5.9 (a) and (b) show solidification model prediction of potential area of hot tear and actual hot tear in the casting respectively.

The first eight castings that were poured before grain refinement showed hot tears. Addition of the grain refiner and thermal management of the permanent mold die during the casting resulted in the elimination of the hot tears. The average grain size before and after grain refinement were 105µm and 65 µm respectively. The successful casting of this component is clearly associated with the effective utilization of solidification modeling to aid mold and casting design, and the use of information from the Hot Tear Control Handbook [6] and an earlier study [7] coupled with strict thermal management of the mold.

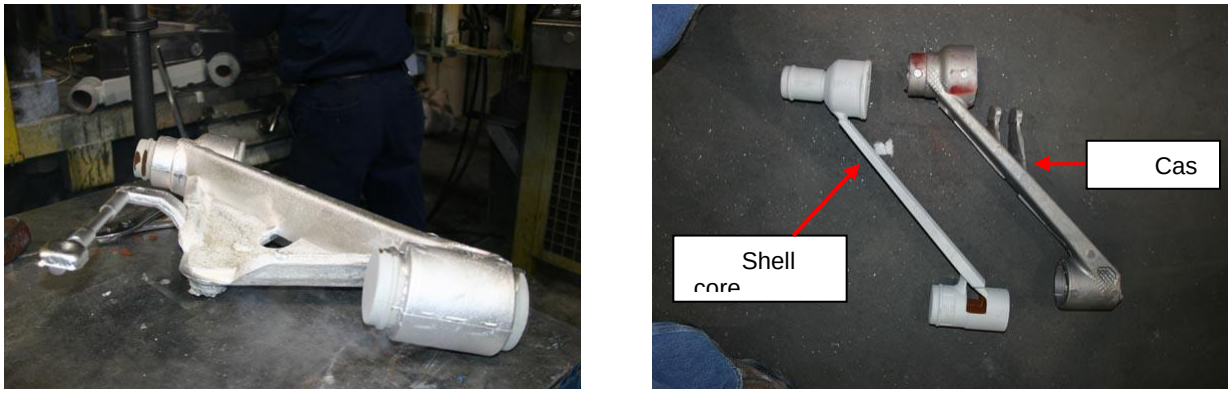

(a) Casting with sand core and test bar prolongation (b) Sand core and finished casting

Figure 4.5.8 *Swing arm casting with gating system, sand core, and finished casting.*

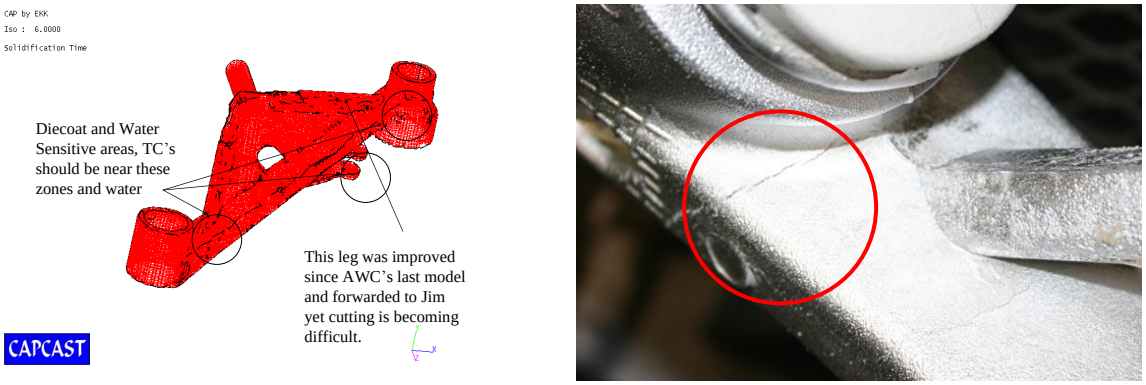

(a) Potential hot spots based on modeling results. (b) Location of hot tear.

Figure 4.5.9 *Predicted and observed hot tear location on casting on casting.*

3.5.3 Characterization

Swivel Component

The swivel casting is a production part normally poured from alloy 356 by gravity tilt-pour casting process in a four-cavity mold with built-in metal cores. Photographs of the swivel head castings are shown in Figure 4.5.4. As previously described, the swivel head castings were sectioned transverse to the parting line through the 45 mm thick section of the casting and macroetched to reveal the internal quality. Photographs of the macroetched sections from alloys 206 and 535 are shown in Figures 4.5.10 (a) and (b). The sections are well grain refined, and there are no gross shrinkage porosity or inclusion defects.

(a) Alloy 206, 1.3x.

(b) Alloy 535, 1.3x.

Figure 4.5.10 *Sectioned and macroetched swivel head castings from alloys 206 and 535.*

Examples of anodized grain structure from the 19 mm (0.75 in.) thick section of the swivel-head casting from alloys 206 and 535 are shown in Figures 4.5.11(a) and (b), respectively. The estimated average grain size for alloys 206 and 535 are 75 µm and 125 µm, respectively.

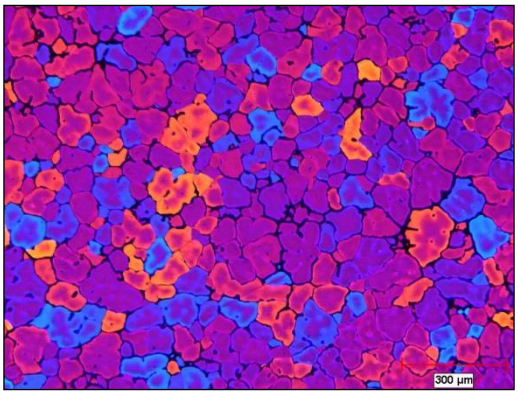

(a) Alloy 206, 50x.

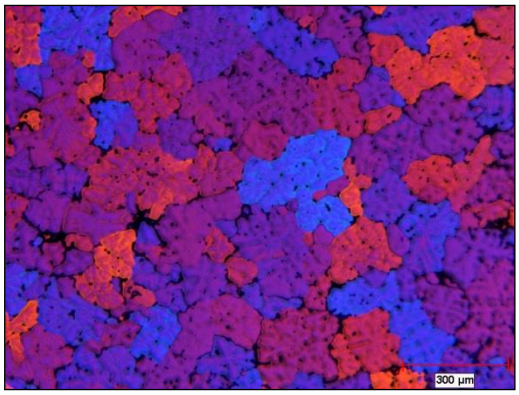

(b) Alloy 535, 50x.

Figure 4.5.11 *Anodized microstructures from grain refined swivel-head casting from alloys 206 and 535. Etched with 1.8% fluoboric acid (HBF4) in water (Barkers's anodizing method).*

Swing-Arm Component

Figures 4.5.12 (a) and (b) show examples of the microstructure at low and high magnifications from the swing arm casting shown in Figure 4.5.8. It is noted that these micrographs are in the as-cast condition. The characteristic dendritic structure is readily apparent in these figures. The grain boundary is decorated with copper-rich eutectic phase (Figure 4.5.12).

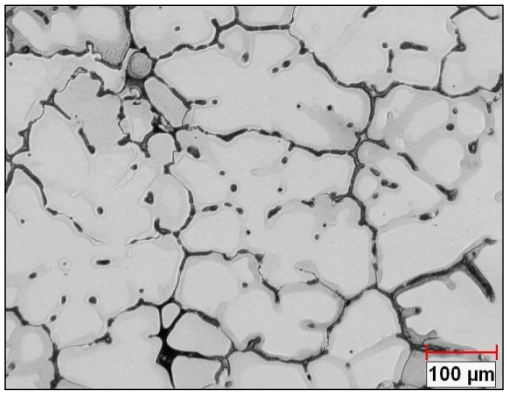

(a) B206-17, Keller's etch, 100x.

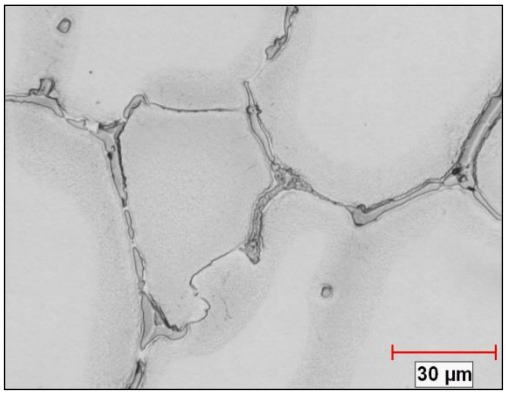

(b) B206-17, Keller's etch, 500x.

Figure 4.5.12 *Microstructures from swing arm castings.*

Examples of SEM images of the fracture surface from the swing-arm component are shown in Figures 4.5.13(a) to (d). Figure 4.5.13(a) shows the progression of hot tear along the grain boundary and also within grains. Figure 4.5.13(b), taken at higher magnification, shows the dendritic solidification structure with the eutectic phase towards the left side of the micrograph. Examples of SEM EDS spectra obtained from both the general area and the eutectic area are shown in Figures 4.5.13(c) and (d). The EDS spectra indicate strong peaks of copper, magnesium, and manganese in the eutectic area.

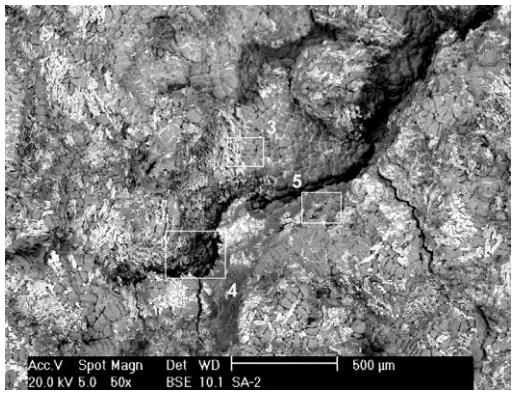

(a) SA-2, 206.0, 50x, fracture through grain boundary.

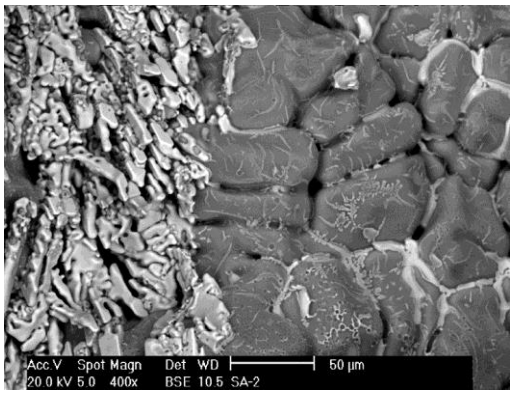

(b) same as (a) at 400x.

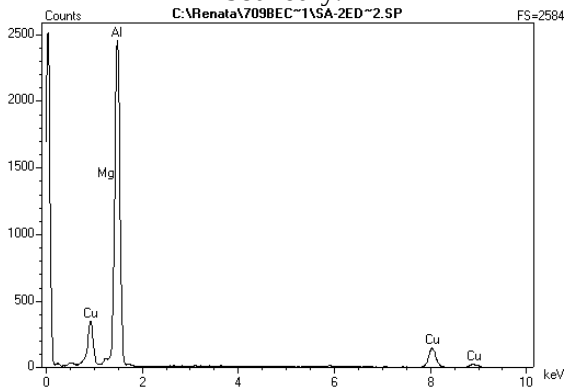

(c) SA-2, 206, EDS, general area.

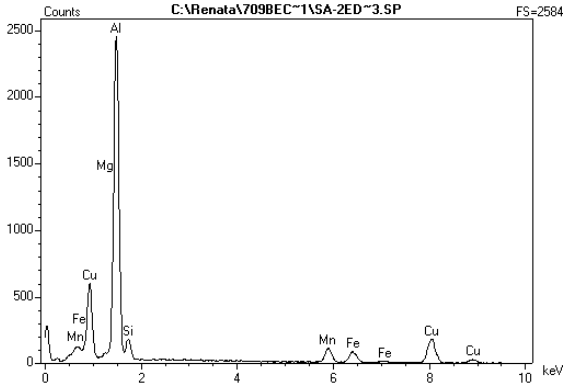

(d) SA-2, 206, EDS, eutectic area.

Figure 4.5.13 *SEM of fracture surface from swing arm casting.*

4.5.4 Control of Hot Tearing

The results from the prototype castings of both alloys has demonstrated some of the key factors that create hot tearing and also how hot tearing can be controlled. For alloys that solidify dendritically over a long freezing range, hot tearing is more prevalent close to 100 percent solid fraction because of lack of liquid metal to feed the voids created by contraction and shrinkage during solidification. It is believed that hot tearing occurs close to the solidus temperature of the alloy where the growth of the primary interlocking dendrites commonly associated with long freezing range alloys is present with some residual liquid film. The trapped residual liquid freezes progressively until the process is complete at the solidus temperature. Grain refinement improves the hot tearing resistance of A535 and A206. As observed, reduction in hot tearing after grain refinement could be associated with the break down and refinement of the interdendritic structure leading to improved feeding and a decrease in the amount of residual liquid during the last stages of solidification. There is agreement that hot tearing occurs when contraction of solidifying castings is excessively restrained by the mold or cores, and that the tears occur in the weak areas where the strain resulting from the solidification contraction is concentrated. It was shown in a recent study that hot tearing of constrained rod castings from A206.0 and A535.0 in a metal mold was improved when the mold temperature was $\geq 400°C$ (10). As the mold temperature falls below 400ºC, the castings begin to show signs of hot tearing. The hot mold provided the required thermal gradient during solidification leading to improved feeding and reduced hot tearing. It has been reported that when there is steep thermal gradient any developed shrinkage stresses is compensated for by the availability of liquid metal to fill the voids created during solidification and result in no hot tearing [6].

4.5.5 Summary and Conclusions

1. Design and Key Processing Control

CANMET-MTL has demonstrated in their casting trials that prototype components can be successfully produced from the hot tear susceptible aluminum alloys A535 (Al-Mg alloy family) and A206 (Al-Cu alloy family). Following this, production parts and industrial scale casting machines were used to try out some of the ideas that made this possible. The casting trials at two production foundries clearly show that with proper equipment and process control, engineering components can be produced successfully in permanent mold without hot tears from both alloys. For this to happen, special attention must be paid to the following:

- Casting and mold design (avoidance of sharp corners, utilization of generous tapers and draft angles, and avoidance of abrupt changes in section thickness),
- Mold coating and mold temperature,
- Effective ejector mechanism (placement and generous ejector pin allowances),
- Molten metal processing (effective degassing and grain refinement techniques),
- Processing temperatures (melting and pouring), and
- Establishment of appropriate thermal gradient (effective cooling rate control) during casting solidification.

Other considerations follow.

2. Molten Metal Treatment

- It is shown for all the casting trials that the metal must be fully grain refined to eliminate hot tearing for both alloys. This was achieved when the titanium level ranged from 0.02 to 0.26 %, with 5 to 20 ppm (estimated) boron content. However, a combination of grain refinement and

strict thermal management of the mold temperature provided the best chance for producing hot tear free castings. It is desirable to have effective degassing and removal of oxide films and other non-metallic inclusions that could lead to the formation of hot tears during solidification. The use of the reduced pressure test (RPT) technique was effective in ensuring gas-free castings.

- The five components were poured from fully degassed and fully grain refined metal. It is noted that the swing arm component incorporated filters in the feed tube and the casting ingate to ensure that only clean metal was used during the low pressure casting process.

3. Mold Coating, Mold Temperature and Casting Ejection

- Although the effect of mold coating was not specifically studied, it was demonstrated that the use of commercially available insulating and refractory coatings, and sometimes followed by a lubricating graphitic top coating to promote casting release were effective for all the castings poured.

- Control of mold temperature is very important to the production of hot tear free castings. Our results show the need to pour these hot tear susceptible alloys in hotter metal molds than normally used for A356.0 to prevent the formation of hot tearing from fully grain refined metal. Based on casting design and cooling conditions, there appears to be a minimum mold temperature at which hot tearing is less prevalent. For our casting trials, these temperatures ranged from about 350˚C to 400˚C.

- Casting ejection time must be carefully controlled to allow the casting to cool with minimum restraint in the mold before it is ejected.

4. Mold and Casting Design

- Successful production of the swing arm casting can be associated with the utilization of solidification modeling to aid mold design. The model helped in the prediction of hot spots so that appropriate thermal management of the mold could be implemented to avoid hot tearing.

- Water-cooling of the perimeter of the part opposite to the gates facilitated the creation of a strong thermal gradient and reduced solidification time that resulted in the elimination of hot tears.

- Utilization of a shell core with a hollow center provided the required core collapsibility after solidification. The incorporation of reusable steel chills within the core provided aggressive chilling in the inside radii that would have had a propensity to tear.

- Cross hatching of stress concentration locations and ejection of casting as early as possible after solidification to limit stress on the parts.

- Successful casting of the swivel and elbow components could be associated with the fact that both castings were designed without sharp corners, with generous taper, and effective ejection mechanism.

- Some challenges of producing the engine mount and rocker arm components are associated with the mold design that was not optimized for alloys A535.0 and A206.0.

4.5.2 Phase II: 4.5.2 Mounting Bracket Casting

The component selected for the casting trials is a mounting bracket used in medical equipment application which is currently produced from aluminum alloy A356 in a metal mold. The current design ensures that the alloy can be cast without hot tearing. The component requires passing grade C radiographic quality in alloy A356. The component was selected for the casting trials because of its fairly complex geometry that seems to suggest that it would be difficult to produce without hot tearing from alloys 206 and 535 by traditional production techniques. Photograph of a finished casting poured from alloy A356 is shown in Figure 4.5.14. Being a production component, no design change is allowed in the tooling design during the casting trials. Therefore, the focus of the casting trials was to establish casting processing parameters that would lead to the casting of hot tear free components using alloy 206 and 535.

Figure 4.5.14 *Bracket component poured from A356.*

4.5.2.1 Computer Simulation

A 3D model of the casting with gating system, mold halves, and cooling channels were provided in STEP format by ECK Industries. The casting was poured from two down sprues and fed by two top risers and one central blind riser located on the lower tie bar. Two thermocouples located in each mold half were instrumented for capturing the actual mold temperature and time during the casting trials. These thermocouples were located at identical locations as shown in Figures 4.5.15 and 4.5.16 in solid models of the molds.

The computer simulation of the bracket component was limited to varying selected processing parameters without making changes to the tooling. The main objective of the computer simulation was to establish and refine casting processing parameters such as: the initial mold preheating temperature, pouring temperature, mold fill time, and total die cycle dwell time from mold filling till the ejection of the cast component. The computer simulation is also capable of identifying sections of the cast component where hot tearing and shrinkage/porosity defects are likely to occur during solidification. The baseline processing parameters used for A356 were used as a starting point. Based on the pre-trial run results; refinements were made to the processing parameters such as mold preheating temperature and total die cycle time used for the casting trials. Some of the key findings from the report are that: the computer simulation results predicted areas where hot tearing and/shrinkage porosity can be expected in alloys A206 and 535.

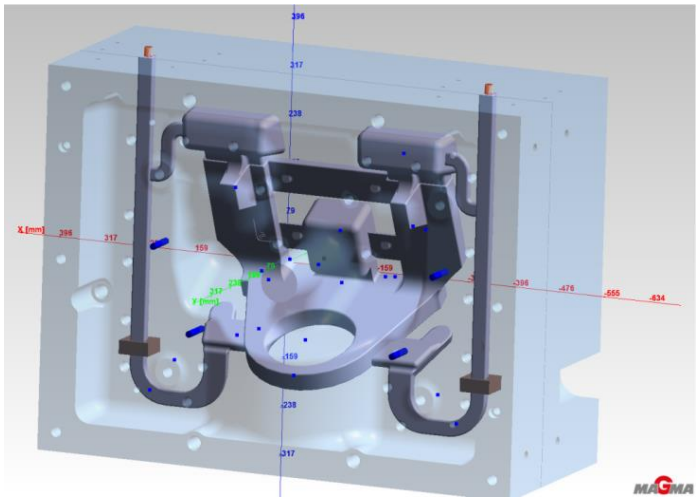

Figure 4.5.15 *Bracket casting with gating system.*

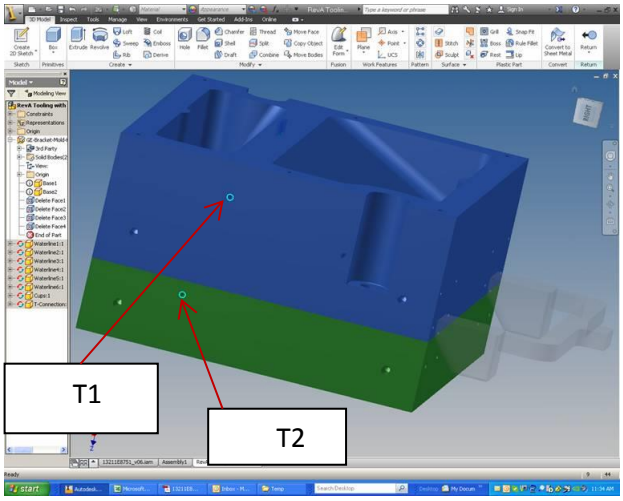

Figure 4.5.16 *Thermocouple locations for the casting trials and simulation.*
T1 and T2 are locations of thermocouples in the mold.

The preliminary computer simulation of the bracket component validated the current casting processing parameters used for alloy A356, and no hot tearing was predicted. Based on the pre-trial casting trial results, refinements were made to the processing parameters, namely the mold preheating temperature and die cycle time. Casting of the bracket component from alloy A206 was conducted at the production foundry. Following the A206 process modeling simulation, casting process modeling simulations for 535 alloys was performed and the rigging was refined to eliminate the shrinkage predicted underneath the top risers. Various iterations of casting process modeling (filling, solidification, residual stress and hot tear modeling) were run by Product Development & Analysis (PDA) LLC, and their detail reports are provided in Annexes 1 to 4, Appendix 3.

Modeling of A356

The pretrial casting processing inputs and boundary conditions for the various casting process simulations for alloy A356 are given in Table 4.5.4.

Table 4.5.4 *Processing parameters for A356*

Parameters	Comments
Cast alloy	A356 : Liquidus - 613°C; Solidus - 542°C
Pouring temperature	782°C
Pouring time:	40 sec
Permanent Mold material	4140 Steel
Mold preheating temperature at the start of the 1st cycle	482°C
Filters	Sivex FC 10 ppi
Mold coating	Dycote 8, insulating type
Water cooling bubblers	6 locations
Database	Standard Magma Database for Alloys, HTC, Cooling Water Channels
Die Cycles	Total die cycle time 325 sec, total 5 die cycles are run; stress estimated after 5th cycle (only in Iteration #3 - V06).

The key finding from A356 simulation was that for the die cycle times and processing parameters used, no hot tearing was predicted for the bracket casting. This is associated with much higher liquid fraction by volume when the die was opened and casting ejected. However, some minor shrinkage was predicted underneath the two top risers. The die cycle time was too short for complete solidification and that could lead to severe distortions. The simulation with and without mold coating indicates that the casting will have more liquid fraction with mold coating. It was established that hot tearing modeling of bracket component of A206 can be performed by using some of the processing parameters and results of the A356 casting baseline trials. Detail results of the computer simulation provided in Annex 1, Appendix 3.

Modeling of A206

The casting processing inputs and boundary conditions for the various casting process simulations for alloy A206 are given in Tables 4.5.5 and 4.5.6. A summary of the number of iterations and die cycle time are given in tables 4 and 5 for A206 and 535. Full details of the computer simulation results for A206 are provided in Annexes 2 and 3, Appendix 3.

Table 4.5.5 *Processing parameters for A206*

Parameters	Comments
Cast alloy	A206: Liquidus - 649°C, Solidus 548° C
Pouring temperature	767°C
Permanent Mold material	4140 Steel
Mold preheating temperature at the start of the 1st cycle	482°C
Filters	Sivex FC 10 ppi
Mold coating	Dycote 8, insulating type
Water cooling bubblers	6 locations
Database	Standard Magma Database for Alloys, HTC, Cooling Water Channels

Table 4.5.6 *Summary of iterations and die cycle for A206*

Iteration Number	Variables	Die Cycle
	Prerun	Total die dwell time (from the start of filling till ejection from the die) 370 or 410 sec; Total 5 die cycles are run; stress is estimated after 5th cycle.
V08	with mold coat initial mold preheat temperature of 482 C;	Closed 40 s; pour prep 20 s; pouring for 40 s; solidification/die closed 210s; die open after ejection 60 s Dwell time – 250s Total cycle time 370s Ran Filling in Cycle 5.
V09, V10 and V11	with mold coat, initial mold preheat temperature of 482C;	Closed 40 s; pour prep 20 s; pouring for 40 s; solidification/die closed 250s; die open after ejection 60 s Dwell time – 290s Total cycle time 410s Ran Filling in Cycle 5.
V12	with mold coat, initial mold preheat temperature of 460 C	Closed 40 s; pour prep 20 s; pouring for 40 s; solidification/die closed 190s; die open after ejection 60 s Dwell time – 230s Total cycle time 350s Ran Filling in Cycle 5.
V13	with mold coat, initial mold preheat temperature of 460 C; die close for 250 sec after filling – 290 sec dwell time).	Closed 40 s; pour prep 20 s; pouring for 40 s; solidification/die closed 190s; die open after ejection 60 s Dwell time – 230s Total cycle time 350s Ran Filling in Cycle 5.

Modeling of 535

The casting processing inputs and boundary conditions for the various casting process simulations for alloy 535 are given in Table 4.5.7. A summary of the number of iterations and die cycle time are given in Table 4.5.8. Full details of the computer simulation results for 535 are presented in Annex 4.

Table 4.5.7 *Processing parameters for 535*

Parameters	Comments
Cast alloy	535: Liquidus - 625°C, Solidus 478°C
Pouring temperature	777°C
Permanent Mold material	4140 Steel
Mold preheating temperature at the start of the 1st cycle	460° C used as starting value.
Filters	Sivex FC 10 ppi
Mold coating	Dycote 8, insulating type
Water cooling bubblers	6 locations
Database	Standard Magma Database for Alloys, HTC, Cooling Water Channels
Die Cycles	Dwell time of 290 sec; total 5 die cycles are run; stress is estimated after 5th cycle till 100% solidified.

Table 4.5.8 *Summary of iterations and die cycle for 535*

Iteration Number		Die Cycle
V15	with mold coat, initial mold preheat temperature of 460 C;	Closed 40s; pour prep 20s; pouring 40s; solidification/die closed 250s; die open after ejection 60s; Dwell time 290s; Total cycle time 410s;

4.5.2.2 Simulation Results

Alloy A206 Prerun

At pouring temperature of 767°C, die cycle dwell time of 310 or 350 sec and mold preheating temperature of 482°C, hot tearing was predicted as shown below in Figure 4.5.17. It was observed that towards the end of solidification, hot tearing develops in the top post to journal transition areas.

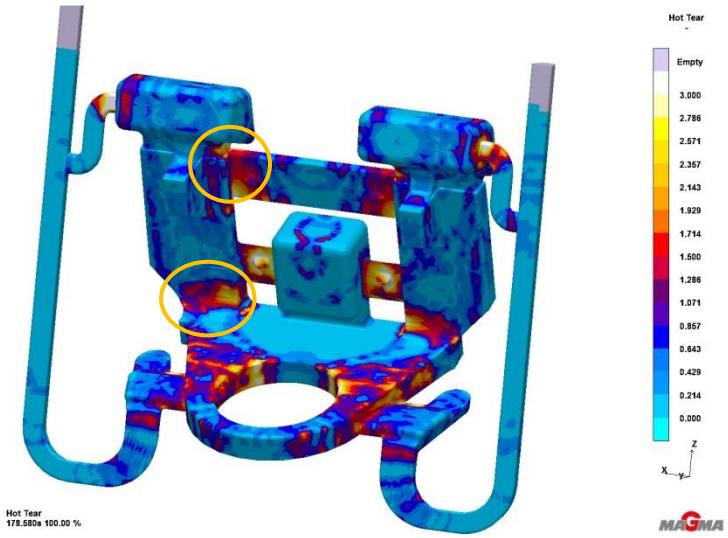

Figure 4.5.17 *Hot tearing predicted in the cross bracket.*

The mechanical hot tearing appears to be driven by the amount of solid fraction % at the time of casting ejection. This is controlled by the dwell time. When the dwell time was longer, hot tearing was found to be pronounced when the solid fraction is around 75% to 90%. The mechanical hot tearing predicted in Figure 4.5.17 at the cross members was noticed while the casting was still in the mold and at the time of ejection from the casting. However, the hot tearing predicted in the top post transition to the journal occurred during cooling to 100% solidified stage after ejection. At higher mold temperature of 482°C the predicted and actual hot tearing found was severe. On the other hand when the casting was ejected with lower solid fraction in the range of 45 to 65% at a dwell time of 310s, no hot tearing was predicted. The lack of hot tearing was due to the presence of liquid metal to feed solidification shrinkage. However, caution should be exercised during casting ejection from the die to avoid mechanical damage that can induce hot tearing. It was shown that longer dwell time increased the hot tearing tendency mainly due to the constraint imposed by the metal mold. The computer simulation results correlated with the actual pre-trial casting results. Figures 4.5.18 and 4.5.19 show the hot tearing found in castings #12 and #10 respectively during from A206 pre-casting trials, which was poured during initial mold pre-heating temperature of 482°C.

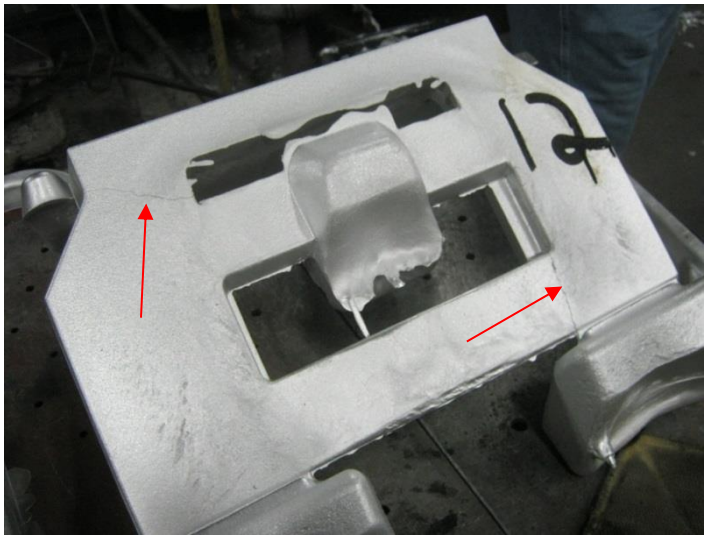

Figure 4.5.18 *Casting #12 showing hot tearing location in the upper cross member junctions.*

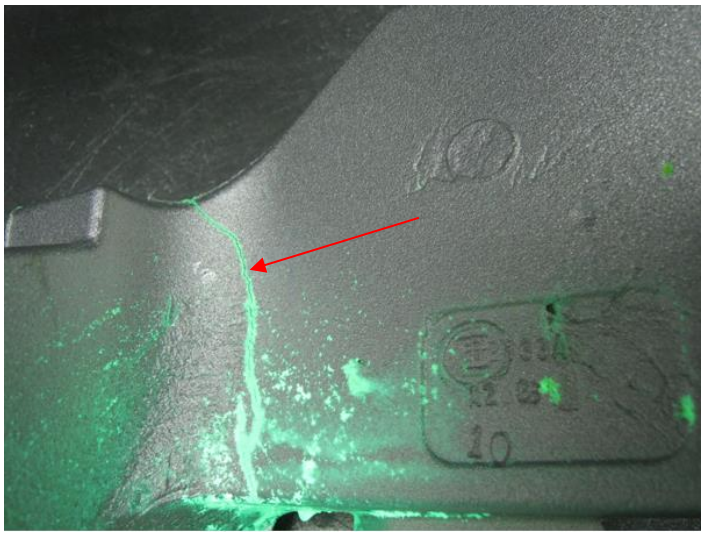

Figure 4.5.19 *Casting #10 showing hot tearing in the transition from the post to the journal area.*

Process Optimization

Alloy A206

Based on the pre-run simulation and casting trial results, following processing parameters were used to simulate the production trials: the pouring temperature; 767°C; initial mold pre-heating temperature of 460°C; and die dwell cycle time of 290 seconds. The predicted hot tearing at the top cross bar and shrinkage below the top risers are shown in Figures 4.5.20 and 4.5.21 respectively. It is observed that the hot tearing and shrinkage defects are relatively minor for this mold temperature and die dwell time.

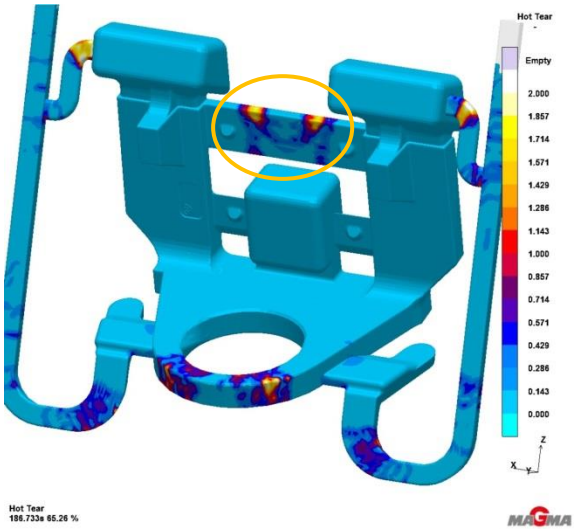

Figure 4.5.20 *Minor hot tearing tendencies at the top cross bar.*

Figure 4.5.21 *Minor secondary shrinkage predicted underneath top risers.*

Apart from hot tearing prediction, mold filling and solidification conditions were also evaluated. Figures 4.5.22 (a) and (b) show examples of mold filling result based on iteration V08 shown in Table 4.5.7. The computer simulation predicted an ingate velocity greater than 0.5 m/sec. This is not desirable as this could lead to the generation of oxide films inclusion in the casting. The gating system should be modified by using of wider tangential ingates to reduce metal velocity and splashing during mold filling.

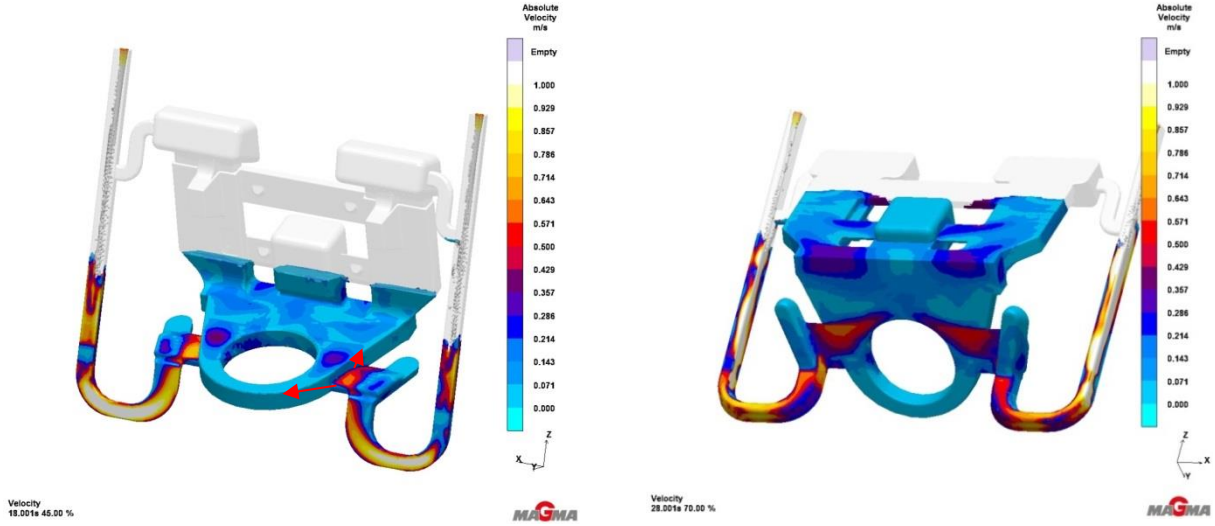

(a) Front. (b) Back.

Figure 4.5.22 *Example of mold filling results.*

Figure 4.5.23 shows examples of solidification results after 70% and 80% volume solidified. The results show potential areas where contraction stresses can be expected during solidification and this could lead to mechanical hot tearing. Considering the 70% volume fraction solidified, the rest was either liquid or in mushy stage when the die was opened 210 seconds after filling. Considering 80% volume fraction solidified, the rest was either liquid or in mushy stage when casting was ejected 270 seconds after solidification. Figure 4.5.24 shows predicted areas where solidification shrinkage can be expected. The shrinkage can be eliminated by increasing the riser contacts at the three locations. Alternately, using of cylindrical instead of rectangular risers for better feeding modulus can improve feeding. The predicted maximum principal total stresses and strains after solidification are shown in Figures 4.5.25(a) and (b) respectively. The predicted areas with mechanical hot tearing just before die opens towards the tail end of solidification, when maximum stresses due to die constraints are expected are shown in Figure 4.5.26. Detailed modeling results are provided in Annexes 2 and 3, Appendix 3.

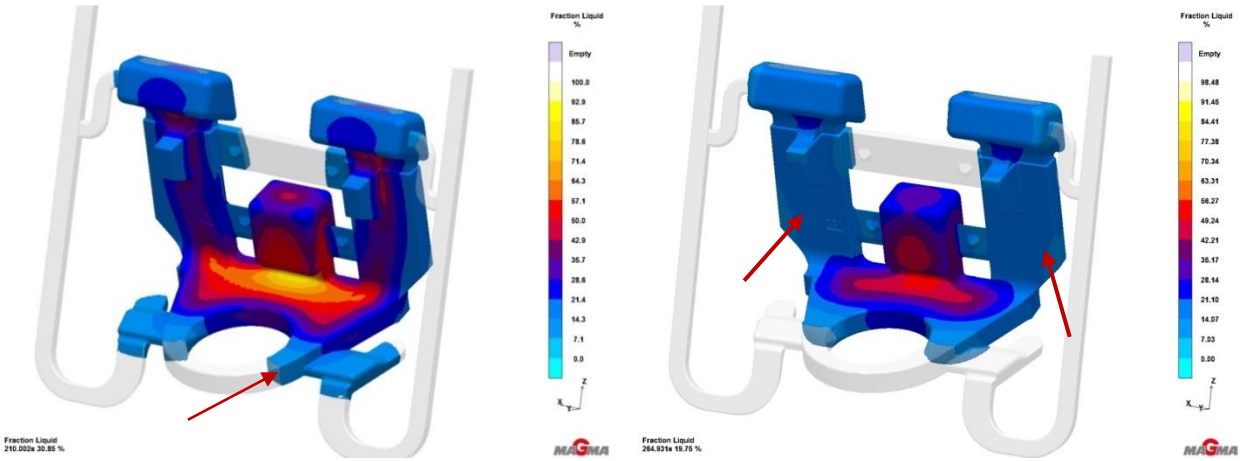

(a) 70% volume solidified, t=210 sec. (b) 80% volume solidified, t=270 sec.

Figure 4.5.23 *Potential areas where contraction stresses can develop and promote mechanical hot tearing are shown by the arrows.*

Figure 4.5.24 *Areas where minor shrinkage is predicted when die opens*.

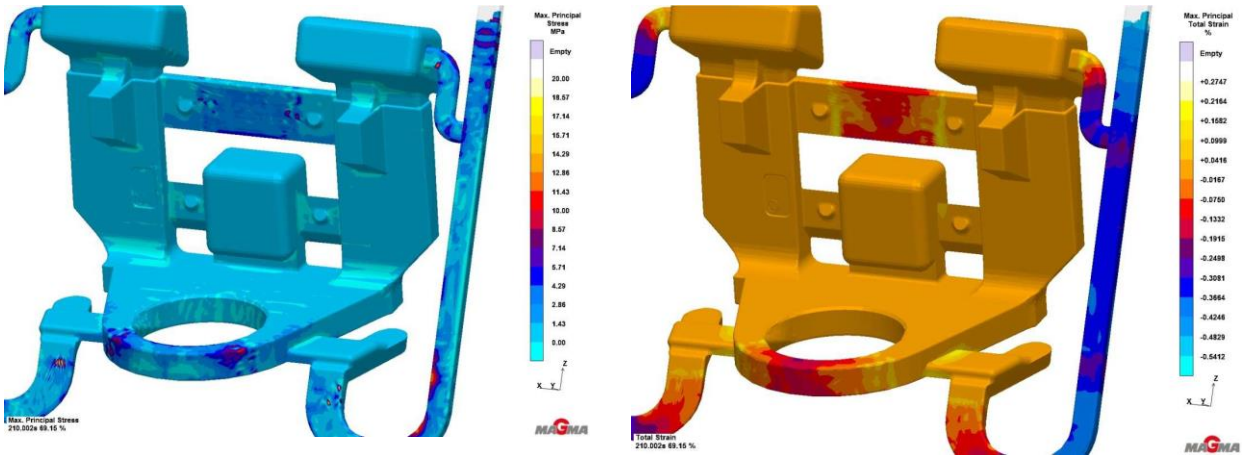

(a) Maximum principal stress. (b) Maximum principal strain.

Figure 4.5.25 *Predicted maximum principal stress and maximum principal strain when die was opened after 120 seconds.*

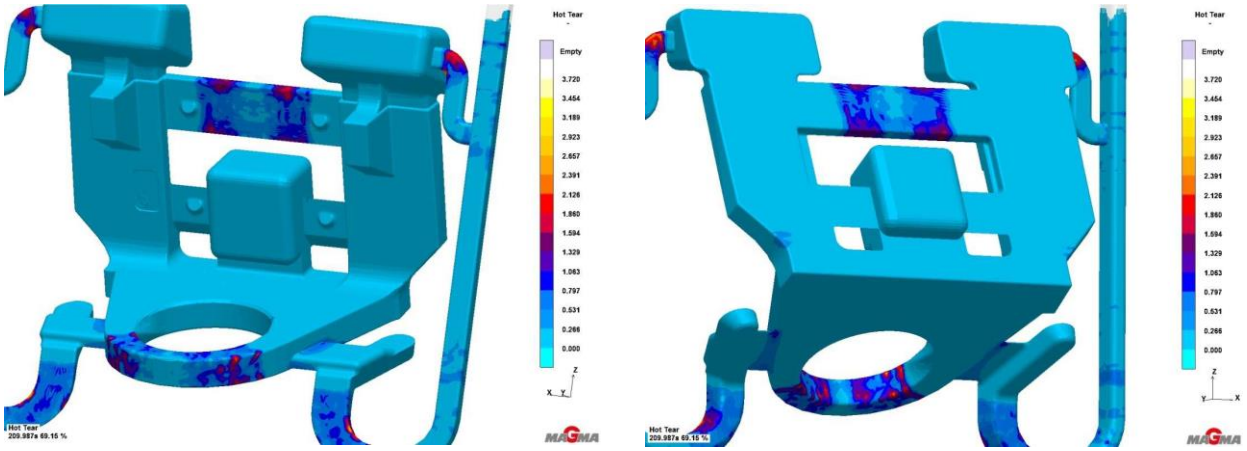

(a) Front. (b) Back.

Figure 4.5.26 *Predicted areas where hot tearing will develop towards the end of solidification*.

Alloy 535

Only one iteration (V09; Table 4.5.8) was simulated for alloy 535; the predicted hot tearing and shrinkage during solidification locations are shown in Figures 4.5.27 and 4.5.28. The selected initial preheating mold temperature was 460°C and die cycle dwell time was 290 sec; other boundary conditions are reported in Table 4.5.7. Figure 4.5.27 shows that hot tearing can be expected during cooling after casting ejection from the die when the component was 90% solidified. A minor hot tearing is also predicted at the time of casting ejection in the lower cross member to riser junction. Figure 4.5.28 shows predicted minor shrinkage below the right top riser that was not insulated. The left side insulated riser provided effective feeding with no secondary shrinkage. This prediction result confirms the well-known fact that riser insulation can contribute to improved casting soundness especially, when there is constraint from casting design and tooling to increase riser size. Detailed results of the computer simulation are provided in Annex 4, Appendix 3.

.

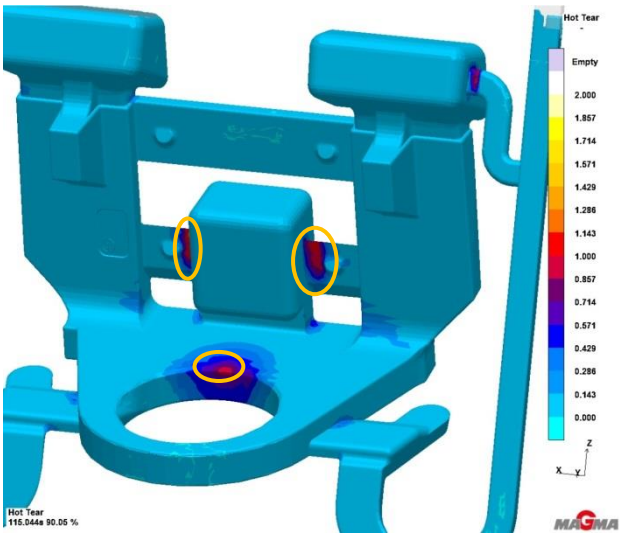

Figure 4.5.27 *Minor hot tearing tendencies at the bottom cross bar.*

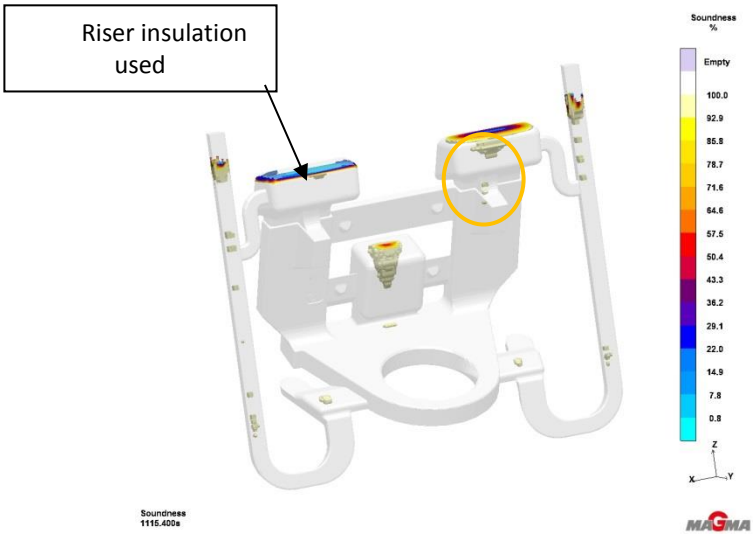

Figure 4.5.28 *Minor secondary shrinkage predicted underneath un-insulated top riser.*

4.5.2.3 Summary and Conclusions

1. The predicated hot tearing locations of A206 bracket component correlated with observed hot tearing locations during the casting trials.

2. In A206, mechanical hot cracking seems to develop when the fraction solid is in the range from 75 to 90%. In some cases, it can develop after ejection while casting is solidifying. Increased initial mold preheating temperature over 480°C, tends to lead to more severe mechanical hot tearing.

3. The extent of hot tearing is less when the casting has lower fraction solid ranging from 65 % to 75 %. This is due mainly due to the presence of liquid metal available to feed solidification shrinkage.

4. A die cycle dwell time of over 290 seconds seems to produce more severe hot tearing, mainly due to the constraint of the metal mold. Therefore, dwell cycle time of 200 to 230 seconds and mold preheating temperature from 460°C to 480°C provided the best results.

5. The areas prone to mechanical hot cracking is driven by the casting design related to variation in section thickness that could cause premature solidifications in some areas of the component. Controlled localized heating elements in those hot spots of the mold can reduce the hot tearing.

6. The minor shrinkage predicted underneath the two top risers and the junctions, if not desirable, can be eliminated by either redesigning of the risering system, using cylindrical insulating risers with increased contact or insulating the current top risers.

7. The risering system design of the bracket casting can be optimized to eliminate shrinkage. The presence of secondary shrinkage in 535 was eliminated by iteration with an insulated top riser. Secondary shrinkage may contribute to the hot tearing tendency.

8. Hot tearing, though predicted in the journal areas, was not seen in the actual casting trial results; which needs to be further investigated.

9. Gating system needs to be redesigned such to reduce the in-gate velocity below 0.5 m/sec to eliminate the risk of oxide inclusions in the casting.

4.5.2.4 Casting Trials

Mold Preparation

The mold was preheated by gas torch and coated using Dycote 8 because of its good insulating and refractory properties. The mold temperature was measured at two locations by two thermocouples (TC) placed inside the molds. Also two infrared (IR) pyrometers were used to measure the mold surface temperatures at two locations. Thermocouples TC1 and TC2 were located respectively in the top and bottom of the moving half of the mold to measure the internal die temperatures. The thermocouples were each about 19 mm depth from the die cavity surface. TC1 was located closer to the pouring cups than TC2. The die surface temperature between the two risers was measured by IR#3.The surface temperature that produces the flange under the hoop section of the casting was measured by IR#4. Figures 4.5.29 to 4.5.31 show the location of the thermocouples and infrared pyrometer spots in the mold.

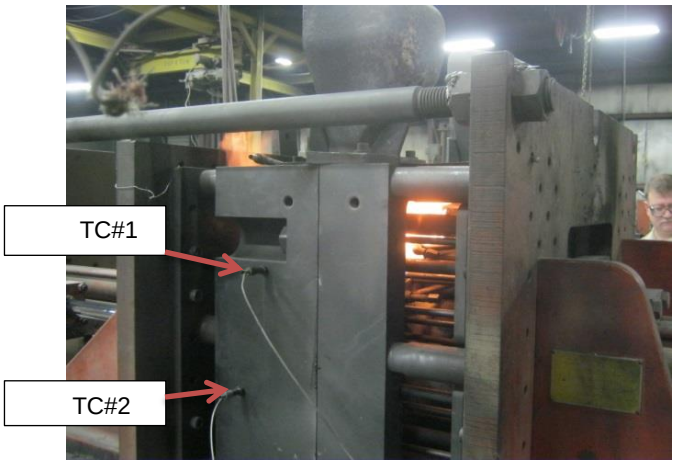

Figure 4.5.29 *Closed mold showing location of the two thermocouples.*

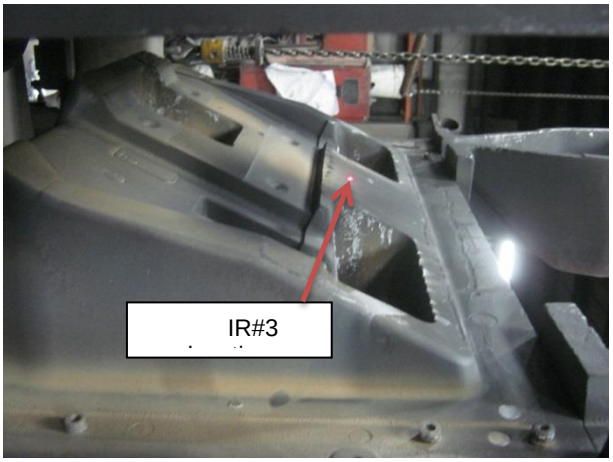

Figure 4.5.30 *Spot where mold surface temperature (IR #3) was measured, near the pouring cup.*

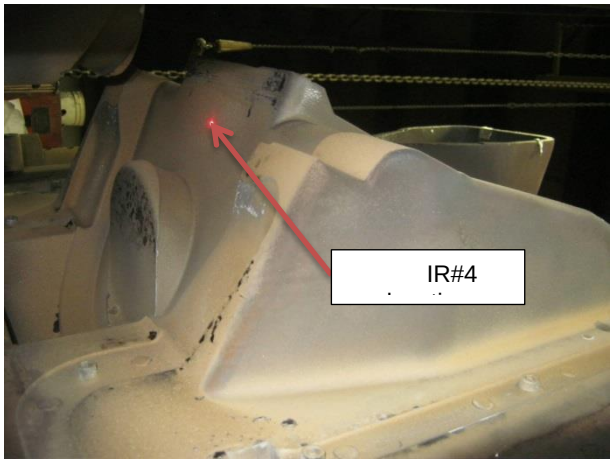

Figure 4.5.31 *Spot where mold surface temperature (IR #4) was measured, flange under the hoop section.*

Melting and Casting

Commercial purity ingots of aluminum alloys 206 or 535 were melted using a gas fired furnace. The charge size was 227 kg. The charge materials were fully grain refined using Ti-B master alloy. The dissolved hydrogen was evaluated by the RPT technique to ensure gas free metal before pouring the castings. The metal temperature was measured by thermocouple immersed in the molten metal and samples for chemical analysis were obtained during the casting trials.

In the preliminary casting trial, twelve components were poured from alloy A206 using a gravity tilt-pour casting machine. The weight of the component with its gating system was about 20 kg and finished weight of about 9 kg. The first three castings were used to warm up the mold to operating temperature and discarded. In general, the mold cavity was filled but surface shrinkage (depressions) was noted in the castings poured. The casting dwell time tried were 270, 290, and 300 seconds. Majority of the castings were poured at 290 seconds dwell time. There was no hot tearing in castings 4, 5, and 6. The mold temperatures from TC1 ranged from 476ºC to 489ºC. There was hot tearing in castings 7 to 12. The mold temperature from TC1 ranges from 498ºC to 530ºC. There appears to be a mold temperature range above which hot cracking can become significant. Additional details on the preliminary trial results are given in Appendix 4.

Following the preliminary casting trials, the bracket component was poured using alloys with different variations of alloys 206 and 535: A206-1 (primary ingots), A206-2 (50% primary ingots + 50% in-house revert), B206 (primary ingots), and 535 (primary ingots). In all fifty two (52) castings were poured, 13 castings each per alloy variation. Using the pre-trial casting results as a guide, the computer simulation trials with this observed hot tearing performance showed that even further reduction in cycle time (by way of dwell time reduction) was desirable and therefore, the machine dwell time used for each of the cast component was set at 230 seconds. A visual examination of each casting was conducted to detect any surface defects such as hot tearing or cracking. Seventeen castings were evaluated using dye penetrant and X-ray radiography, the standards normally used by the production foundry for this component when poured from alloy A356. Two tensile blanks were sectioned from selected castings to evaluate the mechanical properties of the component.

4.5.2.5 Casting Trial Highlights

Chemical Composition

The chemical composition and Aluminum Association (AA) composition specification for the alloys are shown in Tables 4.5.9 to 4.5.11. The compositions fall within specification.

Table 4.5.9 *Chemical analysis of alloy A206*

Alloy	Composition, Wt. %							
	Si	Fe	Cu	Mn	Mg	Ni	Zn	Ti
AA Spec	0.05 max	0.10 max	4.2 - 5.0	0.20 - 0.50	0.15 - 0.35	0.05 max	0.10 max	0.15 - 0.30
A206-1	0.0481	0.0397	4.83	0.397	0.271	0.0088	0.0164	0.184
A206-2	0.0425	0.0344	4.56	0.357	0.176	0.0020	0.0207	0.190

Table 4.5.10 *Chemical analysis of alloy B206*

Alloy	Composition, Wt. %							
	Si	Fe	Cu	Mn	Mg	Ni	Zn	Ti
AA Spec	0.05 max	0.10 max	4.2 - 5.0	0.20 - 0.50	0.15 - 0.35	0.05 max	0.10 max	0.10 max
B206	0.0476	0.0641	4.60	0.306	0.185	0.0026	0.0095	0.098

Table 4.5.11 *Chemical analysis of alloy 535*

Alloy	Composition, Wt. %						
	Si	Fe	Cu	Mn	Mg	Zn	Ti
AA Spec	0.15 max	0.15 max	0.05 max	0.10 - 0.25	6.2 - 7.5	-	0.10 - 0.25
535	0.073	0.061	0.028	0.169	6.760	0.018	0.198

Evaluation of Bracket Component

Overall, visual observation of the casting quality was similar to that normally obtained from A356 poured in the same mold. The mold temperatures used for alloys 206 and 535 were higher than normally used for alloy A356. The surface shrinkage in the castings is associated with the casting geometry that was not optimized for alloys 206 and 535. For casting and tooling optimized for alloys 206 and 535, the shrinkage observed could be avoided. The castability of A206 alloy with 50% primary and 50% in-house scrap was not observed to be different from the primary metal, as the charge material was similar to that castability observed for A206 and B206 100% virgin primary ingots.

Photographs of a bracket component with gating system and finished casting are shown in Figures 4.5.32 and 4.5.33 respectively. Hot tearing was not observed visually on the casting surface. However, surface shrinkage (depressions) in the area marked in Figure 4.5.33 was present in all the castings poured due to component geometry. The dye penetrant inspection and X-ray radiography of the seventeen castings show the presence of shrinkage through the section thickness. The dye penetrant inspection also shows the presence of hot tearing in two castings that were not seen during visual examination. The X-ray radiography images and dye penetrant inspection show the visual surface depression shown in Figure 4.5.33. Examples of X-ray radiography from components poured from alloys 206 and 535 are shown in Figures 4.5.34 (a) and (b). Based on the results of X-ray radiography and dye penetrant inspection, all the castings were rejected due to shrinkage. The result shows that there was lack of proper feeding of the

component during solidification where the surface shrinkage was observed. It is recalled that the mold and its gating system was not optimized for alloys 206 and 535. It is expected that the shrinkage problem can be eliminated by providing adequate risers in an improved component design to promote directional solidification.

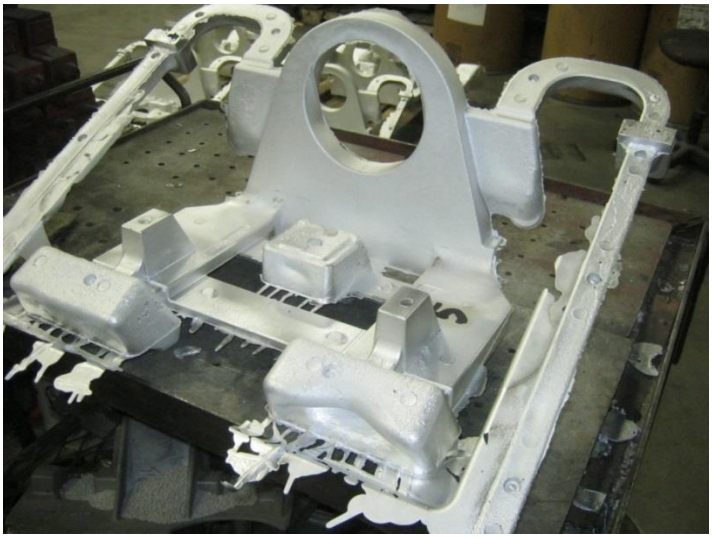

Figure 4.5.32 *Photograph of casting with gating system.*

Figure 4.5.33 *Photograph of finished component.*

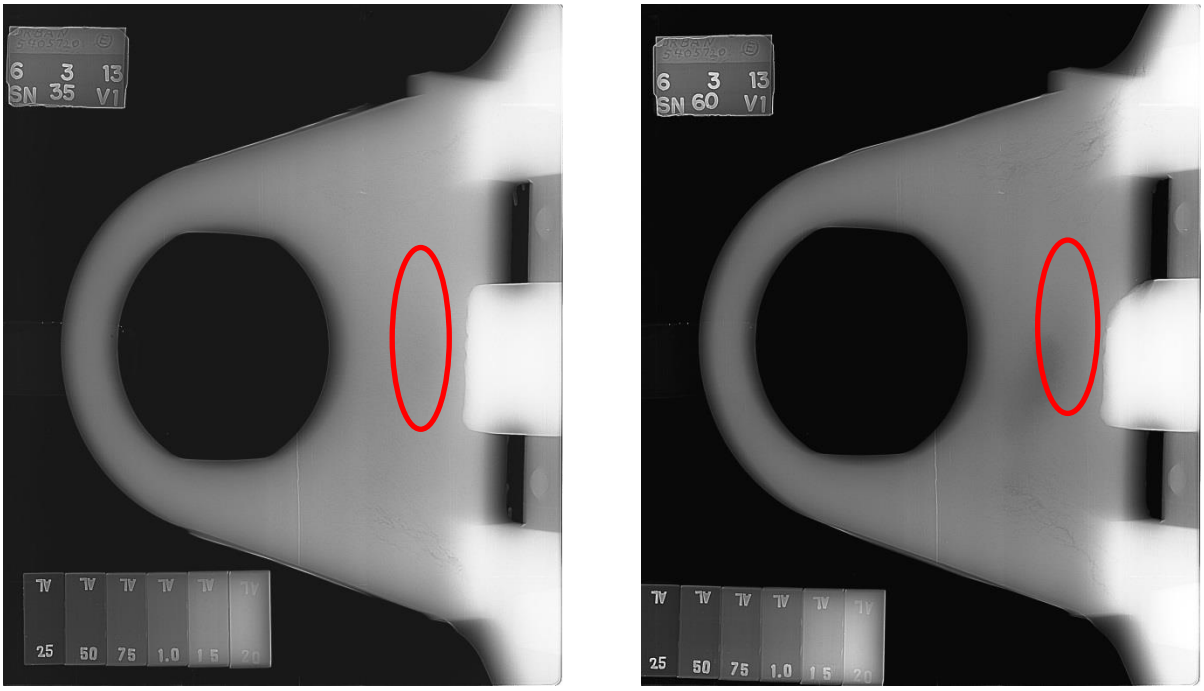

(a) SN 35, A206. (b) SN 60, 535.

Figure 4.5.34 *Examples of X-ray radiographs showing area where surface shrinkage was observed.*

Casting Processing Parameters

The casting processing parameters are summarized in Tables 4.5.12 to 4.5.15. The mold and pouring temperatures are plotted in Figures 4.5.35 to 4.5.38. The mold surface temperatures at two locations were measured by IR#3 and IR#4. The following observations are made from the casting processing parameters. The mold temperatures from TC#1 and IR#3 are usually higher than from TC#2 and IR#4 because of their location in the mold. It was observed that majority of the castings were free of hot tearing during the casting trials. However, in situations where the mold temperatures in certain sections of the mold were close to or higher than 500°C, some castings broke on ejection from the mold. For example, casting #28 poured from A206 broke on ejection from the mold, and the highest temperature measured by TC#1 was 502°C. Casting #32 also broke on ejection from the mold. The temperature readings from TC#1, IR#3 and IR#4 were all above 500°C. In this particular case, the temperature reading from IR#4 was as high as 543°C. To lower the mold temperature, the cooling water flow rate was turned to its highest level. Subsequent castings poured in the colder mold were free of cracking or visible hot tearing. Casting #41 poured from B206 also broke on ejection and the mold surface temperature from IR#4 was 527°C. The mold cooling water flow rate was increased to its maximum level to lower the mold temperature. As observed in the preliminary casting trials, there appears to be a mold temperature range above which mechanical hot cracking can become significant.

The application of mold coating during the casting trial was effective in controlling hot cracking by helping with mold temperature control. For example, it was observed that both riser pocket bottoms were visually red hot during the casting trial but there was no thermocouple located in the area of the die. To control the mold temperature, die coat and top graphite coatings were applied before the next castings were poured and this controlled the cracking. None of the castings poured from alloy 535 show hot tearing or broke on ejection. This is consistent with previous observations that hot tearing in less severe in alloy 535.

These results show that mold temperature is one of the important processing parameters, and that there is mold temperature range above which mechanical hot cracking can become significant. The locating of thermocouples at appropriate section of the mold and the implementation of effective thermal management of the mold by cooling is critical to the casting of hot tear free components.

Although promotion of directional cooling is necessary to avoid hot tearing, and this can be achieved by targeted heating and cooling of the mold areas. However, high spikes in the mold temperature in certain locations especially close to hot spots in the mold could result in mechanical hot tearing as observed during the casting trials. Even though higher temperatures in hot spot can promote directional solidification but longer solidification times makes the casting vulnerable for cracking during ejection.

Table 4.5.12 *Processing temperatures from thermocouples and infrared pyrometer for A206-1*

Casting Number	Pouring Temp. (°C)	TC - Mold Temp. (°C)		IR - Mold Surface Temp. (°C)	
		#1	#2	#3	#4
13	802	472	441	488	416
14	793	477	441	482	427
15	783	488	443	510	432
16	777	507	456	510	441
17	774	507	454	504	438
18	772	523	466	516	449
19	774	519	471	510	449
20	776	506	477	510	454
21	769	504	485	510	452
22	764	489	476	493	438
23	766	516	484	499	454
24	776	529	485	510	441
25	776	536	487	499	443
AVG	777	506	467	503	441
STD	10	20	18	10	11

Table 4.5.13 *Processing temperatures from thermocouples and infrared pyrometer for A206-2*

Casting Number	Pouring Temp. (°C)	TC - Mold Temp. (°C)		IR - Mold Surface Temp. (°C)	
		#1	#2	#3	#4
28	772	502	363	460	482
29	771	505	395	493	513
30	772	514	403	504	527
31	773	517	438	499	538
32	774	517	449	510	543
33	769	513	410	499	463
34	763	515	386	499	438
35	767	520	376	499	438
36	780	518	369	504	443
37	785	518	365	-	-
38	772	522	367	510	435
39	-	520	363	516	432
40	-	508	350	496	418
AVG	772	515	387	499	472
STD	6	6	31	14	46

Table 4.5.14 *Processing temperatures from thermocouples and infrared pyrometer for alloy B206*

Casting Number	Pouring Temp. (°C)	TC - Mold Temp. (°C)		IR - Mold Surface Temp. (°C)	
		#1	#2	#3	#4
41	768	483	423	510	527
42	771	494	432	499	488
43	769	502	390	504	463
44	764	512	374	510	463
45	766	516	366	518	452
46	772	514	364	527	452
47	777	521	362	521	443
48	773	518	358	510	438
49	771	504	347	507	427
50	778	507	334	504	432
51	-	509	353	510	435
52	-	512	356	510	443
53	-	514	358	506	439
AVG	771	508	371	511	454
STD	4	11	28	8	27

Table 4.5.15 *Processing temperatures from thermocouples and infrared pyrometer for alloy 535*

Casting Number	Pouring Temp. (°C)	TC - Mold Temp. (°C)		IR - Mold Surface Temp. (°C)	
		#1	#2	#3	#4
54	779	483	429	496	474
55	771	489	427	491	466
56	771	497	387	488	438
57	773	483	362	488	427
58	771	500	351	485	418
59	763	488	341	485	418
60	768	502	342	491	418
61	778	503	339	491	421
62	777	506	342	488	410
63	768	498	343	491	421
64	764	502	343	493	416
65	772	503	342	491	416
66	766	504	343	493	416
AVG	771	497	361	490	428
STD	5	8	33	3	20

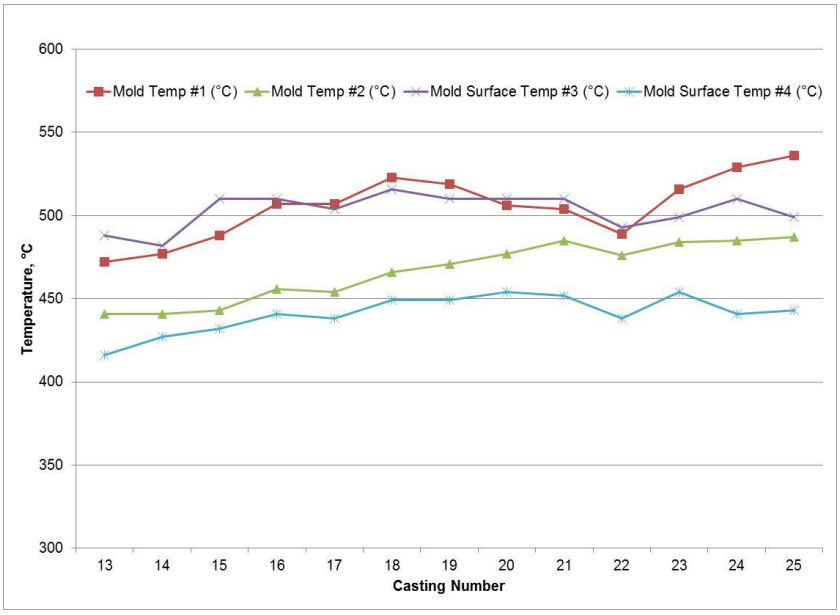

Figure 4.5.35 *Mold and pouring temperatures from melt A206-1.*

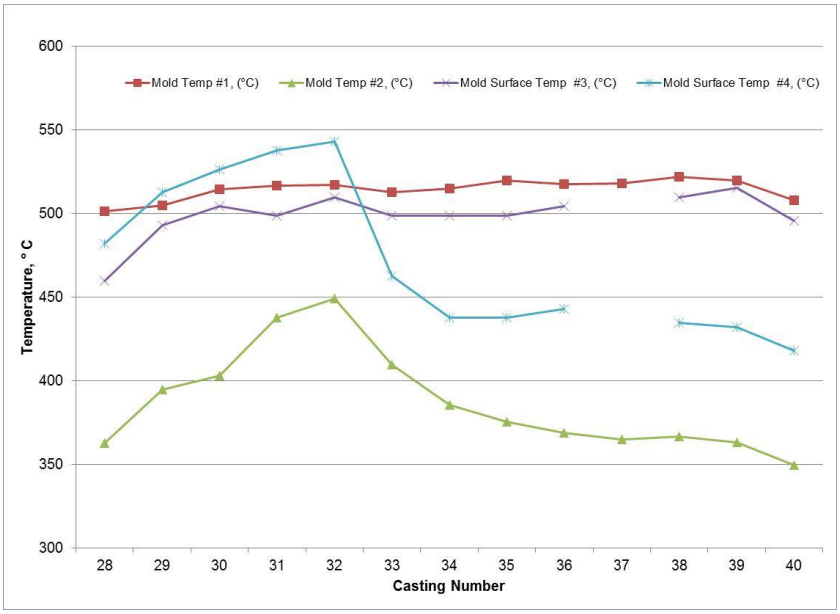

Figure 4.5.36 *Mold and pouring temperatures from melt A206-2.*

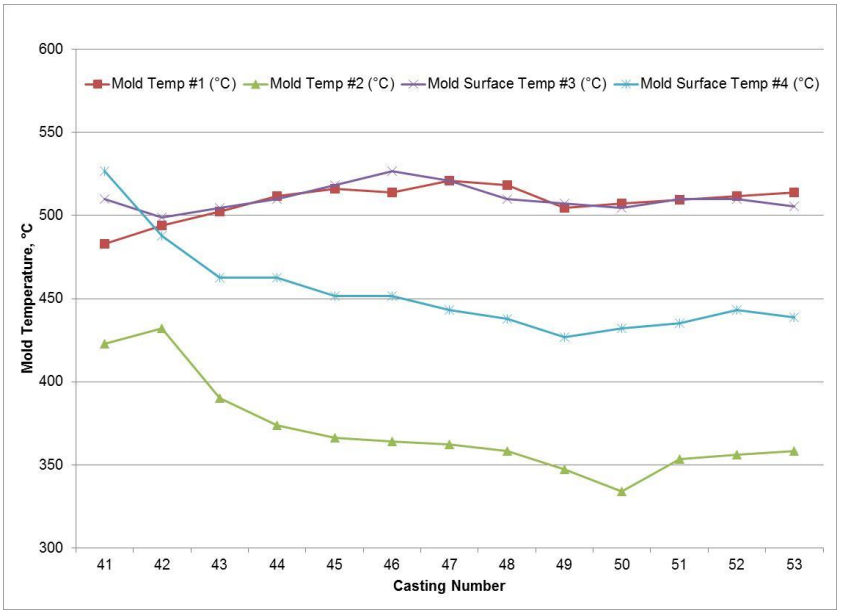

Figure 4.5.37 *Mold and pouring temperatures from melt B206.*

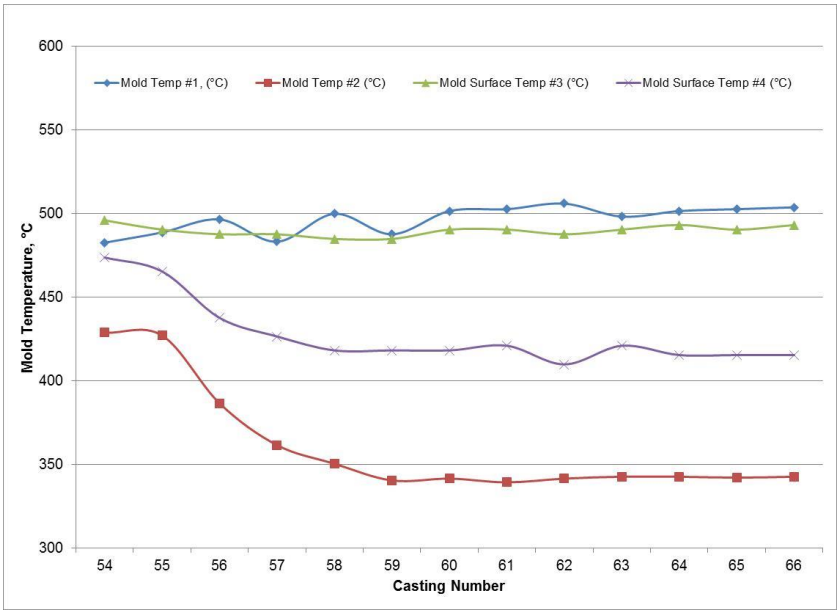

Figure 4.5.38 *Mold and pouring temperatures from melt 535.*

4.5.2.6 Microstructures from Selected Bracket Components

The bracket component was sectioned through the riser located on the lower tie bar. The samples for microstructure evaluation were sectioned from locations A and B in Figure 4.5.39. The thickness of sections A and B are 34 mm and 13 mm respectively and correspond with the thickest and thinnest section of the casting. The surface shrinkage (depression) in location A that is directly under the riser on the lower tie bar is readily apparent. The areas where shrinkage is observed are marked in the photographs.

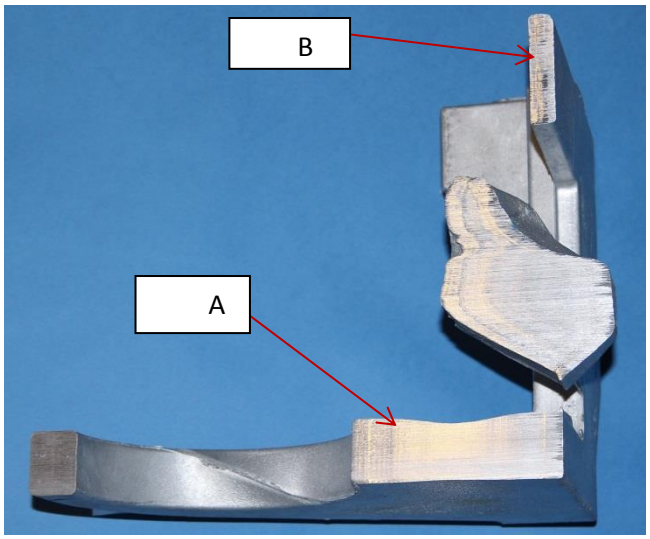

Figure 4.5.39 *A sectioned casting showing locations A and B where samples for microstructure evaluation were removed.*

Examples of unetched microstructures from sections A and B of selected bracket components poured from alloys A206 and 535are shown Figures 4.5.40 and 4.5.41. As would be expected the shrinkage defect in section A is more severe than in the thinner section B. The shrinkage observed in B206 is similar to that shown for A206 and 535.

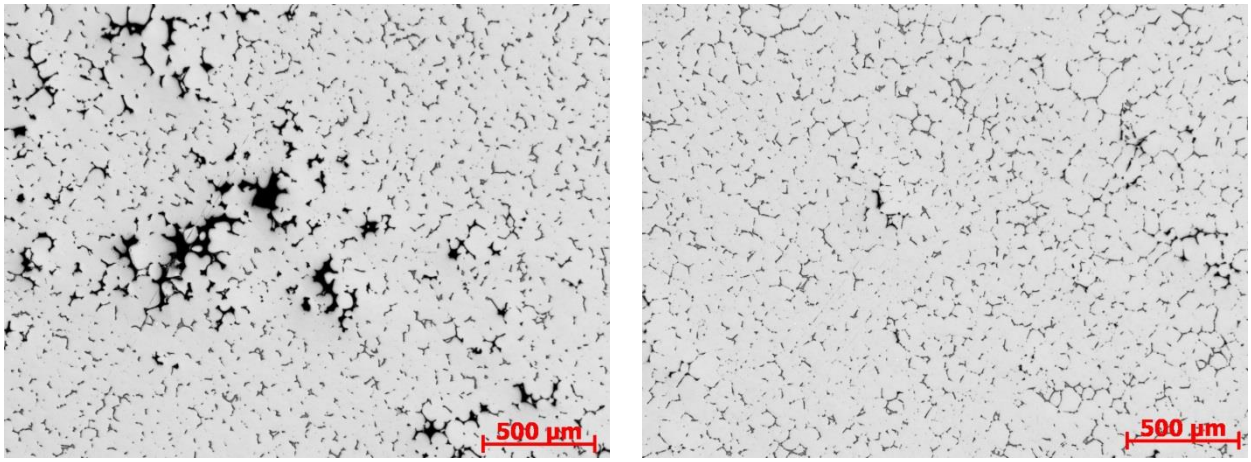

(a) Casting 35, location A, 50x. (b) Casting 35, location B, 50x.

Figure 4.5.40 *Unetched as-cast microstructures from component #35 alloy A206.*

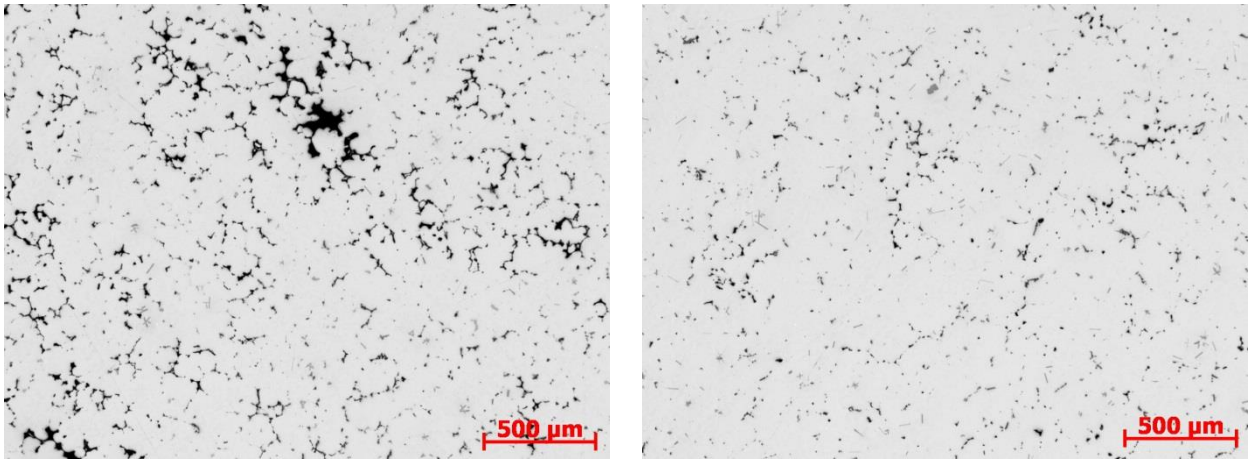

(a) Casting 64, location A, 50x. (b) Casting 64, location B, 50x.

Figure 4.5.41 *Unetched as-cast microstructures from component #64 alloy 535.*

Examples of etched as-cast and heat treated microstructures at low and high magnifications from bracket component poured from alloys A206, B206, and 535 are shown Figures 4.5.42 to 4.5.45. The relatively fine grain structure from sections A and B that are 34 mm and 13 mm in thickness shows the effectiveness of the grain refiner. This is more apparent at lower magnification. For the as-cast samples, a copper-rich eutectic phase ($CuAl_2$) is present at the grain boundary. This eutectic phase along the grain boundary is readily observed at higher magnification shown in Figures 4.5.42(b) and (d) and Figures 4.5.43 (b) and (d). After solution heat treatment, the eutectic phase in Figures 4.5.42 and 4.5.43 were broken down and replaced with fine precipitates of $CuAl_2$ phase along the grain boundaries and within the grains as shown in Figures 4.5.44 (b) and (d). The relatively fine grain structure is also readily apparent in the heat treated samples from alloy B206 shown in Figures 4.5.44 (a) and (c). Figures 4.5.45(a) and (c) show similar fine grain structure from alloy 535.

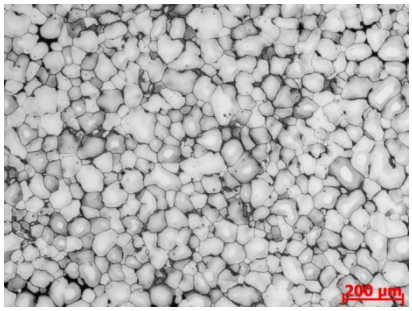

(a) Casting #35, Location A, 100x.

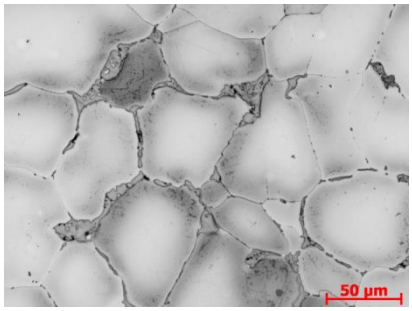

(b) Casting #35, Location A, 500x.

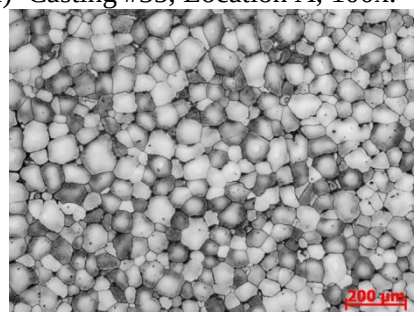

(c) Casting #35, Location B, 100x.

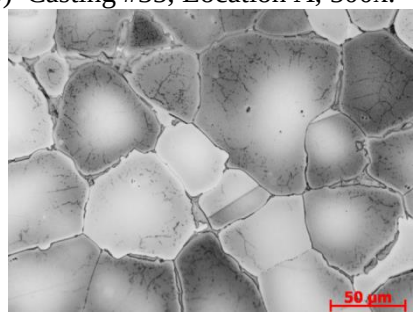

(d) Casting #35, Location B, 500x.

Figure 4.5.42 *As-cast microstructures from component #35 alloy A206.*

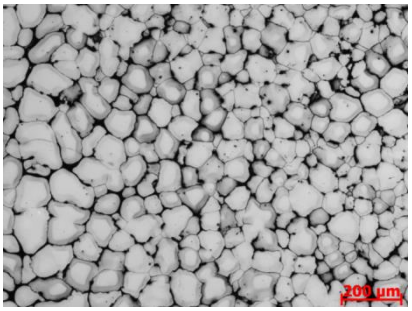

(a) Casting #44, Location A, 100x.

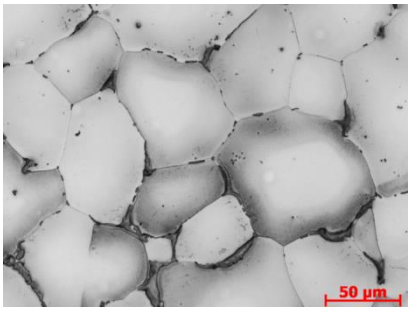

(b) Casting #44, Location A, 500x.

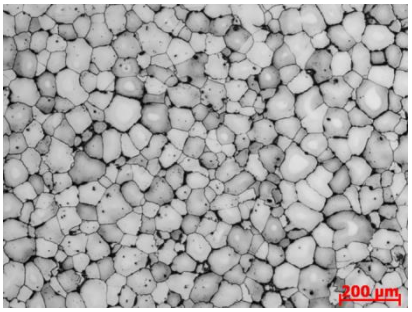

(c) Casting #44, Location B,100x.

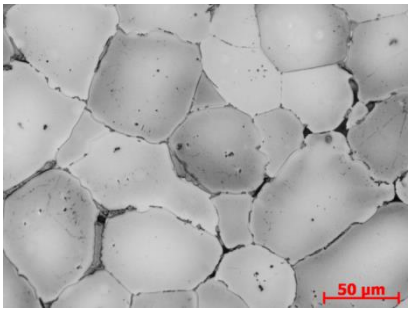

(d) Casting #44, Location B, 500x.

Figure 4.5.43 *As-cast microstructures from component #44 alloy B206.*

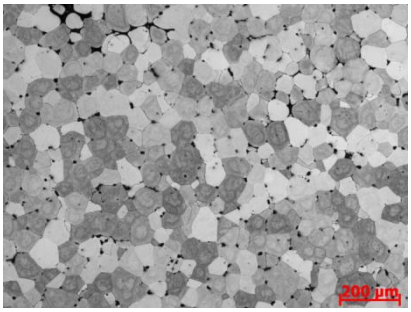

(a) Casting #51, Location A, 100x.

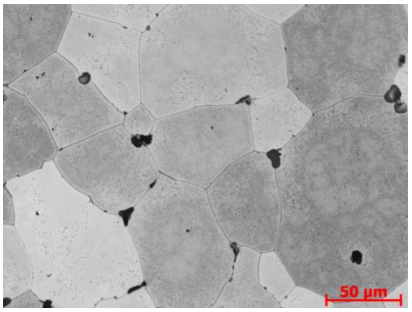

(b) Casting #51, Location A, 500x.

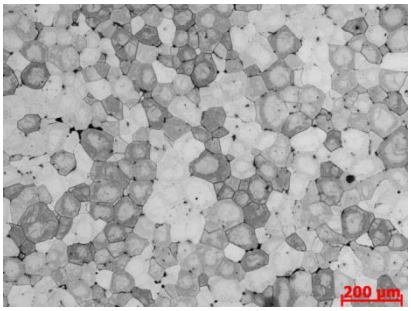

(c) Casting #51, Location B, 100x.

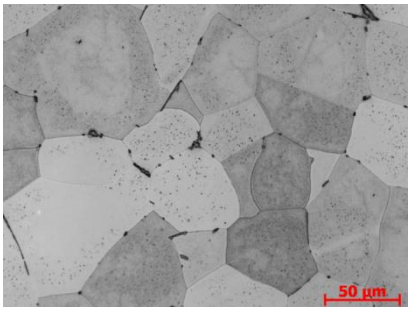

(d) Casting #51, Location B, 500x.

Figure 4.5.44 *Heat treated microstructures from component #51 alloy B206.*

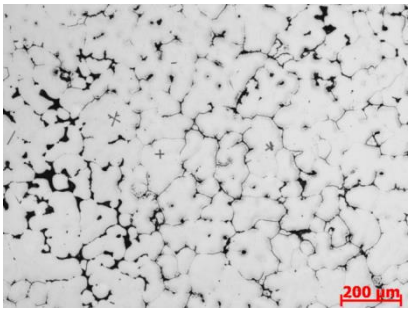

(a) Casting #64, Location A, 100x.

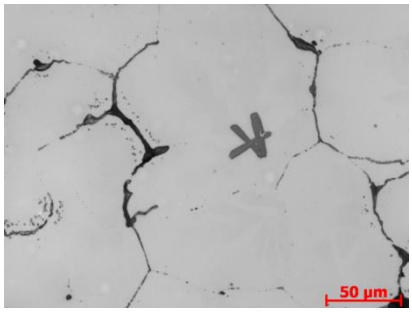

(b) Casting #64, Location A, 500x.

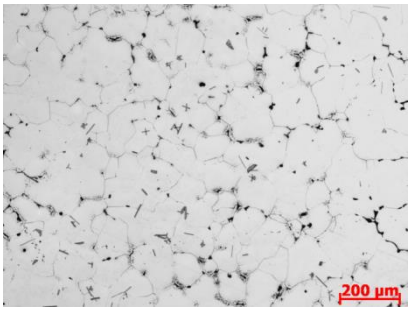

(c) Casting #64, Location B, 100x.

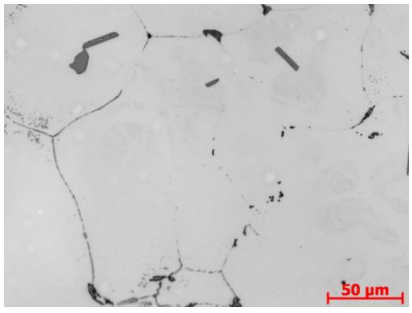

(d) Casting #64, Location B, 500x.

Figure 4.5.45 *As-cast microstructures from component #64 alloy 535.*

Microstructures from a Broken Casting

A photograph of the fracture surface of broken casting #10 from pretrial casting is shown in Figure 4.5.46. The fracture of the casting is associated with the relatively high mold temperature near the hot spot in the casting. The fracture surface shows predominantly inter-crystalline fracture with strong evidence of dendritic solidification. This is more evident from the SEM photographs of the fracture surface (from the edge) at low and relatively high magnifications shown in Figures 4.5.47(a) and (b) respectively. There is also strong evidence of shrinkage porosity on the fracture surface. Examples of unetched microstructures at low and high magnifications from a sample sectioned perpendicular to the fracture surface are shown in Figures 4.5.48(a) and (b). Figures 4.5.49 (a) and (b) show etched microstructures and areas where shrinkage cavity was observed at low and relatively high magnifications. The progression of hot tearing through the section thickness and presence of shrinkage cavities is evident in Figure 4.5.48. The hot tearing and shrinkage cavity appears to follow the grain boundaries. The effectiveness of the grain refiner is evident by the relatively fine grain structure.

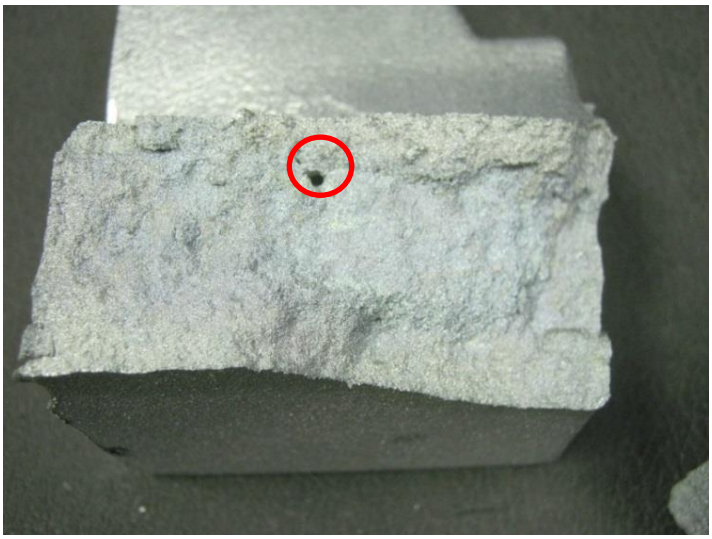

Figure 4.5.46 *Photograph of fracture surface from casting #10 alloy A206, 1.2x.*

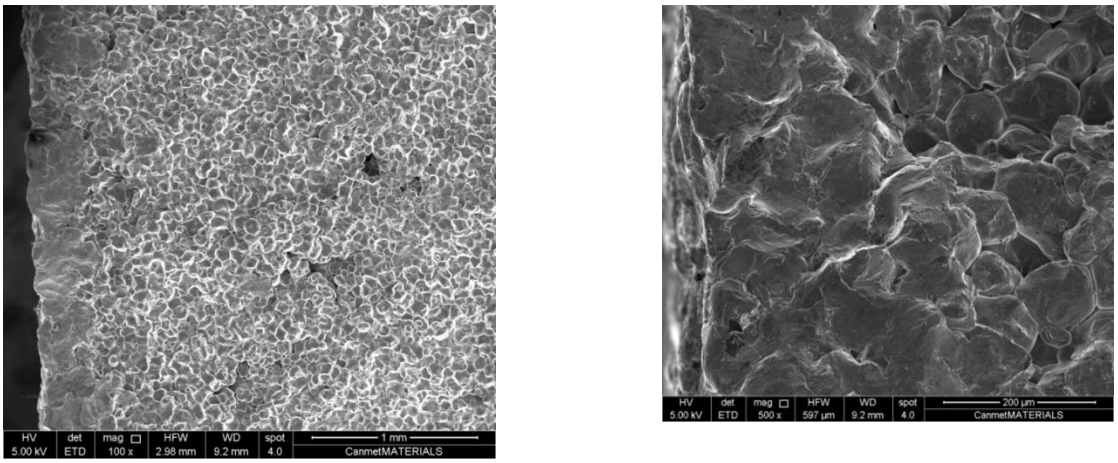

(a) 100x. (b) 500x.

Figure 4.5.47 *SEM photographs of fracture surface from casting #10 of A206.*

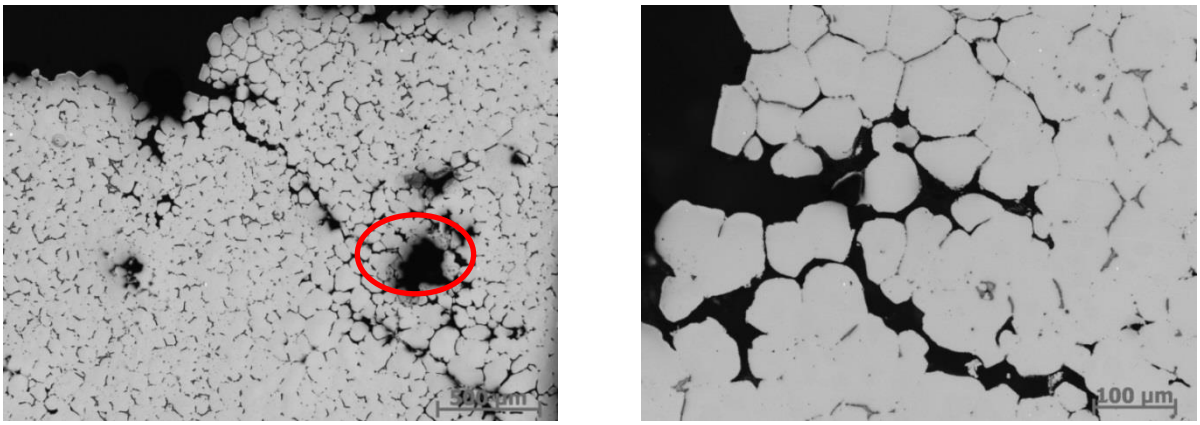

(a) 100x. (b) 500x.

Figure 4.5.48 *Unetched microstructures from casting #10 perpendicular to the fracture surface.*

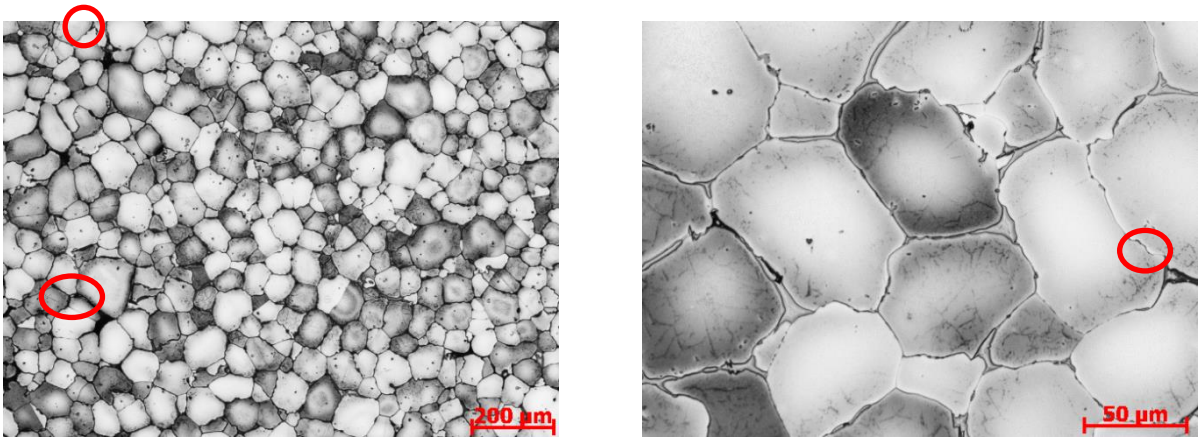

(a) 100x. (b) 500x.

Figure 4.5.49 *Etched microstructures from broken casting #10.*

4.5.2.7 Summary and Conclusions

1. Overall, the casting trials performed at the partner foundry using a production tool that was designed for A356 was successful in that many castings poured from alloys A206, B206 and 535 in a rather challenging production tool were free of hot tearing.

2. There appears to be minimum mold temperature necessary and maximum mold temperature allowable for some areas of this specific casting geometry. To accurately monitor the mold temperature during the casting cycle, more temperature sensors should be located within the die to know the mold temperature in critical locations. This will facilitate rapid implementation of effective thermal management of the mold.

3. Hot tearing could be prevented by effective thermal management of the mold by adjusting the cooling water flow rate in the cooling channels in the mold. These results show that the mold temperature must be controlled within a certain range and mold temperature control is one of the important processing parameters that must be controlled. Effective heat extraction from the mold and effective thermal management of the solidus/liquidus transition within the casting with specific regard to time at temperature's effect on inducing residual stress and relative hot tensile strength at ejection are significant parts of the process control.

4. High spikes in the mold temperature in certain locations especially close to hot spots in the mold can result in casting breakage. Implementation of effective thermal management of the mold by heating and cooling in appropriate areas is critical to casting of hot tear free components.

5. Although metal casting temperature and dwell time remained the same, effective thermal management of the mold by location of thermocouples, mold heating and cooling in specific locations and taking into consideration the casting geometry and section thicknesses are important considerations.

6. Promotion of directional cooling is necessary to avoid hot tearing and this can be achieved by targeted heating and cooling of the mold areas. However, as was shown in the results, high spikes in the mold temperature in certain locations especially close to hot spots in the mold could result in casting breakage. Even though higher temperatures in hot spots can promote directional solidification, longer solidification times make the casting vulnerable for cracking during ejection.

7. The castability of A206 alloy with 50% primary and 50% in-house as the charge material was similar to that observed for A206 and B206 100% virgin primary ingots. This observation could lay the groundwork for future development of these alloys for permanent mold casting without requiring 100% primary virgin ingot. Achieving that goal should make the casting of alloy 206 in metal mold more economically viable and promote wider industry acceptance.

8. Although dye penetrant inspection and radiographic inspection show shrinkage porosity in many of the castings, optimization of casting and mold design should eliminate the shrinkage problem in these hot tearing susceptible alloys.

4.5.3 Characterization (Mechanical Properties)

4.5.3.1Test bars

The tensile bars were machined from coupons obtained from the bracket castings of alloys 206 and 535. The coupons were either vertically (1) or horizontally (2) oriented in the brackets as shown in Figure 4.5.50. In all sixteen coupons were obtained from the four melts. The tensile bars machined from the components conform to the Standard Specimen in ASTM B 557 [19]. The nominal diameter and gage length are 12.7 mm and 50.8 mm respectively. The overall length of each bar was 152.4 mm. The test bars from alloy 206 were also machined from bracket castings and heat treated to T7 temper. Alloy 535 was tested in the as-cast condition (F temper) only. Samples for microstructural evaluation were sectioned from the gauge section of the fractured test bars. The fracture surfaces were examined by SEM for qualitative analysis on shrinkage porosity volume.

The mechanical properties of alloy 206 were also determined from ASTM B108 standard tensile bars. Photographs of a machined tensile bar and a separately cast tensile bar that was poured during the casting trial at the partner foundry are shown in Figure 4.5.51.

The tensile bars were heat treated following standard procedure to obtain T4, T6 or T7 tempers. The T4 temper solutionizing heat treatment consists of heating samples from room temperature to 495ºC in 2 hours and holding at 495ºC for 2 hours. The furnace temperature was then increased to 525ºC and samples were held for 8 hours. These solutionized samples were immediately quenched in water at 80ºC. This was followed by natural aging for a few days before testing. For T6 temper samples, starting from T4 temper samples, the samples were naturally aged for 18 hours at room temperature. This was followed by artificial aging at 155°C for 20 hours, followed by cooling down to room temperature. For T7 temper samples, starting from T4 temper samples, the samples were naturally aged for 13 hours at room temperature. This was followed by artificial aging at 200°C for 4 hours and cooling down to room temperature.

4.5.3.2 Results and Discussion

ASTM B108 Test Bars

The composition evaluated is shown in Table 4.5.16. The minimum Aerospace Material Specifications (AMS) 4236 and 4235 (T4 and T7 tempers) from cast to size test bars and the average mechanical properties in the as-cast condition, T4, T6, and T7 tempers from this study are shown in Table 4.5.17. The detailed properties from each test bar are shown in Appendix 5. The data are plotted in Figures 4.5.52(a) and (b). The data points for T4 and T7 tempers were an average of six test bars each, and four test bars each for the as-cast and T6 temper. The alloy is usually used in the T4 and T7 tempers because T6 temper can result in stress corrosion cracking. The YS in the as-cast condition is 168 MPa. As expected and shown in Table 4.5.17, there is significant improvement in properties after heat treatment. Comparing the results from this study with the minimum AMS in Table 4.5.17 for the T4 and T7 tempers, the UTS, YS, and % elongation met or better than the minimum requirements.

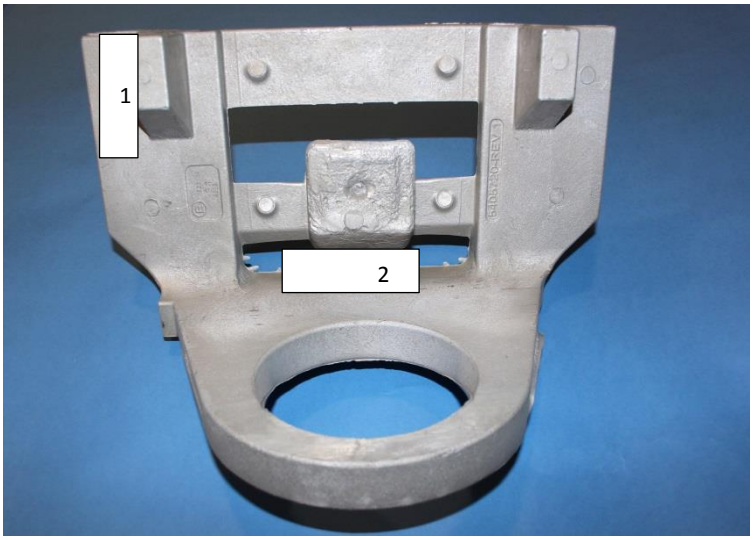

Figure 4.5.50 *Bracket casting showing areas where test bars were removed.*

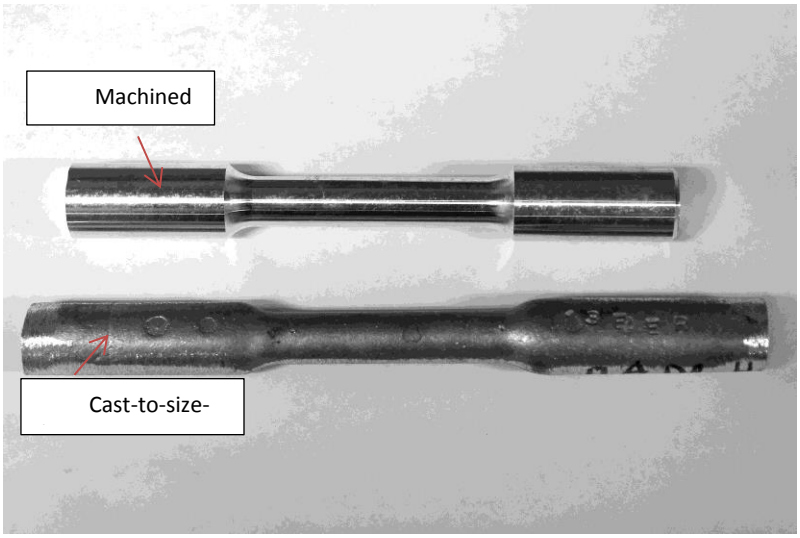

Figure 4.5.51 *Photographs of machined and separately cast test bars.*

Microstructures from as-cast and heat treated samples are shown in Figures 4.5.53(a) to (d). The as-cast microstructure showing the presence of characteristic $CuAl_2$ eutectic phase along the grain boundary is shown in Figure 4.5.53(a). After solution heat treatment, the dendritic network of the eutectic $CuAl_2$ along the grain boundary was broken down and replaced by fine precipitates of $CuAl_2$ phase within the grains and at grain boundaries shown in Figures 4.5.53(b) to (d).

Table 4.5.16 *Chemical analysis of alloy 206*

Melt Number	Composition, wt. %						
	Cu	Mn	Mg	Ti	B	Fe	Si
N2054B	4.60	0.43	0.33	0.059	0.010	0.074	0.038

Table 4.5.17 *Average Properties and standard deviation from ASTM B108 test bar of alloy 206*

Condition	Properties		
	UTS (MPa)	YS (MPa)	Elong. (%)
AMS 4236 -T4	345	205	10
AMS 4235-T7	345	275	3
As-Cast	244 ± 3.8	168 ± 1.0	4 ± 0.5
T4	392 ± 14.9	256 ± 2.3	12 ± 3.1
T6	402 ± 12.4	280 ± 8.8	8 ± 0.8
T7	410 ± 9.0	359 ± 4.1	4 ± 0.8

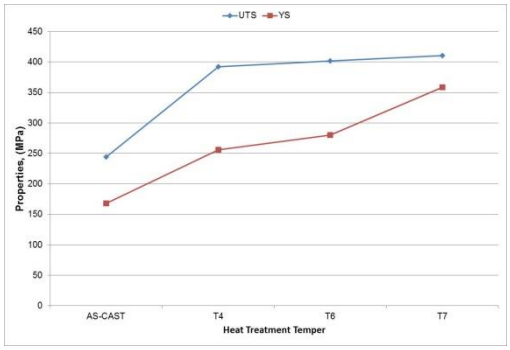

(a) Tensile strengths

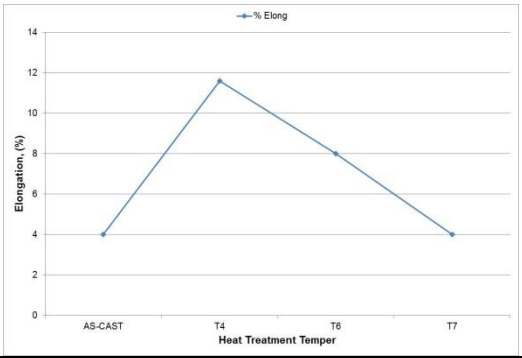

(b) Elongation.

Figure 4.5.52 *(a) Tensile properties and (b) elongation from as-cast and after heat treatment.*

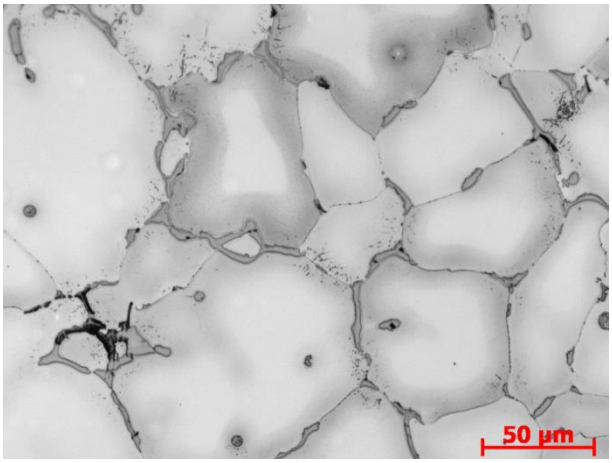

(a) 7-2, As-cast F temper.

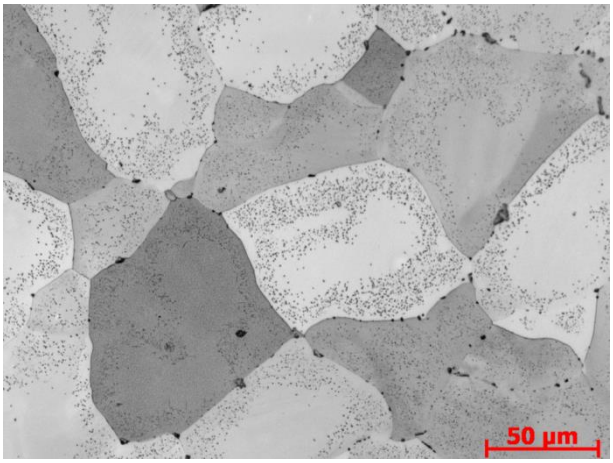

(b) 7-1, T4 temper.

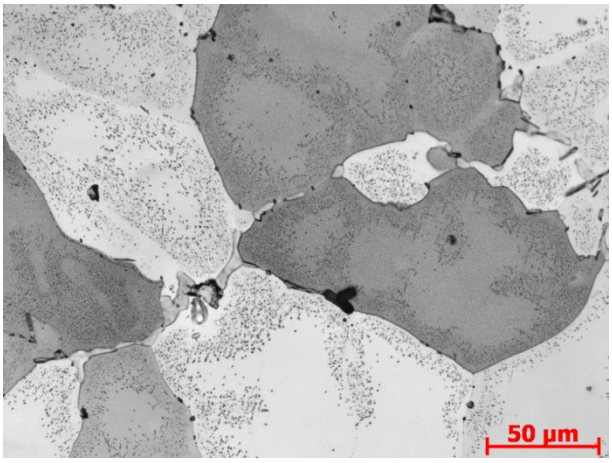

(c) 13-2, T6 temper.

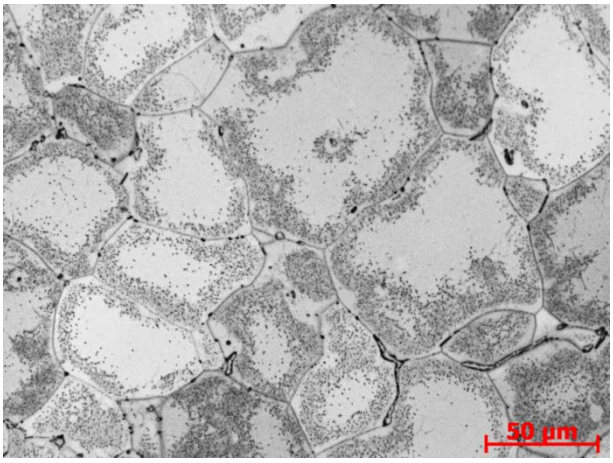

(d) 11-1, T7 temper.

Figure 4.5.53 *Microstructures from test bars poured from B206 in as-cast and after heat treatment. Keller's etch, 500x.*

Test Bars Machined from Bracket Component

The chemical analyses from the melts prepared are shown in Tables 4.5.18 and 4.5.19. The chemical compositions are within the range specified by AA specification. The average mechanical properties from the machined test bars and separately cast bars are given in Table 4.5.20. The minimum Aerospace Material Specifications (AMS) 4236 and 4235 (T4 and T7 tempers) for properties of test bars machined from undesignated casting areas are also given in this table. It is recalled that the bracket components from alloy 206 were heat treated to T7 temper only. Detailed properties from each test bar are shown in Tables 1 to 5, Appendix 6. The results from Table 4.5.20 are plotted in Figures 4.5.54 to 4.5.57. For the samples machined from melt 206-1, 100% primary ingot, the UTS, YS, and % Elongation from the samples in vertical orientation (e.g. 17-1, 19-1), Figures 4.5.54, are higher than those in horizontal orientation (e.g. 17-2, 19-2). A similar observation is made in the samples from melt 206-2, 50% primary ingot + 50% revert. As shown in Figures 4.5.55, the properties from tensile bars in vertical orientation (34-1, 38-1) are higher than those in horizontal orientation (34-2, 38-2). Figure 4.5.56 shows that the properties from tensile bars in vertical (45-1, 49-1) orientation are higher than those in horizontal (45-2, 49-2) orientation. The properties determined from the separately cast tensile bars shown in Figure 4.5.57 are higher than those from the machined bars because they are free from shrinkage porosity defects. The

reason for this is that samples in the horizontal orientation tend to have higher shrinkage defects than those in vertical orientation. The trend observed in alloy 535 is similar to that for alloy 206, except that alloy 535 tends to show higher shrinkage. Effective risering and gating techniques must be used during casting and mold design stages to eliminate the shrinkage defects.

The minimum properties required by AMS 4235 for A206-T7 were usually met by test bars obtained from vertical orientation of the castings. The results from the horizontal orientation were slightly lower. For alloy B206, the UTS and YS were slightly lower, but the minimum elongation was met. For the cast to size test bars (E1 to E4) from A206, the average UTS (433 MPa), YS (360 MPa) and Elongation (5.6%) are higher than the minimum AMS 4235 T7 specification. Despite the shrinkage porosity defects, the minimum 1.5% elongation could be easily obtained. Examples of microstructures and SEM fractograph of fracture surface of selected test bars are shown in Figures 4.5.58 and 4.5.59 respectively. The level of porosity is higher in the test bars in horizontal orientation. The relatively fine grain structure shows that the castings were poured from fully refined metal.

Table 4.5.18 *Chemical analysis of alloy A/B206*

Alloy	Composition, Wt. %							
	Si	Fe	Cu	Mn	Mg	Ni	Zn	Ti
AA Spec	0.05 max	0.10 max	4.2 - 5.0	0.20 - 0.50	0.15 - 0.35	0.05 max	0.10 max	0.15 - 0.30
A206-1	0.0481	0.0397	4.83	0.397	0.271	0.0088	0.0164	0.184
A206-2	0.0425	0.0344	4.56	0.357	0.176	0.0020	0.0207	0.190
B206	0.0476	0.0641	4.60	0.306	0.185	0.0026	0.0095	0.098

Table 4.5.19 *Chemical analysis of alloy 535*

Alloy	Composition, Wt. %						
	Si	Fe	Cu	Mn	Mg	Zn	Ti
AA Spec	0.15 max	0.15 max	0.05 max	0.10 - 0.25	6.2 - 7.5	-	0.10 - 0.25
535.0	0.0731	0.0613	0.0278	0.169	6.760	0.0179	0.198

Table 4.5.20 *Average properties from bars machined from component*

Alloy and Sample Id.	Properties		
	UTS (MPa)	YS (MPa)	Elong. (%)
AMS 4236 -T4	*310*	*180*	*8*
AMS 4235-T7	*345*	*275*	*1.5*
A206-1			
17-1 and 19-1	376 ± 4.2	314 ± 1.4	4 ± 0.4
17-2 and 19-2	314 ± 36.1	269 ± 12.0	2.6 ±1.7
A206-2			
34-1 and 38-1	350 ±14.1	284 ± 0	3.5±1.3
34-2 and 38-2	278 ± 9.2	240 ± 0	1.6 ±0.3
B206			
45-1 and 49-1	329 ± 7.1	272 ± 0.7	3 ± 0.2
45-2 and 49-2	261± 1.4	225 ± 0	1.5 ± 0.1
A206			
E1, E2, E3 and E4	434 ±10.3	360± 1.6	5.6 ± 1.3
535			
60-1 and 63-1	243 ± 3.5	129 ± 0.7	10 ± 0
60-2 and 63-2*	121 ± 44.5	93 ± 19.1	1.6 ± 1.3

*Sample broke at the shoulder, data not accurate.

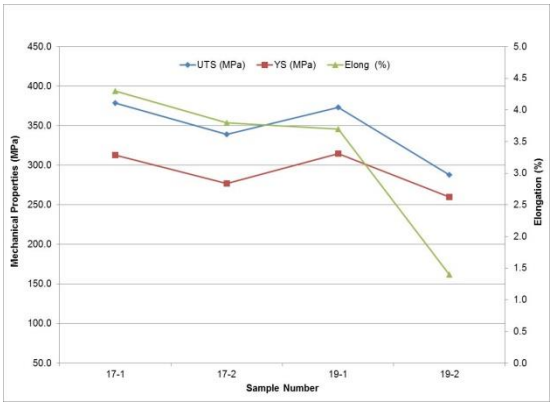

Figure 4.5.54 *Mechanical properties of test bars machined from bracket casting of A206-1.*

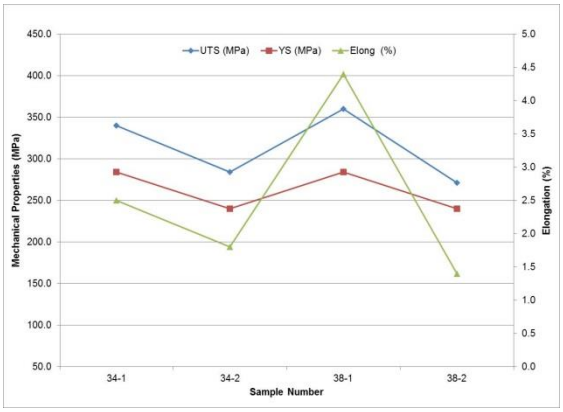

Figure 4.5.55 *Mechanical properties of test bars machined from bracket casting of A206-2.*

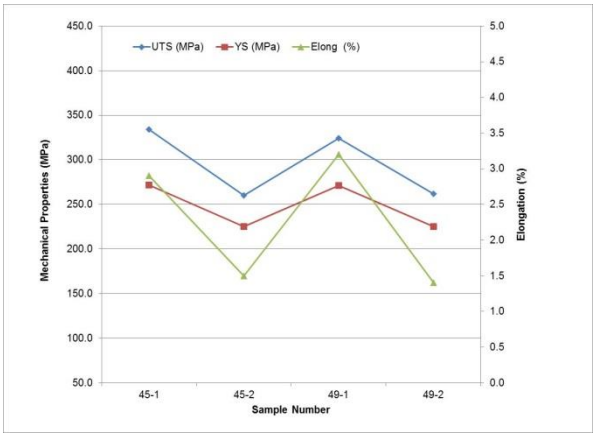

Figure 4.5.56 *Mechanical properties of test bars machined from bracket casting of B206.*

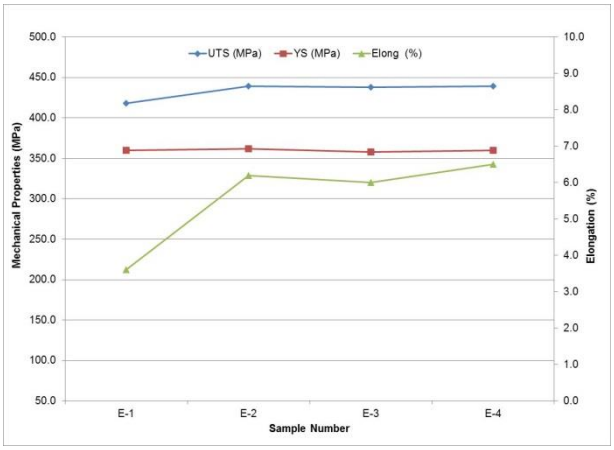

Figure 4.5.57 *Mechanical properties of separately cast test bars of A206.*

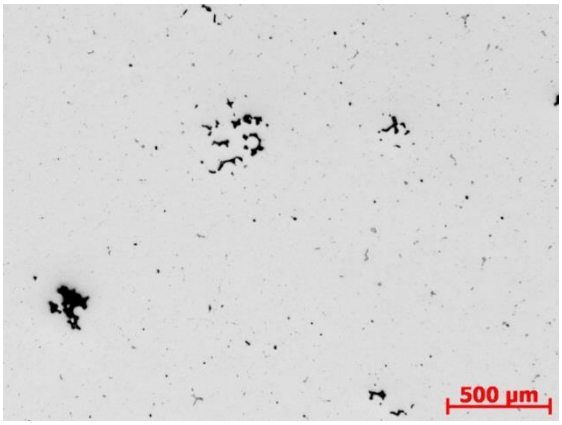

(a) Sample 17-1, unetched, 50x.

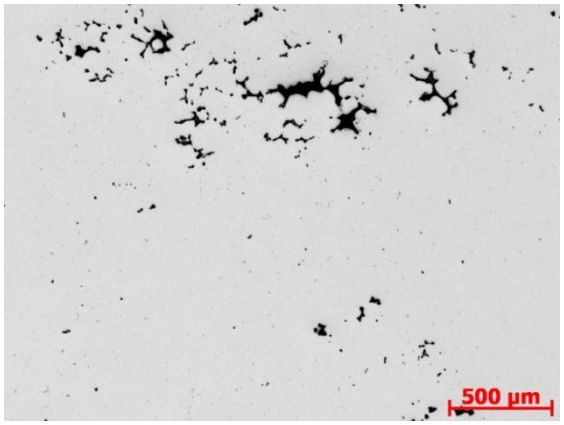

(b) Sample 17-2, unetched,50x.

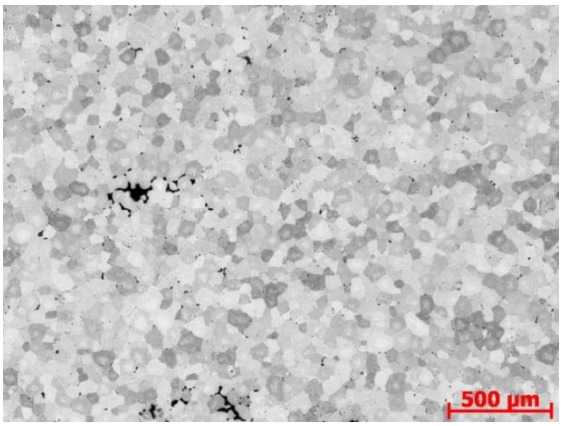

(c) Sample 17-1,50x.

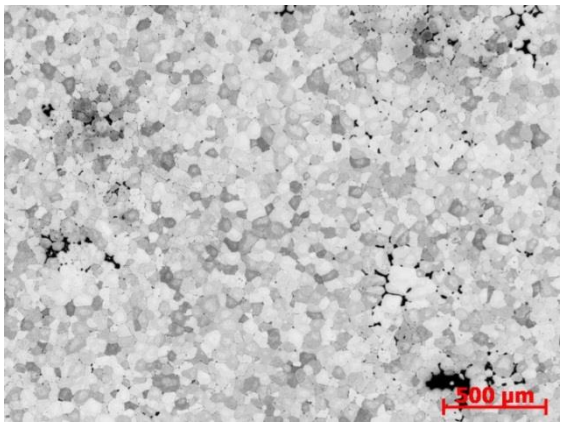

(d) Sample 17-2, 50x.

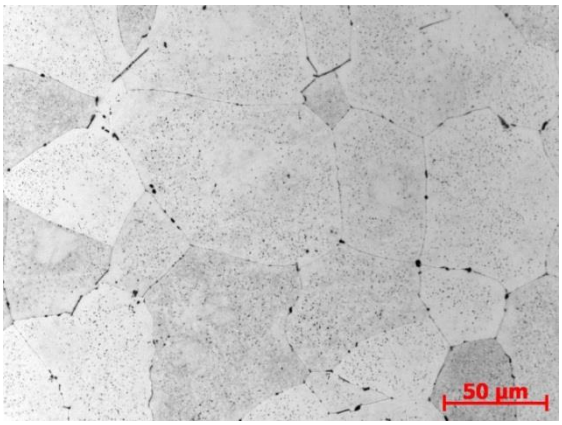

(e) Sample 17-1,500x.

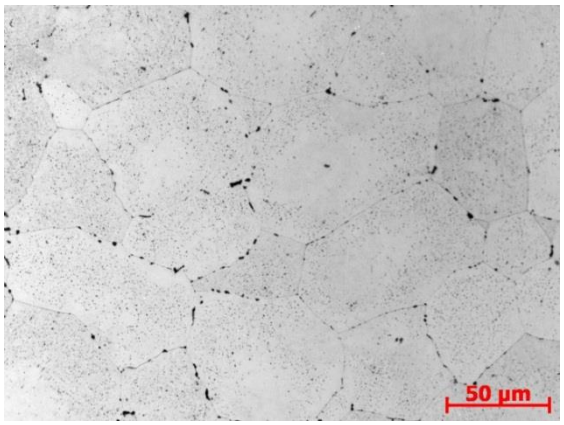

(f) Sample 17-2, 500x.

Figure 4.5.58 *Microstructures from test bars machined from the bracket component in vertical (17-1) and horizontal (17-2) orientation. Etchant is Keller's reagent.*

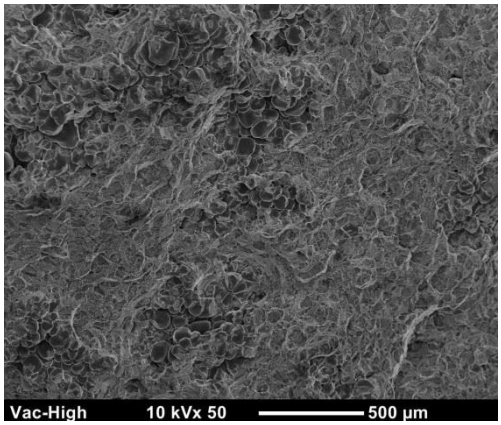

(a) Sample 17-1, 50x.

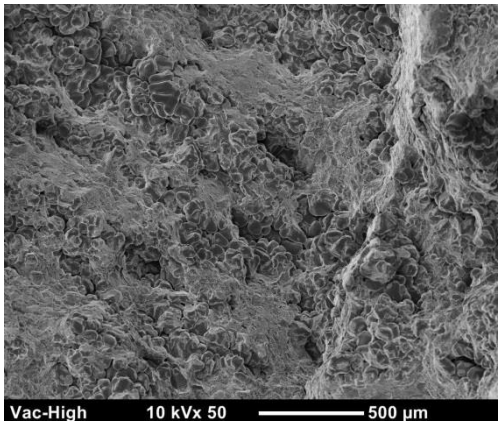

(b) Sample 17-2, 50x.

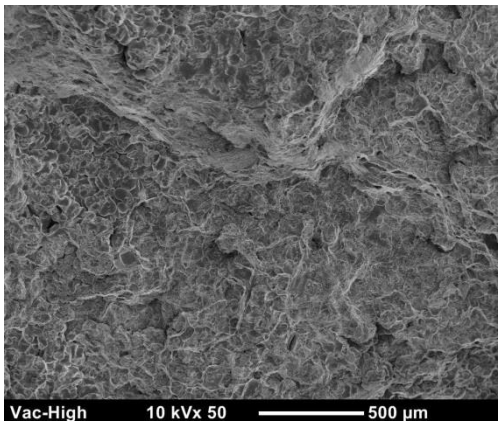

(c) Sample 60-1, 535,50x.

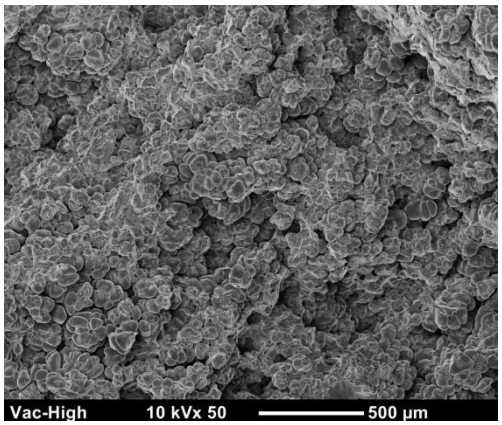

(d) Sample 60-2, 535, 50x.

Figure 4.5.59 *SEM of fracture surface of tensile bars in vertical (17-1) and horizontal (17-2) orientation. Dendritic structure and shrinkage voids are shown.*

4.5.3.3 Summary and Conclusions

1. The UTS, YS, and % elongation from the ASTM B108 tensile bars met the AMS 4236 (T4) and 4235(T7).

2. The higher tensile properties from tensile bars in vertical orientation compared to those in horizontal orientation are associated with higher shrinkage porosity in the samples in horizontal orientation.

3. The minimum properties required by AMS 4235 for A206-T7 were usually met by test bars in vertical orientation from A206. The results from the horizontal orientation were slightly lower.

5 Benefits Assessment

Alloy 206 is used in applications where high strength is required. It can be heat treated to either a high yield strength or high toughness condition. Examples of use include military, aerospace, and heavy-duty transportation applications. Regrettably, alloy 206 have higher tendency for hot tearing than in 300 series alloys when poured in metal mold, therefore it is usually produced by sand casting process. The results from the casting trials at partner foundries have shown that the processing parameters developed in this project can be used to produce components that are free of hot tearing when alloys 206 and 535 are poured in metal molds.

The energy and environmental savings that can be achieved by using permanent mold casting and high strength alloys are relate to: elimination of and/or reduced sand use; energy saved from sand molding; energy saved by reduced finishing operations due to higher tolerances and better surface finish; improved casting yield around 65% compared with 50% or less for sand castings; reduced scrap for remelting / recycling; and potential for reduced heat treatment costs. Significant energy savings can be achieved by using gravity and/or low-pressure permanent-mold casting processes, with sand or permanent-mold cores. It has been estimated that energy savings of about 250 kWh per ton of castings can be realized by switching from sand to permanent mold casting. The environmental problems associated with sand disposal and working conditions in the foundries would also be improved.

Considering the high strength of alloy 206, thinner and lighter structural components can be used in automotive and other applications compared to Al-Si alloys 356 and 319. Similarly alloy 535 exhibits good mechanical properties and dimensional stability in the as-cast condition. For alloy 535 a more cost effective T5 heat treatment can be used because it does not require the more expensive solution treatment, water quenching and aging treatment, commonly used for aluminum alloys 356 and 319.

6 Commercialization

Some of our industry partners are looking into taking advantage of the results and expand their use of alloy 206 in current and new applications where its higher tensile properties provide clear economic advantage over other alloys. By following the processing route developed in this project hot tearing free components can be produced from alloys 206 and 535 poured in metal molds. Therefore alloy 206 can be used in heavy-duty transportation applications (e.g. automotive chassis, gear housings, and suspension components) where high tensile and yield strengths and moderate elongation are needed.

7 Accomplishments

Unique processing techniques were developed and six journal and conference proceeding publications from the outcome of completed tasks.

7.1 Control of Hot Tearing

A link between grain refinement, mold temperature and formation of hot tearing was discovered when alloy 206 is cast in metal mold. It was determined that a combination of grain refinement and mold temperature greater than 400˚C is necessary to prevent hot tearing during the solidification of alloy 206 in metal molds. Grain refinement of the molten alloy breaks down the interdendritic solidification structure leading to improved feeding, and the hotter mold provided effective thermal gradient, reduced cooling

rate, and reduced principal strain during the last stages of solidification to preclude the formation of hot tear.

7.2 Publications

1. Fasoyinu, Y., and Sahoo, Mahi., "Factors Influencing Hot Tearing of Aluminum Alloy 206.0 Poured in Metal Molds", Proceedings of the 48th Conference of Metallurgists: Materials Development and Performance of Sulphur Capture Plants, August 23-26, 2009, Sudbury, ON, Canada, pp 3-17.
2. Fasoyinu, F. A., J Thomson, J.P., Sullivan, L., and Sahoo, M., "Characterization of Microstructures and Mechanical Properties of Aluminum Alloys 206.0 and 535.0 Poured in Metal Molds", AFS Transactions Vol. 116 (2008).
3. Fasoyinu, F. A.,, and Sahoo, Mahi., "Permanent Mold Casting of Aluminum Alloys 206 and 535", MTL 2008-19(CF), 60 pages.
4. Fasoyinu, F.A., and M. Sahoo, "Hot Tearing of Aluminum Alloys 206 and 535 Poured in Metal Mold", Proceedings AFS 6th International Conference on Permanent Mold Casting of Aluminum and Magnesium, Dallas, TX, February 11-12, 2008.
5. Fasoyinu, F. A., Thomson, J.P., Burke, P., Weiss, D., and Sahoo, Mahi., "Permanent Mold Casting of Aluminum Alloys A206.0 and A535.0", AFS Transactions, Vol. 115, (2007).
6. Fasoyinu, Y., Thomson, J.P., Burke, P., and Sahoo, M.,"Mahi Sahoo, "Studies on Hot Tearing Resistance and Permanent Mold Casting of Aluminum Alloys 535.0 and 206.0 For Automotive Applications", Proceedings of the International Symposium on Aluminum, Edited by G. Dufour, F. Paray, and J. Tessier, October 1-4, 2006, Montreal, COM2006, pp 131-147.

8 Conclusions

1. The utilization of intensive solidification modeling to aid mold and casting design was effective in predicting the areas on a cast component that could produce hot cracking where the die hit certain maximum temperatures based on the wall thickness and casting geometry.

2. The computer simulation results of the bracket component show that increasing initial mold preheating temperature over 480°C tends to lead to mechanical hot cracking due to ejection stresses. Hot tearing is reduced or not present when fraction solid ranges from 65 % to 75 %. This is due to the presence of liquid metal to feed solidification shrinkage. A die cycle dwell time of over 290 seconds tends to create more severe hot tearing due to longer metal mold constraint time. Therefore, die cycle dwell time of 200 to 230 second and initial mold preheating temperature from 460°C to 480°C provided the best results.

3. Overall, the casting trials performed at the partner foundries using production tools designed for A356 was successful in that many castings poured from alloys A206, B206 and 535 in rather challenging production tools were free of hot tearing.

4. Optimization of the grain structure and good control of casting cycle time are critical to producing hot tear free components. High spikes in mold temperature in locations close to hot spots in the mold can result in casting breakage. Effective thermal management of the mold by location of temperature sensors and controlled heating and/or cooling at the right time in hot spots are critical to producing hot tear free components.

5. Although dye penetrant inspection and radiographic inspection show shrinkage porosity in some of the components, optimization of casting and mold design should eliminate the shrinkage problem in these hot tearing susceptible alloys.

6. The castability of A206 with 50% primary ingot plus 50% in-house scrap as the charge material was similar to that observed for A206 and B206 100% primary ingots. This could lay groundwork for future work on developing appropriate charge material primary/scrap ratio for alloy 206. Achieving that goal should make the casting of alloy 206 more economically viable and wider industry acceptance.

7. Laboratory scale experiments show that a combination of grain refinement and preheating of metal mold to a minimum of 400°C or higher is necessary to prevent the formation of hot tearing of alloys 206 and 535 poured in restrained metal mold. Hot tearing occurs when the contraction of solidifying castings is excessively restrained by the mold or cores, especially in hot spots of the casting where the strain resulting from solidification contraction is concentrated.

8. The comparative computer simulation results of the restrained rod castings poured in metal molds at 290°C and 450°C, from alloys 206 and 535 show that hot tearing is reduced at the higher mold temperature. The computer simulation results closely match the hot cracking trends observed experimentally during the casting trials. The improvement in hot tearing resistance is associated with the reduced principal strain developed at the higher mold temperature during the last stages of solidification (90-100% fraction solid). Therefore, casting conditions that would create a combination of a high strain rate and high solid fraction during the later stages of solidification should be avoided.

9. The areas prone to mechanical hot cracking is driven by the casting design related to variation in section thickness that could cause premature solidifications in some areas of the component. Controlled localized heating elements in those hot spots of the mold can reduce the hot tearing.

10. The mechanical properties of the castings produced met or exceeded the required aerospace standards. The results from this work should make it easier for automotive designers to use the high strength alloys in vehicles with confidence.

9 Recommendations

The results from this project have demonstrated that hot tear free structural components can be successfully produced from hot tear susceptible alloys 206 and 535 poured in metal molds by following stringent production control during the casting process. The structural components evaluated were produced from molds and tools designed for alloy A356, with no design changes during the casting trials. The success achieved resulted from manipulating the casting processing parameters such as mold and pouring temperatures, casting ejection control and thermal management of the mold. Therefore, I would recommend a follow-up project where casting, mold, and tooling design are optimized for alloy 206 to take full advantage of its superior tensile properties for a selected structural component. The results of such study should expand the use of alloy 206 by the automotive industry where thinner-wall and lighter structural components can be poured from alloy206.

10 References

1. ASM Handbook, Vol. 2 "Properties and Selection: Nonferrous Alloys and Special-Purpose Materials" published by ASM International pp. 143-144, (October 1990).
2. ASM Specialty Handbook, Aluminum and Aluminum Alloys, edited by J. R. Davis, Published by ASM International, p 46. (1993).
3. Fasoyinu, F. A., Cousineau, D., Newcombe, P., Castles, T. and Sahoo, M. "Grain Refinement and Thermal Analysis of Al-Mg Alloy 535", presented at the 6th International Conference on Molten Aluminum Processing,, Orlando, Florida, USA, Nov. 11-13, (2001).
4. Fasoyinu, F. A., Thomson, J., Cousineau, D., Castles, T. and Sahoo, M. "Gravity Permanent Mold Casting of Al-Mg Alloy 535", AFS Transactions, vol. , pp. 907-912 (2002).
5. Sigworth, Geoffrey "Grain Refining of Aluminum Casting Alloys", Proceedings 6th International Conference on Molten Aluminum Processing, Orlando, Florida, USA, Nov. 11-13, pp 210-221, (2001).
6. Kearney, A. L. and Raffin, J. "Hot Tear Control Handbook for Aluminum Foundrymen and Casting Designers", AFS Publication, (1971).
7. Sigworth, Geoffrey "An Improved A206 alloy for Automotive Suspension Components, USCAR Final report for AMD 305, pp 62 pages (2002).
8. Chamberlain, B., Watanabe, S. and Zabek, V.J. "A Natural Aging Aluminum Alloy, Designed for Permanent Mold Use", AFS Transactions, Vol. , pages 133-142, (1977).
9. Jorstad, John and Rasmussen, Wayne, "Aluminum Casting Technology", 2nd Edition, Edited by Donna Zalensas, Published by AFS, pp. 19-43 (1997).
10. Farrior, Gilbert M, Brillhart, Donald C, and Burkart, Alan R "Simplified Grain Size Test Aids Cast Aluminum Quality", Light Metal Age, Vol. 36, No. 5, 6, pp. 11-912 (June 1978).
11. Fasoyinu, Yemi, Thomson, J.P., Burke, Paul, and Sahoo, Mahi "Studies on Hot Tearing Resistance and Permanent Mold Casting of Alumnium Alloys 535.0 and 206.0 for Automotive Applications", Proceedings Light Metals, Oct 1-4, Montreal, (2006).
12. Solidification Characteristics of Aluminum Alloys Volume 2: Foundry Alloys, Lennart Backerud, Guocai Chai, and Jarmo Tamminen, Published by AFS / SKAN ALUMINIUM, p (1990).
13. Solidification Characteristics of Aluminum Alloys Volume 3: Dendrite Coherency, Lars Arnberg, Lennart Backerud and Guocai Chai. Edited by Susan P. Thomas, AFS, and Jarmo Tamminen, Published by AFS, p (1996).
14. Lees, D.C.G, "Factors Controlling the Hot-Tearing of Aluminum Casting Alloys", Foundry Trade Journal, pp. 211-220, (August 18, 1949).
15. Pellini, William. S "Strain Theory of Hot Tearing", Foundry, p. 125-199, (Nov 1952).
16. Bishop, H.F., Ackerlind, C. G. and Pellini, W. S., "Metallurgy and Mechanics of Hot Tearing", AFS Transactions, Vol. 60, pp. 818-833, (1952).

17. Major, J.F. and Sigworth, G. K. “Chemistry Property Relationship in AA 206 Alloys”, AFS Transactions, Vol. 114, (2006).
18. ASM Handbook, Vol. 7 “Atlas of Microstructures of Industrial Alloys” published by ASM International p. 260, (1972).
19. ASTM Designation B 557-02; “Standard Test Methods for Tension Testing Wrought and Cast Aluminum- and Magnesium-Alloy Products”, Annual book of ASTM Standards, Vol.02-02, ASTM International, West Conshohocken, PA (2002), Fig. 9, page 6, 2002.

11 Appendices

Appendix 1 Mold and Pouring Temperatures from Constrained Castings

Table 1 Mold and pouring temperatures from melts N2051, N2052 and N2054

Sample Id.	Temperature, (°C)		Comments
	Mold	Pouring	
N2051A-4	212	704	Melt not refined. All rod casting show hot tearing and broke off at rod/sprue junction.
N2051A-5	213	702	
N2051B-4	211	701	Melt refined. All rod casting show hot tearing and broke off at rod/sprue junction.
N2051B-5	205	697	
N2052A-4	362	700	Melt not refined. All rod casting show hot tearing and broke off at rod/sprue junction.
N2052A-5	345	695	
N2052B-4	377	705	Melt refined. All rod casting show hot tearing and broke off at rod/sprue junction.
N2052B-5	327	705	
N2054A-4	400	701	Melt not refined: Rod castings show hot tearing.
N2054A-5	376	699	
N2054B-4	350	713	Melt refined: Rod castings show hot tearing.
N2054B-5	-	708	

Table 2 Mold and pouring temperatures from melt N2055

Sample Id.	Temperature, (°C)		Comments
	Mold	Pouring	
N2055A-1	409	696	Melt not grain refined. The rod castings show hot tearing at the three mold temperatures studied. Some rods broke off at the rod/sprue junction, and also close to the rounded end, especially at the lower mold temperatures.
N2055A-2	391	700	
N2055A-3	350	706	
N2055A-4	348	711	
N2055A-5	208	703	
N2055A-6	208	700	
N2055B-1	401	697	Melt grain refined. The rod castings show reduced hot tearing after grain refinement for molds preheated to about 400C.
N2055 B-2	357	700	
N2055 B-3	342	703	
N2055 B-4	342	706	
N2055 B-5	207	697	
N2055 B-6	213	700	

Table 3 Mold and pouring temperatures from melt N3001

Sample Id.	Temperature, (°C)		Comments
	Mold	Pouring	
N3001A-1	424	709	Metal not grain refined. Rods broke off at the rod/sprue junction and sometimes towards the rounded end. Hot tearing most severe at the lowest mold temperature evaluated (~200ºC).
N3001A-2	400	700	
N3001A-3	358	695	
N3001A-4	362	702	
N3001A-5	220	693	
N3001A-6	207	706	
N3001B -7	387	697	Melt grain refined. Minor hot tearing observed at rod/sprue junction. None of the rods broke off completely at the rod/sprue junction.
N3001B-8	382	704	
N3001B-9	353	696	Minor hot tearing observed. None of the rods broke off at the rod/sprue junction.
N3001B-10	349	701	
N3001B-14	222	697	Hot tearing observed on all rod castings.
N3001B-16	218	699	

Table 4 Mold and pouring temperatures from melt N3002

Sample Id.	Temperature, (°C)		Comments
	Mold	Pouring	
N3002A-1	411	708	Metal not grain refined. The longest rod broke off at the rod/sprue junction. No hot tears on the shorter rods.
N3002A-2	399	715	
N3002A-3	359	695	The longest rods broke off at the rod/sprue junction and sometimes along the rod. The shorter rods show hot tearing at the rod/sprue junction.
N3002A-4	342	697	
N3002A-5	229	704	All the rods broke off at the rod/sprue junction and sometimes at the rod/rounded end.
N3002A-6	236	700	
N3002B-7	412	702	Melt grain refined. No hot tear on all the rod castings.
N3002B-8	409	704	
N3002B-9	348	712	The two longer rods show minor hot tearing at the rod/sprue junction.
N3002B-10	344	708	
N3002B-11	239	692	Hot tearing at the rod/sprue junction and also along the longest rod near the rod/rounded end.
N3002B-12	238	700	

.

Table 5 Mold and pouring temperatures from melt N3037

Sample Id.	Temperature, (°C)		Comments
	Mold	Pouring	
1	200	700	Metal not grain refined. Hot tear on bars at riser/rod junctions, and some rod broke off.
2	200	700	
3	300	700	Hot tear on bars at riser/rod junctions, and some rod broke off.
4	300	700	
5	300	700	Melt grain refined: Hot tear on bars
6	300	700	
7	200	700	Melt grain refined: Hot tear on bars.
8	400	700	Melt grain refined: Minor hot tear on bars.
9	400	700	

Table 6 Mold and melt temperature from melt N3038

Casting Id.	Temperature, ºC		Comments
	Mold	Pouring	
N3038-1	200	705	Metal not grain refined Hot tear on all bars
N3038-2	300	706	Hot tear on all bars
N3038-3	400	708	Minor hot tear on bars
N3038-4	400	703	Melt grain refined: No hot tear
N3038-5	300	705	Minor hot tear
N3038-6	200	699	Hot tear on all bar

Appendix 2 Cooling Curves from Constrained Rod Castings

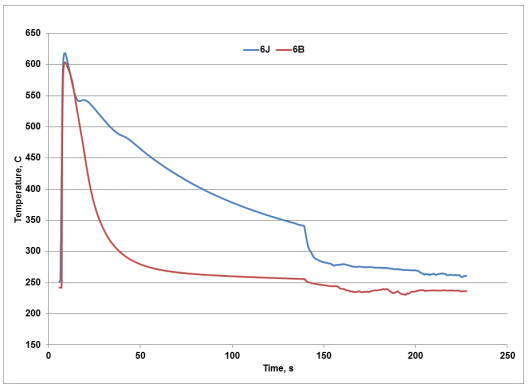

(a) 200-6Jand6B.

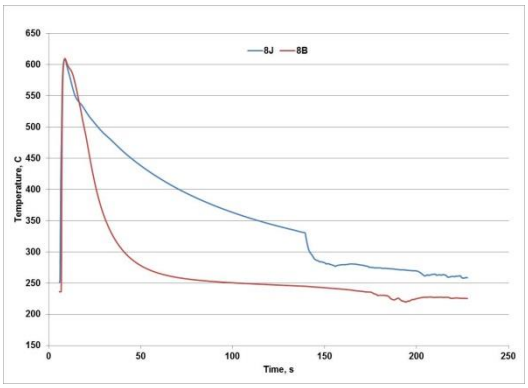

(b) 200-8Jand8B.

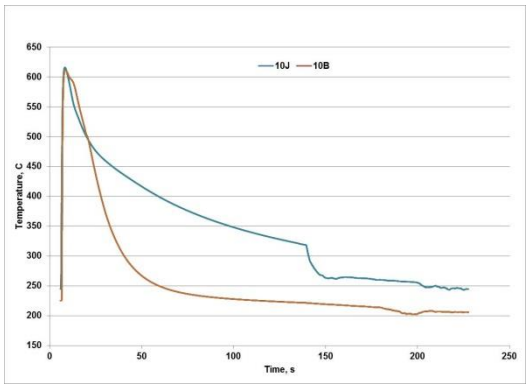

(c) 200-10Jand10B.

Figure 1 Cooling curves from mold preheated to 200°C poured from unrefined metal.

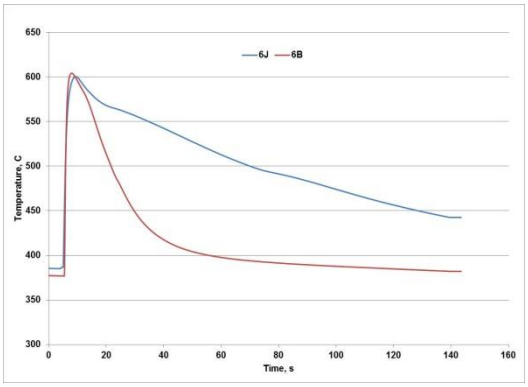

(a) 350-6Jand6B.

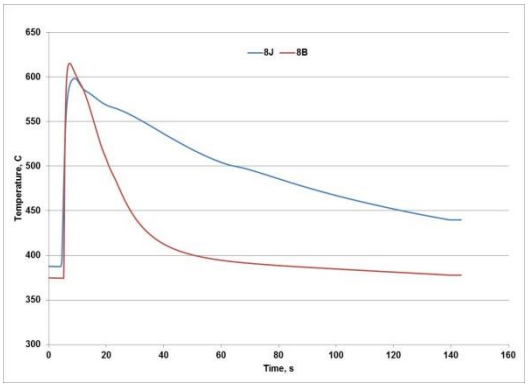

(b) 350-8Jand8B.

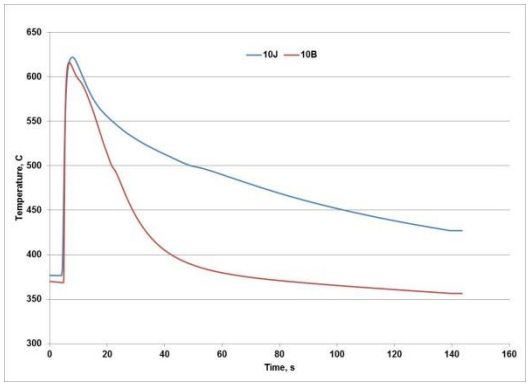

(c) 350-10Jand10B.

Figure 2 Cooling curves from mold preheated to 350°C poured from unrefined metal.

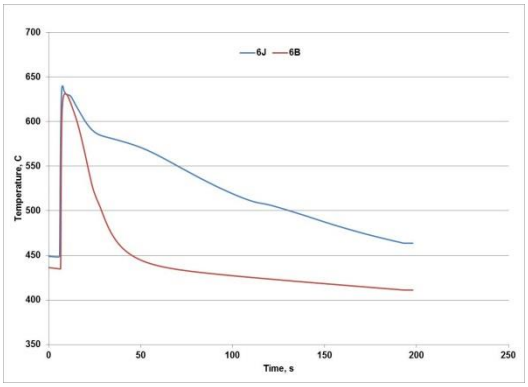

(a) 400-6Jand6B.

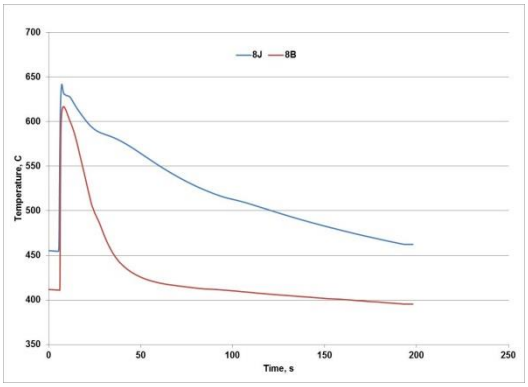

(b) 400-8Jand8B.

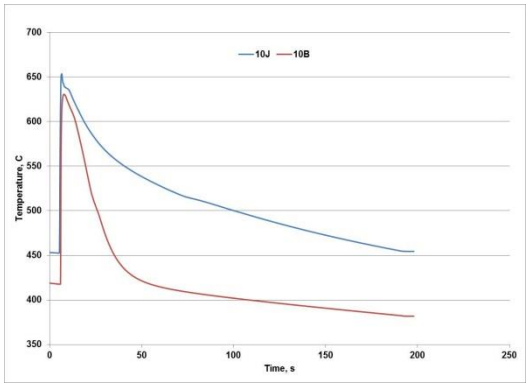

(c) 400-10Jand10B.

Figure 3 Cooling curves from mold preheated to 400°C poured from unrefined metal.

Appendix 3 Computer Simulation

Annex 1 Computer simulation results from A356

Report on A356
Bracket Hot Tear Simu

Annex 2 Computer simulation results from A206

Report on A206
Bracket Baseline Trials

Annex 3 Computer simulation results from A206

Report on A206
Bracket Upcoming Tria

Annex 4 Computer simulation results from 535

Report on 535
Bracket Upcoming Tria

Appendix 4: Preliminary Casting Trial Results

Preliminary Casting Trial

The mold temperature was measured by two thermocouples (TC) and two infrared (IR) pyrometers to measure mold surface temperatures. The casting processing parameters are summarized in Tables A1. It is noted that the mold temperatures from TC1 and IR#3 are usually higher than from TC#2 and IR#4 because of their location in the mold. The mold surface temperatures at two locations were measured by IR#3 and IR#4. In general, there was good mold filling and the casting show minor drags at low draft area. Casting #7 was broken on ejection broken casting at ejection. The casting dwell time for most of the casting was 290 seconds. Castings 1 to 3 were discarded as they were used to warm up the mold to operating temperatures. There was no hot tearing in castings 4 to 6 but castings 7 to 12 show hot tearing. The hot tearing in casting 7 to 12 is associated with the generally higher mold temperatures in those castings as shown in Table 1. The mold temperature is an important processing parameter that must be controlled within a given range. There appears to be a mold temperature range above which mechanical hot cracking can become significant. Example of hot tearing observed in the component from casting #12 is shown in Figure 1. The locations of the cracks are usually at the hot spots. It was observed that reducing the dwell time to 270 seconds in combination with increasing of mold temperature resulted in the formation of hot tearing. The 290 seconds dwell time appears to be adequate and served as input to the subsequent computer simulation.

Table 1 Processing temperatures from Pre-Trial for A206

Casting Number	Pouring Temp. (°C)	Mold Temp. (°C)		Mold Surface Temp. (°C)		Casting Dwell time (s)
		TC#1	TC#2	IR#3	IR#4	
4	781	476	431	549	510	290
5	781	484	437	538	427	290
6	782	489	445	554	466	290
7	779	498	446	571	510	290
8	778	511	450	560	477	290
9	787	518	452	560	482	290
10	781	517	454	577	488	270
11	773	530	468	577	504	270
12	781	521	473	582	527	300
AVG	780	505	451	563	488	-
STD	4	19	13	15	30	-

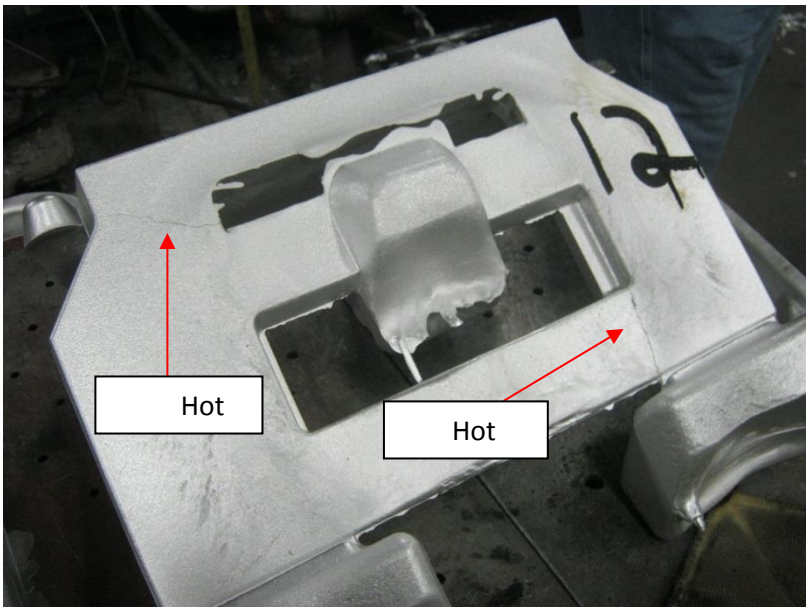

Figure 1 Photograph of casting #12 showing location of hot tearing.

Appendix 5 Mechanical properties from ASTMB108 bars

Table 1 Summary of mechanical properties from alloy 206

Samples	UTS (MPa)	YS (MPa)	Elong. (%)
As-Cast			
N2054B-10-1	247	167	4.4
N2054B-15-2	244	169	3.9
N2054B-6-1	247	168	4.4
N2054B-7-2	239	167	3.3
AVG	244.3	167.8	4.0
STD	3.8	1.0	0.5
T4 - Samples			
N2054B-12-2	404	259	13.0
N2054B-14-2	385	258	9.0
N2054B-6-2	365	255	6.8
N2054B-7-1	401	253	15.0
N2054B-8-1	400	256	12.0
N2054B-9-1	399	254	14.0
AVG	392.3	255.8	11.6
STD	14.9	2.3	3.1
T6 - Samples			
N2054B-11-2	410	281	9.0
N2054B-13-2	390	272	7.2
N2054B-8-2	393	275	7.5
N2054B-10-2	415	292	8.4
AVG	402	280	8.0
STD	12.4	8.8	0.8
T7 - Samples			
N2054B-9-2	416	361	4.5
N2054B-11-1	417	358	4.7
N2054B-13-1	394	351	2.8
N2054B-12-1	415	363	4.1
N2054B-15-1	414	360	4.4
N2054B-14-1	405	359	3.2
AVG	410.2	358.7	4.0
STD	9.0	4.1	0.8

Appendix 6 Mechanical properties from bracket component

Table 1 Properties from A206-1 (100% Primary Ingot)

Sample No.	UTS (MPa)	YS (MPa)	Elong. (%)
17-1	379.0	313.0	4.3
19-1	373.0	315.0	3.7
AVG	376.0	314.0	4.0
STD	4.2	1.4	0.4
17-2	339.0	277.0	3.8
19-2	288.0	260.0	1.4
AVG	313.5	268.5	2.6
STD	36.1	12.0	1.7

Table 2 Properties from A206-2 (50% Primary Ingot + 50% Revert)

Sample No.	UTS (MPa)	YS (MPa)	Elong. (%)
34-1	340.0	284.0	2.5
38-1	360.0	284.0	4.4
AVG	350.0	284.0	3.5
STD	14.1	0.0	1.3
34-2	284.0	240.0	1.8
38-2	271.0	240.0	1.4
AVG	277.5	240.0	1.6
STD	9.2	0.0	0.3

Table 3 Properties from B206

Sample No.	UTS (MPa)	YS (MPa)	Elong.(%)
45-1	334.0	272.0	2.9
49-1	324.0	271.0	3.2
AVG	329.0	271.5	3.1
STD	7.1	0.7	0.2
45-2	260.0	225.0	1.5
49-2	262.0	225.0	1.4
AVG	261.0	225.0	1.5
STD	1.4	0.0	0.1

Table 4 Properties from separately cast A206

Sample No.	UTS (MPa)	YS (MPa)	Elong. (%)
E-1	418.0	360.0	3.6
E-2	439.0	362.0	6.2
E-3	438.0	358.0	6.0
E-4	439.0	360.0	6.5
AVG	433.5	360.0	5.6
STD	10.3	1.6	1.3

Table 5 Properties from 535

Sample No.	UTS (MPa)	YS (MPa)	Elong. (%)
60-1	245.0	128.0	10.0
63-1	240.0	129.0	10.0
AVG	242.5	128.5	10.0
STD	3.5	0.7	0.0
60-2	152.0	106.0	2.5
63-2*	89.0	79.0	0.7
AVG	120.5	92.5	1.6
STD	44.5	19.1	1.3

* Sample broken at shoulder.